博士学位論文

Doctoral Dissertation

Design and Development of Soft Fiber-Reinforced Polymer Composites with Extraordinarily High Crack Resistance

非常に高い亀裂耐性を示すソフト繊維強化ポリマー複合材料の設計と創製

崔 為

Cui, Wei

北海道大学大学院生命科学院

Graduate School of Life Science, Hokkaido University

2020 年 09 月

September 2020

Contents

Chapter 1-General Introduction

1.1. Overview

Engineering materials, for instance, metals, ceramics, are widely applied in industry owing to their desirable mechanical performance (high strength, stiffness, and good corrosion resistance, etc.).[1-3] However, they also show obvious shortcomings, such as heaviness, brittleness, and notch sensitivity. For decades, scientists and engineers have been attempting to overcome the limitations by developing novel structural materials that can offer prominent incorporations of stiffness, strength, toughness, and lightness at low cost. As science and technology advanced, synthetic compounds from multiple components, usually termed as composites, are invented and gradually replacing traditional industrial products due to the efficient combination of various mechanical properties that surpass those of their components by orders of magnitude.[4-6] One type of the most common composites at present, fiber-reinforced polymers (FRPs), are frequently used to substitute neat metals or ceramics in industry because of their improved comprehensive performance.[7, 8] These composites are generally composed of rigid elastic matrices (polymers, metals, ceramics, etc.) and rigid fibers, demonstrating high strength and stiffness.[9-11] Nevertheless, due to poor interfacial bonding and force transmission between matrix and

fibers (**Figure 1.1**), the rigid/rigid combinations usually exhibit unsatisfactory fatigue crack resistance.[12-17] Namely, conventional fiber or fabric reinforced composites, with an isotropic high modulus (~several or tens of GPa), are intrinsically rigid materials with limited and resulting low toughness. More unfortunately, incorporating multiple and mutually exclusive properties into one system, as exemplified by high toughness, strength, and stiffness, results in materials that compromise one essential property at the expense of another.[18-20] Therefore, a pivotal challenge for current composite field is that how to improve material toughness without sacrificing strength, lightness, etc.

In fact, nature has managed to circumvent the dilemma and developed materials showing superior comprehensive mechanical performance (high fracture resistance, good load-bearing capacity and low density). The creations include, but not limited to, ligament and skin,[21, 22] bone and nacre.[23, 24] The strategy is to combine rigid, brittle components and soft, organic matrices into composite materials. Most of these natural materials have highly sophisticated structures with complex hierarchical designs existing over multiple length scales, which result in composite properties that far exceed what could be expected from a simple combination of the individual components (**Figure 1.2**). Extensive researches have been carried out in an endeavor to mimic the unique natural structure with synthetic approaches, aiming to obtain artificial composites exhibiting

prominent mechanical performance which is comparable to natural materials. For example, a synthetic nacre was fabricated by predesigned matrix-directed mineralization, showing a specific toughness and strength close to natural nacre.[25] Another soft biomimetic composite was designed by incorporating stiff aramid nanofibers into poly (vinyl alcohol) system, whose mechanical properties matched or exceeded those of prototype tissues.[26] Recently, based on the delicate concept learning from nature, our group has developed a new class of tough soft composites from the soft/hard combination of polyampholyte (PA) hydrogel matrix and woven glass fiber fabric (GF).[27-29] The de-swelling tough PA gel, with multiple ionic bonds in the gel network,[30] demonstrates a self-adjustable adhesion to either positively or negatively charged surfaces.[31] Therefore, it is supposed to form good adhesion with negatively charged GF. As expected, the biomimetic composites, having a desirable interface between matrix and fiber, exhibit very high fracture toughness (~250 kJ m^{-2}), strength (~65 N mm^{-1}), and tensile modulus (~600 MPa), which are far superior to those of either the hydrogel or GF (**Figure 1.3**). As the composites contain water and are likely biocompatible, they exhibit some structural similarities with load-bearing natural tissues and hold great potential in biological applications. However, for this kind of hydrogel/fabric composites, a problem is that water evaporation during use occurs inevitably, which significantly influences their mechanical performance under industrial

condition. Hence developing a universal composite system that is tough yet stable for industrial application awaits further exploration.

To overcome the dilemma for hydrogel/fabric composites, replacing water-contained matrices with more suitable ones is necessary. Similar to hydrogels, elastomers are also soft and energy dissipative, and they are usually tougher and water-free, enabling them to be applied in industry. Conventional elastomers, such as polydimethylsiloxane (PDMS), polyurethane (PU), are highly elastic and can hardly form good interfacial bonding with diverse surfaces. Composites from them usually show a limited mechanical performance. Lately, our group has successfully designed and developed a series of novel viscoelastic elastomers via a simple one-step radical polymerization of two kinds of acrylate monomers.[32] The resulting elastomers are not only soft and tough, but also adhesive to diverse surfaces (**Figure 1.4**), which allows the fabrication of composites with superior mechanical properties feasibly.

1.2. Outline of this thesis

The aim of this study is to design extraordinarily crack-resistant, yet strong and lightweight fiber-reinforced polymers (FRPs), and generate a universal criterion by understanding the fracture mechanism. To address these issues, we mainly focus on the following three parts: 1) Selecting suitable matrices to construct crack-resistant FRPs; 2) Investigating the mechanical

behaviors of resulting FRPs; 3) Understanding the fracture mechanism of tough FRPs by virtue of mechanics models.

In **Chapter 2**, a brief view on the concept of crack resistance is introduced. Meanwhile, common experimental methods to characterize the crack resistance of a material are explained. Based on the lessons learned from nature, basic strategy to enhance the crack resistance of materials is put forward. This chapter is helpful to initially understand why composite materials always show fantastic crack resistance.

In **Chapter 3**, the strategy to design an extraordinarily tough fiber-reinforced polymers is introduced in detail. Viscoelastic matrices that are adhesive, soft, and tough are selected to combine with commercial fiber fabrics. The three key properties result in composites showing unique features that are totally different from traditional composites with thermosetting plastics as matrices. The good adhesion between fibers and matrix enables a strong interface, which ensures both components to fully dissipate stored energy; The softness of matrices gives extremely high fiber/matrix modulus ratio, leading to energy dissipation zones several orders of magnitude larger than common composites from rigid matrices; The tough matrices show strain energy density comparable to fibers, highly enhancing the energy dissipation density of composites in the dissipation zone. Therefore, we reasonably expect the composites are able to have a satisfying crack resistance.

In **Chapter 4**, the prepared fiber-reinforced polymer composites are tested to investigate their mechanical properties. The highly anisotropic composites demonstrate multiple fantastic properties such as high strength, high toughness, and low density, which can be rarely achieved by other material systems. The strong interface between matrix and fibers is the premise of high mechanical performance. Moreover, the soft composites can also be polymerized from thermal initiation besides photo initiation, extending the possible application in industry. The design strategy is also universal, strong and tough composites can be obtained by combining various fabrics and matrices that are adhesive, soft, and tough. High temperature influences the performance of soft composites. However, preparing composites from matrices with high glass transition temperature is a way to solve this problem.

In **Chapter 5**, the crack-resistant mechanism of soft composites is analyzed. Consistent with the tearing behaviors at different width, the composites show a size-dependent fracture energy. Two characteristic widths are defined to divide the fracture behaviors of soft composites. According to the characteristic widths, the fracture energy of the materials is determined by the matrix toughness, fiber geometry, and width, when the fracture behavior of composites is fiber pullout and matrix failure. When the fracture behavior of composites is mainly fiber fracture and matrix failure, then the fracture energy is decided by the force transfer

length as well as the energy dissipation density, and the fracture energy become size-independent above this width, reflecting the intrinsic crack resistance of the composites. We show that force transfer length is related to the component modulus ratio while the energy dissipation density results from the volume weighed average work of extension of components. The results point out the way to fabricate tough composite materials. That is, maximizing force transfer length by increasing modulus ratio and enhancing energy dissipation density by using energy dissipative components. Based on this principle, we successfully fabricate composites that show fracture energy of as high as 2500 kJ m^{-2}, 100 times that of current toughest composites and are even tougher than metals.

In **Chapter 6**, we apply the design strategy to hydrogel system, aiming to develop crack resistant composite hydrogels. Alginate hydrogels dried in confined condition are employed as the rigid skeleton. Polyacrylamide hydrogels are used as the soft matrix. The modulus ratio of rigid to soft can be as high as 10^5, which is conducive for a large force transfer length. Meanwhile, the alginate skeleton has an energy dissipation density comparable to commercial fibers, which facilitates high energy dissipation density. The resulting composite hydrogels show improved tensile and tearing properties compared with components and are higher than current toughest hydrogels.

In **Chapter 7**, conclusions of the whole dissertation are summarized.

Figures

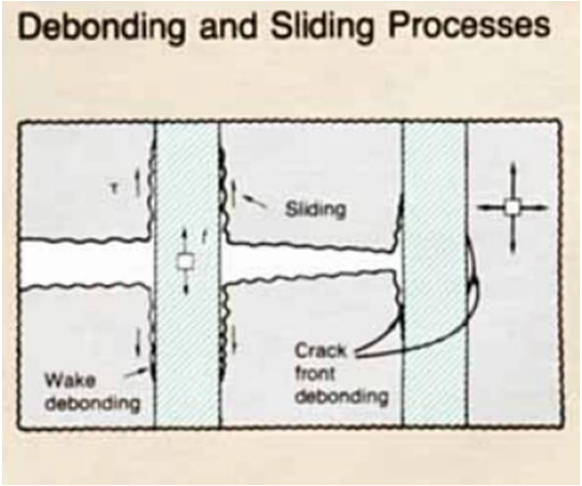

Figure 1.1. Debonding and sliding processes of fiber-reinforced ceramic-matrix composites. For this kind of composites, debonding is a prerequisite for toughening and sliding governs toughening. Crack propagation and fracture involve debonding and sliding processes.

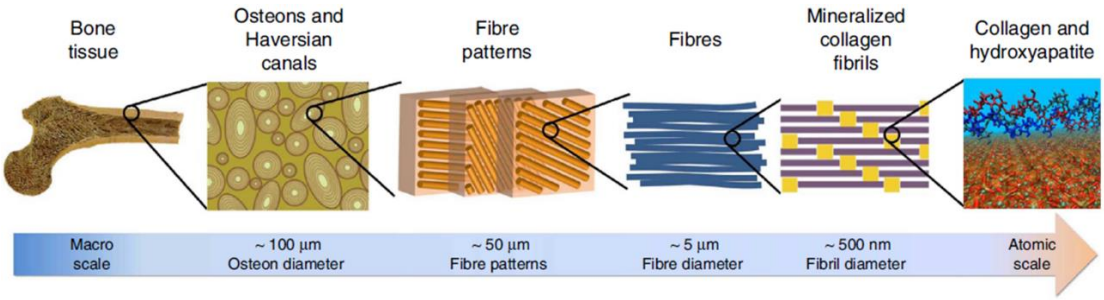

Figure 1.2. Hierarchical structure of bone ranging from the macroscale skeleton to nanoscale collagen and hydroxyapatite.

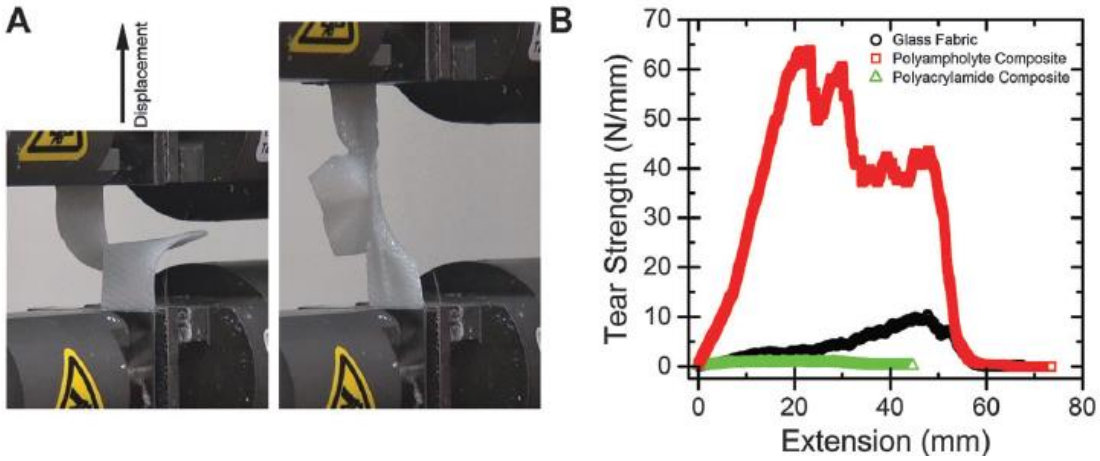

Figure 1.3. Extraordinary mechanical properties of PA/GF soft composites. (A) Tearing behavior. (B) Tearing properties compared with neat components.

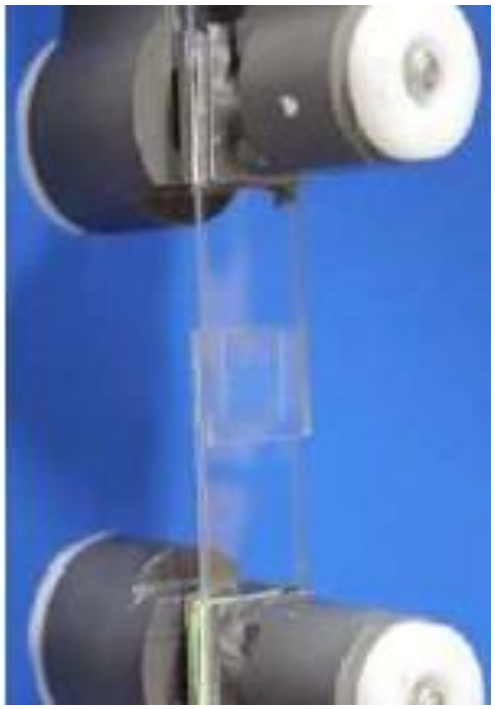

Figure 1.4. Adhesive viscoelastic elastomer from acrylate monomers.

Chapter 2-Recent advances in fiber reinforced polymer composites

2.1. General concepts on crack resistance of composite materials

2.1.1. Fracture in composite materials

Crack resistance, as the name implies, is the ability of a material to resist crack growth before catastrophic failure.[33-35] Compared with homogenous materials, the crack propagation in heterogenous composite materials is more complicated. Depending on the strength of interface, the fracture of composites can be generally divided into two types: 1) crack growth due to interfacial debonding; and 2) crack growth due to components failure.

The interfacial debonding usually occurs in fiber-reinforced polymers (FRPs) made from rigid fibers and rigid thermosetting plastics (**Figure 2.1**).[36] The modulus of fibers is on the order of 10^0~10^2 GPa,[9, 10] while that of matrix is on the order of 10^0 GPa,[11, 37-39] giving rise to a poor interfacial contact and resulting easily occurred delamination. The interface usually fails before matrix rupture and fiber breaking. Thus, fiber sliding friction during pullout is the main energy dissipation mechanism, whereas the matrix and fibers themselves do not dissipate much energy, resulting in a relatively low fracture energy.[40-42]

For the other case, in FRPs with sufficiently strong interface, the crack

will not be able to growth without breaking the components (**Figure 2.2**).[29] This fracture behavior highly enhances the crack resistance of materials because breaking components usually requires large amounts of energy to realize. However, developing this kind of FRP systems is demanding since the stiff reinforcing fibers usually interact weakly with general matrices. Scientists circumvent this problem recently by displacing the commonly used thermosetting matrices with matrices that are adhesive, soft, and tough.[30, 31, 43] The resulting composites with strong interface exhibit superior crack resistance compared with conventional rigid FRPs (**Figure 2.3.**).[27, 28]

2.1.2. Common characterization methods of crack resistance

The essential goal of fracture mechanics is to define a criterion for crack growth and to link this criterion to the physical mechanisms of fracture. Typically, such a criterion involves the comparison between two distinct quantities: one is a material property which quantifies the resistance to crack growth, e.g. the fracture energy, and the other describes the driving force for crack growth as governed by external loading and specimen geometry. For a crack to grow, the latter must reach or exceed the former.

Generally, the crack resistance of a material is characterized by fracture energy, Γ, the energy required to create unit surface area for crack growth.[28, 44] Several kinds of common specimens are employed for

fracture testing to quantify the fracture energy (**Figure 2.4**).

For a pure shear test (**Figure 2.4a**),[45-50] the undeformed sample is a long thin strip of width L_0, height $2H_0$ and thickness b_0 with $L_0 \gg 2H_0$ and b_0. A long crack of length c ($c \gg 2H_0$) is initiated in the middle of the sample. Normally, an external force at a constant velocity is imposed on the grips to displace the sample and propagate the crack. The fracture energy derived in Rivlin and Thomas, is given by

$$\Gamma = 2W(\lambda_s)H_0, \lambda_s = 1 + \frac{\Delta}{H_0} \quad (2.1),$$

where $W(\lambda_s)$ is the strain energy density in materials at a stretch ratio of λ_s far ahead of the crack tip. In practice, $W(\lambda_s)$ is typically measured by subjecting an uncracked sample to tension under the pure shear constraint and calculating the area under the measured stress-strain curve.

For a simple extension test (**Figure 2.4b**),[45, 51-53] the undeformed sample geometry is defined by the length L_0, height $2H_0$ and thickness b_0. Unlike the pure shear test, the two arms of the specimen at the cracked end are clamped and peeled apart. The fracture energy, also derived in Rivlin and Thomas, is given by

$$\Gamma = \frac{2\lambda_a F}{b_0} - 2W(\lambda_a)H_0 \quad (2.2),$$

where F is the applied force to the two arms, λ_a and W are the stretch ratio and strain energy density of the arms, respectively.

For a single notch test (**Figure 2.4c**),[54-57] it was initially proposed by Greensmith to determine the fracture energy of vulcanized natural rubbers.

Using a compliance method, Greensmith found that the fracture energy for short cracks with length $c \ll L_0$ is approximately given by

$$\Gamma = \frac{6}{\sqrt{\lambda}} W(\lambda_b) c \quad (2.3),$$

where $W(\lambda_b)$ is the strain energy density of an uncracked sample subjected to a uniaxial stretch ratio λ_b, and L_0 is the width of the sample which is much less than the height $2H_0$.

For a tearing test (**Figure 2.4d**),[27, 30, 58, 59] the crack deformed by out-of-plane shear loading. The two arms of a pre-cracked specimen are oppositely displaced to impose the tearing load. The fracture energy can be calculated as

$$\Gamma = \frac{2F}{b_0} \quad (2.4),$$

where F is the tearing force, b_0 is the sample thickness.

2.2. Strategies to enhance the crack resistance

The major strategies existing to increase the crack resistance of materials stem primarily from nature. By combining rigid, brittle components (e.g. fibers) with soft components (e.g. collagen), nature has shown us how to fabricate strong and tough composites. The creations include, but not limited to, skin and tendon (soft),[22] bone and scale (hard).[60, 61] Most of these natural materials have very complex hierarchical architectures existing over multiple length scales, resulting in comprehensive properties that far exceed what could be expected from a simple combination of the

individual components.

The extremely high crack resistance of natural materials can be explained from the physics point of view. The crack resistance, usually expressed by fracture energy, is influenced by two factors: 1) energy dissipation zone; 2) energy dissipation density. The former determines the size of area for the material to dissipate energy when the crack advances. The latter determines the amount of energy that is dissipated in the dissipation zone. Natural materials manage to maximize one of these two factors or both. For example, bones have a soft/rigid structure, resulting in extremely high modulus ratio, which generates a huge energy dissipation zone.[62-65] Another example is muscle, which contains strong fibrous skeleton and soft matrix. Fibers are strong and resistant to stretch, giving rise to a high energy dissipation density.[66, 67] These natural materials maximize the essential factors, highly enhancing their crack resistance.

2.3. Objects and design strategy of this thesis

Despite nature has shown us the success of creating high-toughness materials, it is still a big challenge for scientists to make tough artificial materials. Moreover, it is even more demanding to incorporate multiple mechanical properties into one material system, such as strength, toughness, low density, due to the contradiction between these properties.

In this dissertation, we put forward a universal strategy to design

composite materials showing high toughness, high strength, and low density simultaneously. Instead of using traditional thermosetting plastics as matrices, we select a range of newly developed viscoelastic matrices that are adhesive, soft, and tough, to combine with commercial woven fiber fabric, successfully creating a series of extremely tough fiber-reinforced polymers, without sacrificing strength and weight. We elucidate that the high toughness of the composites results from large energy dissipation zone and high energy dissipation density. The former is maximized by the extremely high modulus ratio of fiber to matrix. The latter is enhanced by the high toughness of matrices. This design principle can be further extended to hydrogel systems. Tough composite hydrogel is prepared by combining aligned fibrous alginate and soft polyacrylamide, suggesting the universality of the design strategy. We believe the tough composite materials developed in this work hold great potential in industrial applications and the design strategy can inspire the development of tough materials in various fields.

Figures

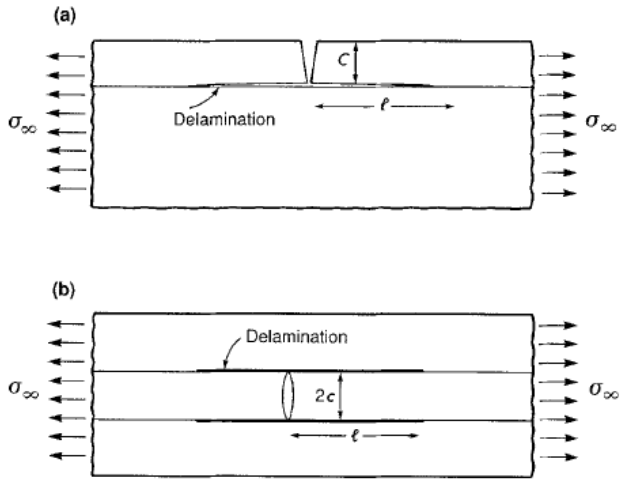

Figure 2.1. Two important geometries for delamination in composites: (a) from an edge crack, (b) from a central notch. The crack growths by interfacial delamination.

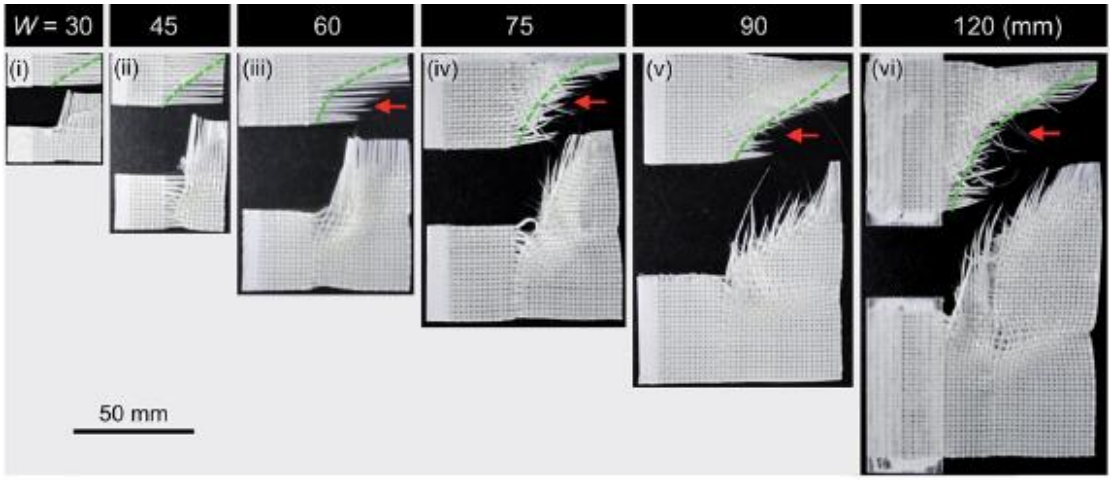

Figure 2.2. Fracture images of the composites with strong interface. The red arrows in (iii–vi) indicate fiber fracture. The green dashed lines in (i-vi) show the fracture path, determined approximately by the fractured hydrogel matrix boundary. The crack growths by breaking both the fibers and matrix without interfacial debonding.

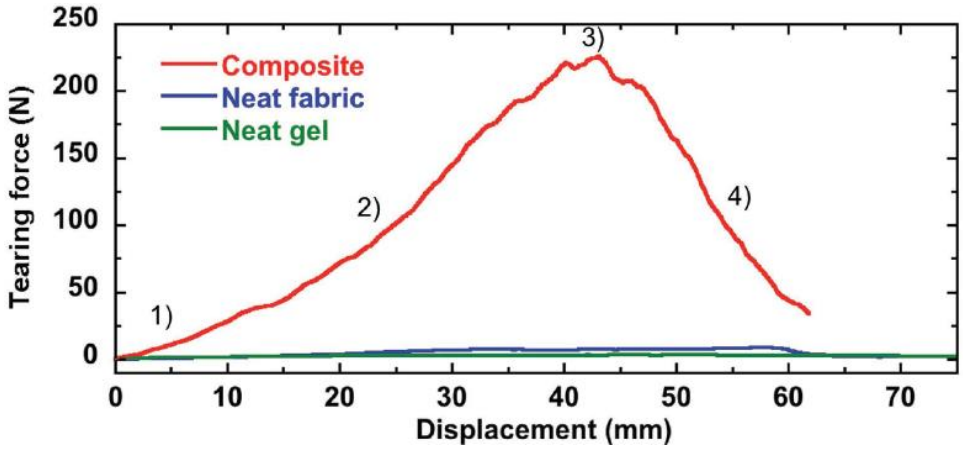

Figure 2.3. The extraordinary crack resistance of FRPs from polyampholyte hydrogels that are adhesive, soft, and tough. The composites show orders of magnitude higher tearing force compared with neat components.

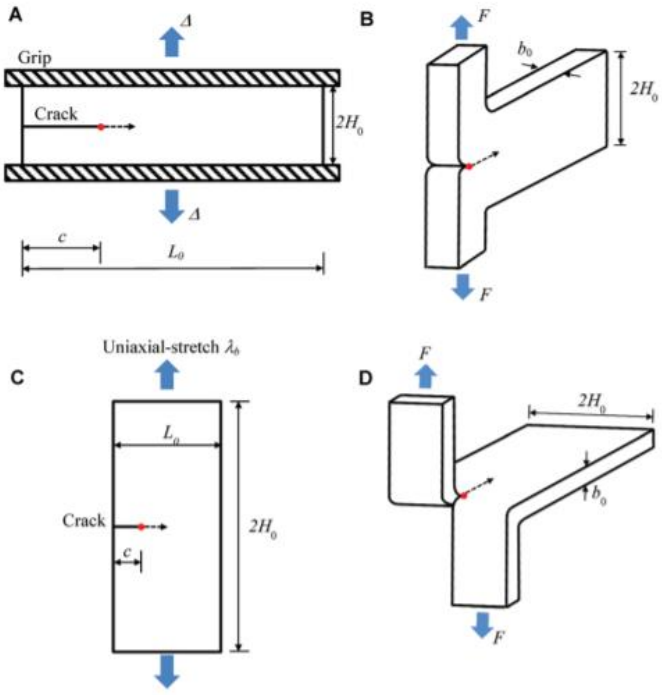

Figure 2.4. Fracture test configurations. (A) Pure shear. The thickness of the specimen is b_0, and the grips assumed to be rigid. (B) Simple extension. (C) Single edge crack. (D) Tearing. For (A and C) the undeformed geometry is shown to illustrate specimen dimensions, while for (B and D) the deformed geometry is shown to illustrate the loading mode. The crack tip is illustrated as a red point and the dashed arrow indicates the projected crack path.

Chapter 3-Design Strategy of Tough Fiber Reinforced Polymers

3.1. Introduction

Synthetic compounds from multiple components, usually termed as composites, are gradually replacing traditional industrial products due to their efficient integration of multiple mechanical properties that surpass neat components by orders of magnitude.[4-6] They have replaced traditional industrial products such as metals and alloys due to their high strength at greatly reduced weight.[7, 8] However, these composites still show poor crack resistance compared with metals, which seriously hampers their reliability in safety-critical applications. Existing composites are usually composed of rigid thermosetting plastics (epoxy, phenolic resin, etc.) and rigid fibers, the moduli of thermosetting matrices and fibers are on the order of 10^0 GPa and 10^0~10^2 GPa, respectively.[9-11, 38] The rigid/rigid combinations give high strength and stiffness, while the fiber/matrix modulus ratio is normally below 10^2, which significantly confines the force transmission between he rigid/rigid components, giving rise to fairly limited process zone and resulting low toughness.[12-17]

Generally, to create a crack-resistant fiber-reinforced polymer (FRP), two factors are considered to play key roles in affecting the toughness, i.e., the energy density, and the process zone size.[29] The energy density

dominates the amount of energy dissipation per area while the process zone determines the area of energy dissipation. The energy density is influenced by mechanical properties of components as well as the interface. Viscoelastic matrix and strong fiber are preferable to have large energy densities and form an excellent interface. For process zone, the concept is similar to the damage zone of tough hydrogels, which is the area surrounding the crack that dissipates energy.[44, 52, 68, 69] The size of process zone is reflected by the force transfer length, which highly depends on the modulus ratio between components.[70] Higher modulus ratio gives better force transfer capability and corresponding larger process zone. Therefore, tough composites can be constructed from energy-dissipative components with strong interfacial bonding and contrasting moduli. This principle is verified in fiber-reinforced hydrogel composites from a polyampholyte (PA) hydrogel matrix and woven glass fiber fabric (GF).[27-29] The soft, de-swelling, and viscoelastic PA gel, with multiple ionic bonds in the network,[30] demonstrates a self-adjustable adhesion to either positively or negatively charged surfaces,[31] which forms strong adhesion with negatively charged GF. On the other hand, the fiber/matrix modulus ratio in this composite system achieves ~10^3 to 10^4, which greatly facilitates the force transfer between components.[29] As a result, the PA/GF composites, with energy-dissipative components (strain energy density above 4 MJ m^{-3}) and a considerable force transfer length (critical width above 45 mm),

exhibit high intrinsic toughness (~1000 kJ m^{-2}), strength (~300 MPa), and tensile modulus (~600 MPa), which fill the gap between soft materials and traditional rigid materials.

To develop soft FRP composites based on elastomers, novel viscoelastic elastomers that are soft, tough, and adhesive to fibers, simultaneously easily to form composites with weave fiber fabrics are required. Existing elastomers, such as PDMS, polyurethane, and natural rubber, could not satisfy these requirements. The three properties of the viscoelastic matrices result in soft FRPs showing unique features that are totally different from conventional rigid FRPs: 1) the good adhesion between fibers and matrices enables a strong interface, which ensures both components to fully dissipate stored energy; 2) the softness of matrices gives extremely high fiber/matrix modulus ratio, leading to energy dissipation zones several orders of magnitude larger than common FRPs from rigid matrices; 3) the tough matrices show strain energy density comparable to fibers, highly enhancing the energy dissipation density of FRPs in the dissipation zone.

In this chapter, we intend to design and develop FRPs based on this principle. For this purpose, we first select a series of novel elastomers by one-step free radical copolymerization of acrylate monomers. The dynamics of the elastomers, characterized by the Kuhn segment relaxation time, can be tuned over six orders by varying the chemical structure and

composition of the acrylate monomers that form hard segment and soft segment of copolymers. The elastomers exhibit maximum energy dissipation when the strain rate is 1/10 of the inverse of the Kuhn segment relaxation time, reaching a work of extension at tensile fracture of ~ 25 MJ m^{-3} and a fracture energy of 20 kJ m^{-2}. Such toughness is comparable to natural rubbers and is among the highest of elastomers ever reported. In addition, these elastomers possess full self-recovery, self-healing, and strong adhesion on various solid surfaces. The wide range of tunable dynamics substantially enriches the choices of elastomers for soft FRP applications, and the facile one-step and solvent-free synthesis of these elastomers from liquid monomers are not only suitable for fabrication of composites with fabrics but also eco-friendly, cost-effective and scalable, which greatly lowers the barrier for the practical applications.[32] By tuning the molar fraction of monomers, the modulus of the energy-dissipative elastomers varies from hundreds of kilopascals to tens of megapascals, which is conducive to adjust the modulus ratio and relevant toughness of composites.

3.2. Results and Discussion

3.2.1. Design strategy of extraordinarily tough fiber-reinforced polymers

To create a crack-resistant FRP, it is necessary to understand the

determinant factors that influence the crack resistance. The crack resistance of a material is characterized by fracture energy, Γ, the energy required to create unit surface area for crack growth.[33-35, 71] Simply, we can envision that Γ is influenced by two factors: 1) the length over which a material is deformed inelastically ahead of the advancing crack, known as the energy dissipation zone size, l_T, and 2) the energy dissipation density of the dissipation zone when the crack advances, W. Accordingly, Γ (J m^{-2}) could be related to l_T (m) and W (J m^{-3}),[72, 73]

$$\Gamma \cong W \cdot l_T. \quad (3.1).$$

Therefore, developing tough materials is a question of how to design structures that maximize W and l_T. For composites consisting of a hard phase embedded in a soft matrix, W results from the contributions of both components, while l_T is related to the force transfer length that is determined by the component modulus ratio (hard to soft).[70, 74, 75]

To enhance the crack resistance of FRPs, we employ viscoelastic polymer matrices that are adhesive, soft, and tough. These properties should not only enable a strong interface with the stiff reinforcing fibers, but also result in large force transfer lengths through high fiber/matrix modulus ratios, which contributes to a high energy dissipation density and large energy dissipation zone (**Figure 3.1**).

3.2.2. Mechanical properties of selected matrices

A class of newly developed "viscoelastomers" are used to fabricate a series of soft/rigid FRPs by combination with various woven fabrics. The viscoelastomer matrices are formed by one step radical copolymerization from liquid acrylate monomers without using solvent (**Figure 3.2**).[32] Chemical structures of used monomers are shown in **Table 3.1**. As a typical example, we first show the mechanical behaviors of the elastomers P(PEA-co-IBA), synthesized from ethylene glycol phenyl ether acrylate (PEA) as soft segment and isobornyl acrylate (IBA) as hard segment. The elastomers are formed by UV initiated free radical copolymerization of the bulk monomers in the presence of small amount of benzophenone (BF) as UV initiator. By tuning the molar fraction of IBA, f ($f = \frac{M_{IBA}}{M_{PEA}+M_{IBA}}$) from 0.1 to 0.3, the mechanical properties of the elastomer can be tuned over a wide range (**Figure 3.3**). Thereafter, the matrix is denoted as M1-*f*. The tearing fracture energy T_m, measured by trousers tearing test at a velocity of 50 mm min^{-1}, can be tuned from 15 to 34 kJ m^{-2}. The tensile modulus (E_m) and the tensile work of extension (W_m) of P(PEA-co-IBA), measured at a strain rate of 0.07 s^{-1}, vary from 0.8 to 4.4 MPa and from 6 to 19 MJ m^{-3}, respectively. Moreover, the matrix is highly viscoelastic, the mechanical properties of which can be easily tuned by altering the testing velocity (**Figure 3.4**). Mechanical parameters of all matrices are summarized in **Table 3.2**.

Therefore, the soft viscoelastomers P(PEA-co-IBA) are highly energy-dissipative, having a work of extension roughly on the order of the rigid CF fiber. In addition, the fiber/matrix modulus ratio, E_f/μ_m, can be as high as $8.0\times10^4 \sim 1.5\times10^4$ when the molar fraction of IBA, f, is varied from 0.1 to 0.3. Accordingly, the combination of the CF and the viscoelastomers is expected to give high energy dissipation density and large force transfer length.

3.2.3. Mechanical properties of used fibers

We try to combine the viscoelastomer with strong and rigid fiber fabrics. Images of all fabrics used in this work are shown in **Figure 3.5**. Taking carbon fiber (CF) fabric as an example, it has plain texture of 0.3 mm-thick and with fabric area density of 200 g m^{-2} woven from fiber bundles. Each fiber bundle is made from hundreds of thin fibers of 5 μm-diameter. The fiber bundles have an ellipsoid cross section of 3.8 mm perimeter and 0.204 mm^2 area. (**Table 3.3**). A single fiber bundle has tensile modulus E_f of 21 GPa and work of extension at fracture W_f of 39 MJ m^{-3} (**Figure 3.6, Table 3.4**).

3.2.4. The strong adhesion between matrix and fibers

To ensure the force transmission between components in fiber-reinforced polymer composites and avoid delamination, a strong interface is critical.

The adhesion tests between matrix and fibers are conducted by pulling out an individual fiber bundle from neat viscoelastomer matrices. The matrix M1-*f* is taken as an example to demonstrate the tests. The fiber bundle is partially embedded in M1-*f* matrix and pulled out unidirectionally. The results show that the fiber bundle outside the matrix breaks at a force of about 130 N for all tested matrices (**Figure 3.7a**), rather than being pulled out (**Figure 3.7b**). This result demonstrates that the interface and matrix do not fail, and the shear bonding strength (τ_s) of the interface should be higher than 2.28 MPa that is estimated by balancing the external force (F = 130 N) with the adhesion force provided by the shear bonding strength, as $F = \tau_s \cdot A$, where A is the embedded surface area of the fiber bundle.

3.2.5. The theoretical load transfer length for a model composite

The theoretical load transfer length l_T for a model composite consisting of parallel fibers embedded in a soft matrix is derived in the literature:[70, 74, 75]

$$l_T = \sqrt{\frac{E_f A_f d}{\mu_m h}} \quad (3.2),$$

where E_f and μ_m are the tensile modulus of the fiber and the shear modulus of the matrix, respectively, d is the effective distance between adjacent fibers, h is the width of the fiber, and A_f is the cross-sectional area of the fiber. Equation (3.2) can also be expressed in terms of the product of the geometric pre-factor $\alpha = \sqrt{\frac{A_f d}{h}}$ and the modulus ratio, as

$$l_T = \alpha \sqrt{\frac{E_f}{\mu_m}} \quad (3.3).$$

Assuming that this model is applicable to our composites, using the geometry parameters of fabrics shown in **Table 3.3**, the geometric pre-factors for CF, GF, and AF are estimated as $\alpha_{CF} = 0.208\ \text{mm}$, $\alpha_{GF} = 0.206\ \text{mm}$, $\alpha_{AF} = 0.201\ \text{mm}$, respectively. The geometry parameters of fabrics are determined from the cross section of corresponding composites shown in **Figure 3.8**.

3.3. Conclusions

In this chapter, the basic design strategy of tough FRPs is introduced. The key idea is to utilize viscoelastic polymer matrices that are adhesive, soft, and tough. The strong adhesion enables a strong interface between matrix and fibers, which ensures both components to fully dissipated stored energy. The softness of matrices is not only conducive for the interfacial bonding, but also gives an extremely high modulus ratio of fiber to matrix, resulting in an extraordinarily large force transfer length. The high toughness of matrices guarantees the high energy dissipation in the energy dissipation zone, facilitating a high energy dissipation density. These unique characteristics are totally distinguished from traditional fiber-reinforced thermosetting plastics, which usually exhibit interfacial delamination during fracture due to the rigid/rigid combinations. In rigid FRPs, the interface usually fails before matrix rupture and fiber breaking. Thus, fiber

sliding friction during pullout is the main energy dissipation mechanism, whereas the matrix and fibers themselves do not dissipate much energy, resulting in a relatively low fracture energy.[40-42] Therefore, the FRPs from adhesive, soft, and tough matrices, showing a strong component interface, are expected to possess crack resistance superior to conventional rigid FRPs.

3.4. Experimental Section

3.4.1. Materials

Plain weave carbon fiber fabric (CF), glass fiber fabric (GF), and aramid fiber fabric (AF) were purchased from Marukatsu Co., Ltd., Japan. All fabrics were used as received. Acrylate monomers, ethylene glycol phenyl ether acrylate (PEA), benzyl acrylate (BZA), di(ethylene glycol) ethyl ether acrylate (DEEA), and isobornyl acrylate (IBA) were provided by Osaka Organic Chemical Industry Ltd, Japan. Ultraviolet initiator benzophenone (BP) was purchased from KANTO Chemical Co., Inc and used without further purification.

3.4.2. Methods

Preparation of viscoelastomers. Samples were prepared by placing 1 mm spacer between two hydrophobic films supported by glass plates to form a reaction mold. Subsequently two monomers, one of the following of

ethylene glycol phenyl ether acrylate (PEA), benzyl acrylate (BZA), or di(ethylene glycol) ethyl ether acrylate (DEEA), along with isobornyl acrylate (IBA), containing initiator (0.1 mol% of the total monomer molar concentration) was injected into the mold. The random copolymerization was allowed to proceed under an argon atmosphere via ultraviolet irradiation (UVP lamp Toshiba-FL15BLB, wavelength 365 nm, light intensity 4 mW cm^{-2}) for 10 h.

Uniaxial tensile tests. The tensile tests were carried out by using a commercial tensile tester (Autograph AG-X, Shimadzu Co., Japan) equipped with a 100 N load cell at 50 mm min^{-1} crosshead velocity in air. Before the tests, the viscoelastomers were cut into a dumbbell shape standardized as JIS-K6251-7 (2 mm in inner width, 12 mm in gauge length) with a cutting machine (Dumb Bell Co., Ltd.) (**Figure 3.9a**).

Trouser tearing tests. The tearing fracture energy of the samples was evaluated by trouser tearing tests. The tensile tester (Autograph AG-X, Shimadzu Co., Japan) equipped with a 100 N load cell was employed to perform the tearing tests. A sample with a prescribed width w and length w + 30 mm was prepared. An initial notch of 30 mm was made in the middle of the sample along the length direction with a laser cutter. To prevent elongation of the legs during tests, stiff and thin tape was glued on both sides of the samples before testing (**Figure 3.9b**). During testing, one leg of the sample was clamped to the base, and the other was clamped to the

crosshead, which was displaced at a velocity of 50 mm min^{-1} at room temperature in the open atmosphere. After testing, the tearing force-displacement curves were obtained to calculate the tearing energy of samples by the following equation:[27-29]

$$T = \frac{\int_0^L F\, dL}{t \cdot L_{bulk}} \quad (3.4),$$

where F is the tearing force, t is the sample thickness, L is the displacement, and L_{bulk} is the projected crack length.

Scanning electron microscopy. Microscale observation was carried out by scanning electron microscopy (SEM) (JEOL JSM-6010LA, Tokyo, Japan). Samples were gold-coated in an ion-sputtering machine (E-1010, Hitachi, Tokyo, Japan) before observation. The acceleration voltage varied from 15 to 20 kV.

Figures

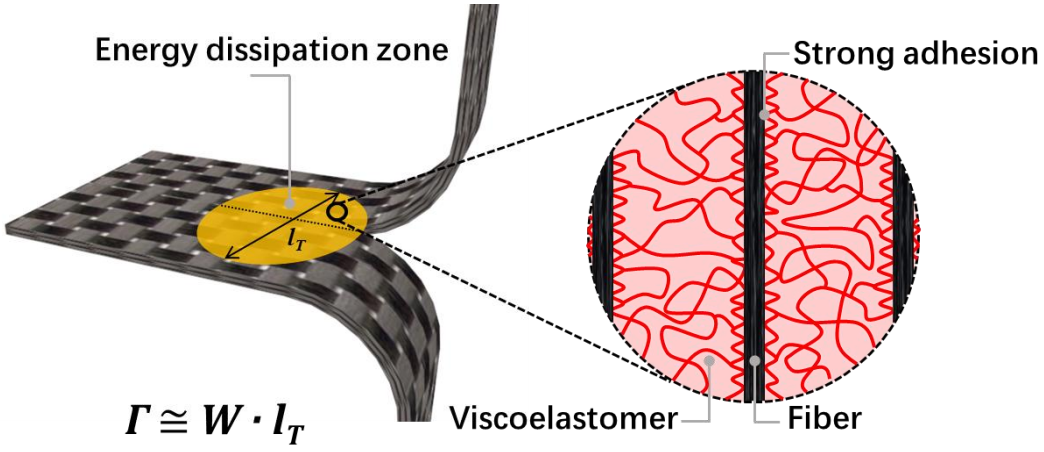

Figure 3.1. Design strategy of extraordinarily tough fiber-reinforced polymers (FRPs). The strategy employed involves combining strong and rigid woven fabrics with viscoelastomer matrices that are adhesive, soft, and tough. Such a combination gives high energy dissipation density, W and large energy dissipation zone, l_T (up to the cm scale) due to the high fiber/matrix modulus ratio (10^4~10^5), guaranteed by the strong fiber/matrix interface.

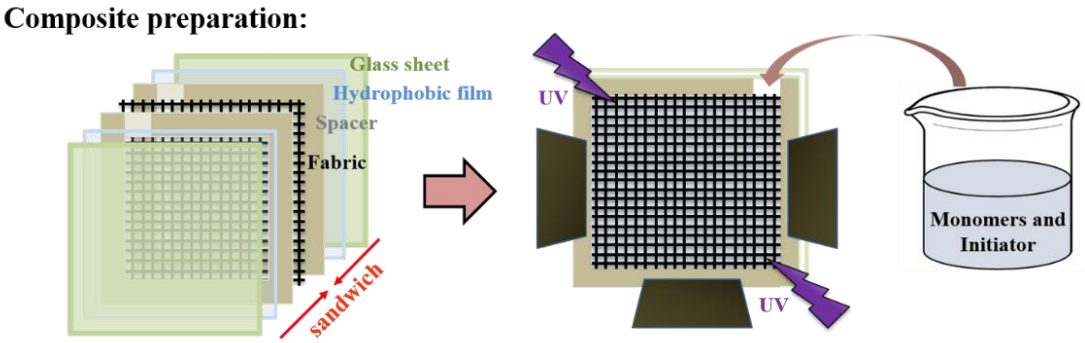

Figure 3.2. Composites were fabricated by random radical copolymerization. During preparation, a sheet of fiber fabric was embedded into a reaction cell made up of two glass plates coated with hydrophobic films, inside which 0.5 mm spacers were used to sandwich the fabric sheet on both sides. Afterwards the precursor solution was injected into the cell under argon atmosphere. Polymerization was initiated by UV irradiation for 10 h.

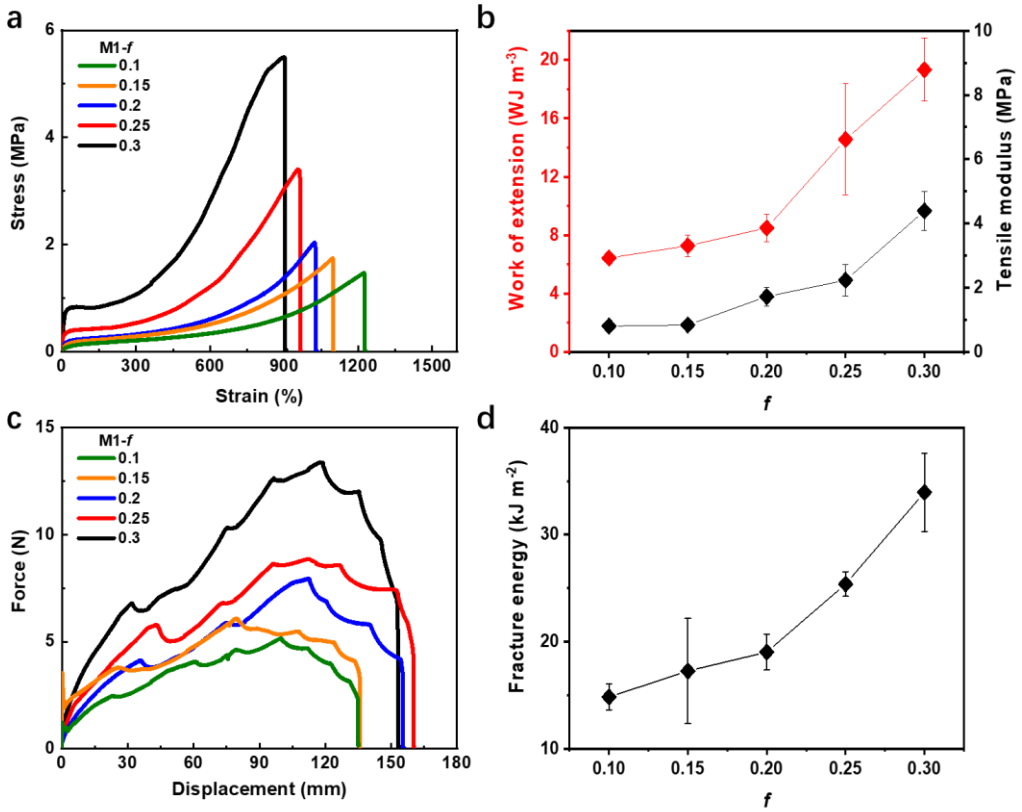

Figure 3.3. Tunable tensile properties of matrices M1-*f* that stands for the copolymer P(PEA-*co*-IBA) with various *f*. (a) Tensile properties of M1-*f* at displacement velocity of 50 mm min^{-1}. The corresponding strain rate was 0.07 s^{-1}. (b) The work of extension and tensile modulus both increase as *f* increases. (c) Tearing properties of P(PEA-co-IBA) with varied *f* at 50 mm min^{-1}. (d) The fracture energy also increases as *f* increases.

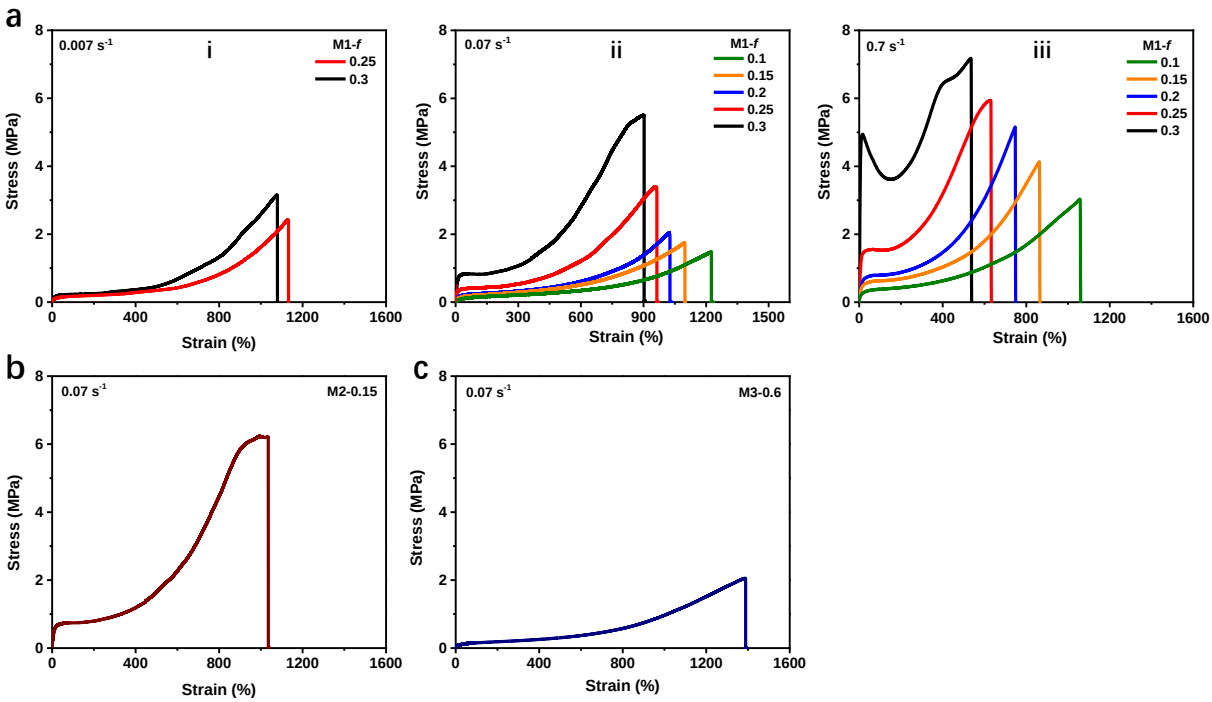

Figure 3.4. Strain rate dependence of viscoelastomer matrix M1-*f* and tensile properties of M2-0.15 and M3-0.6. (a) The matrices M1-*f* with different *f* are tested at strain rates of 0.007 s^{-1}, 0.07 s^{-1}, and 0.7 s^{-1} (Tensile velocities of 5 mm min^{-1}, 50 mm min^{-1}, and 500 mm min^{-1}) (a-i, a-ii, and a-iii), respectively. Results indicate that the tensile property of matrix is highly dependent on strain rate. Tensile modulus and failure stress of matrix increase with increasing strain rate, while tensile strain decreases. Both M1-0.3 and M1-0.25 show obvious yielding and relatively high tensile modulus of 105 MPa and 30 MPa at the strain rate of 0.7 s^{-1}, which behave similarly to thermal plastics. (b) Tensile property of M2-0.15. (c) Tensile property of M3-0.6.

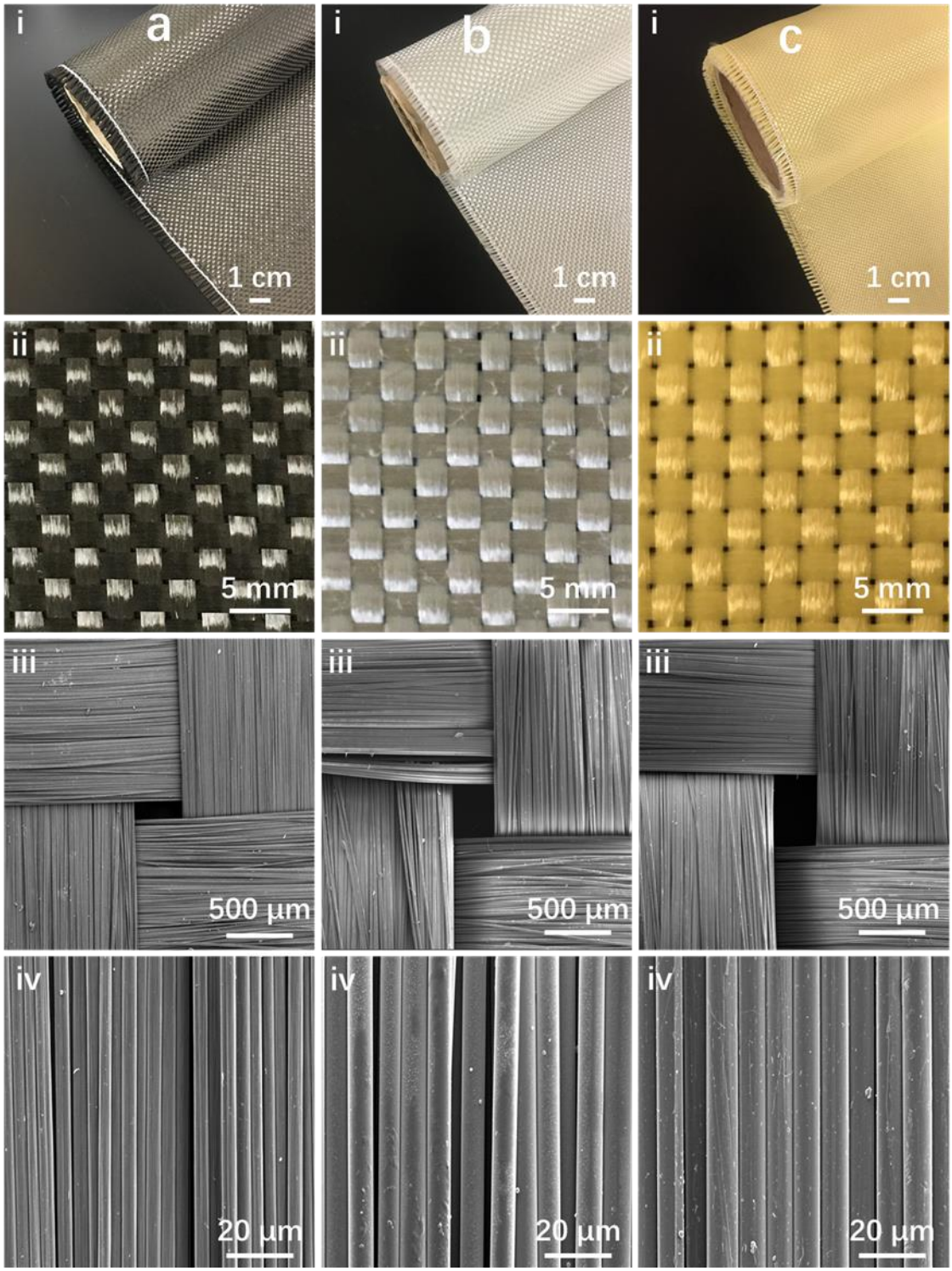

Figure 3.5. Macro- and micrographs of plain weave (a) carbon fiber (CF), (b) glass fiber (GF), and (c) aramid fiber (AF) fabrics used in this work. All fabrics are in a plane weave pattern of fiber bundles that contains thousands of individual thin fibers. (i) The macrographs of all fabrics. (ii) The plain weave structures. (iii) SEM micrographs of woven fiber bundles. (iv) Individual fibers.

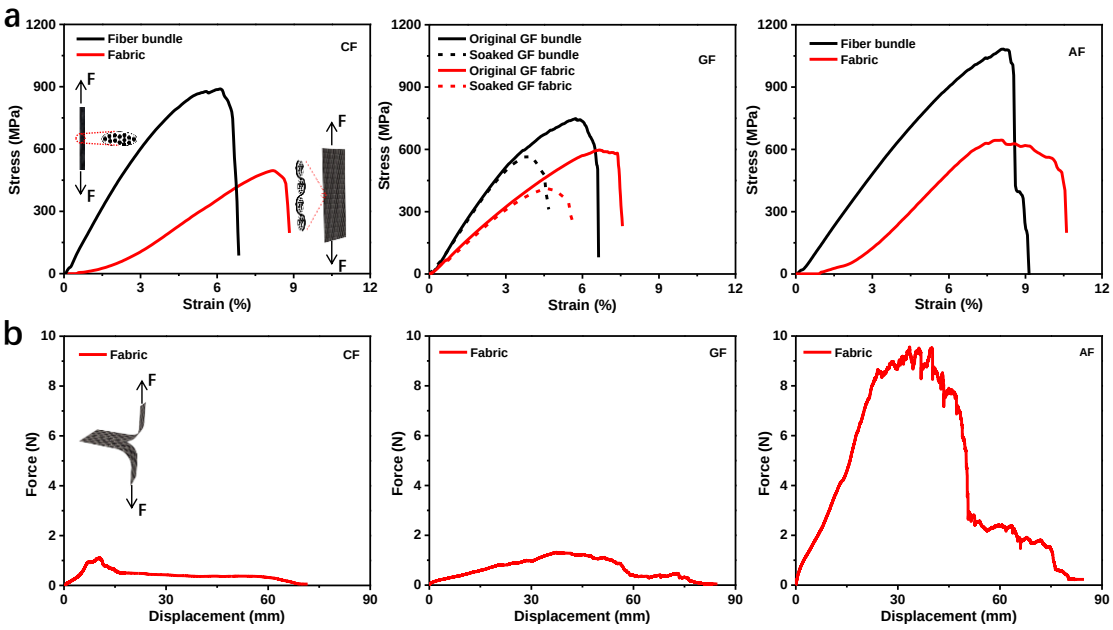

Figure 3.6. Mechanical properties of woven fabrics and individual fiber bundles used in this work. (a) Tensile stress-strain curves for both fabrics and individual fiber bundles of carbon fiber (CF), glass fiber (GF), and aramid fiber (AF) fabrics. The measurement of the fabrics was performed along the axis of meshes. The tensile performance of a single fiber bundle is different from a fabric. For the fabric that is in a weave pattern,[11] the bundles are in a curved geometry to form meshes. The mesh geometry influences the area to calculate stress and corresponding tensile modulus while the curved geometry influences the strain. Therefore, the fabric shows a lower tensile modulus, fracture stress but higher fracture strain. In particular, tensile properties of GF fabric and individual bundle are influenced by the monomer solution while CF and AF are not. Both GF fabric and bundle show decreased tensile stress and strain after soaking in the monomer solution for 10 h. This can be due to the corrosion of coating on GF during soaking, which generates more defects on GF. Therefore, data for GF after soaking is employed in the whole text. (b) Trousers tearing force-displacement curves for CF, GF, and AF fabrics. Tensile and tearing velocity were both 50 mm min^{-1}. Strain rate for tensile tests was 0.07 s^{-1}.

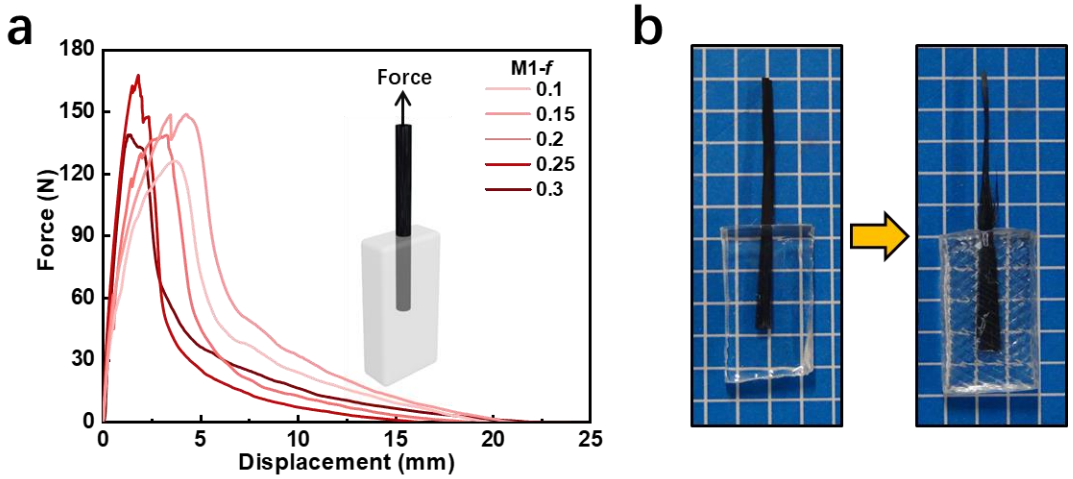

Figure 3.7. Adhesion test to determine the interfacial bonding strength between single carbon fiber bundles and matrices, M1-*f*. (a) A carbon fiber bundle was embedded in the transparent matrix with an embedding surface area of 3.8 mm (cross-sectional perimeter) × 15 mm (length). The pullout velocity was 50 mm min^{-1}. (b) Images showing the samples before and after the adhesion test. The length of a lattice is 5 mm. The fiber bundle fractures without being pulled out from the matrix, indicating the high strength of the interface as well as the matrices.

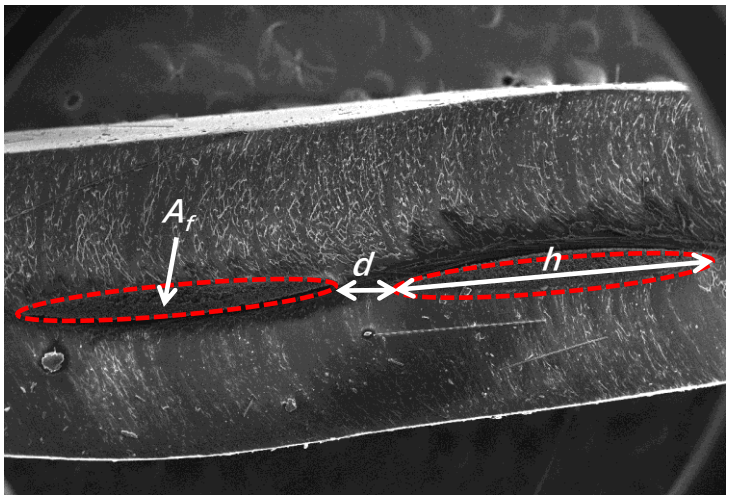

Figure 3.8. Cross-section SEM view of the composite shows the cross-sectional area of fiber bundles (area of red dotted circle) in the matrix, from which geometry parameters are estimated.

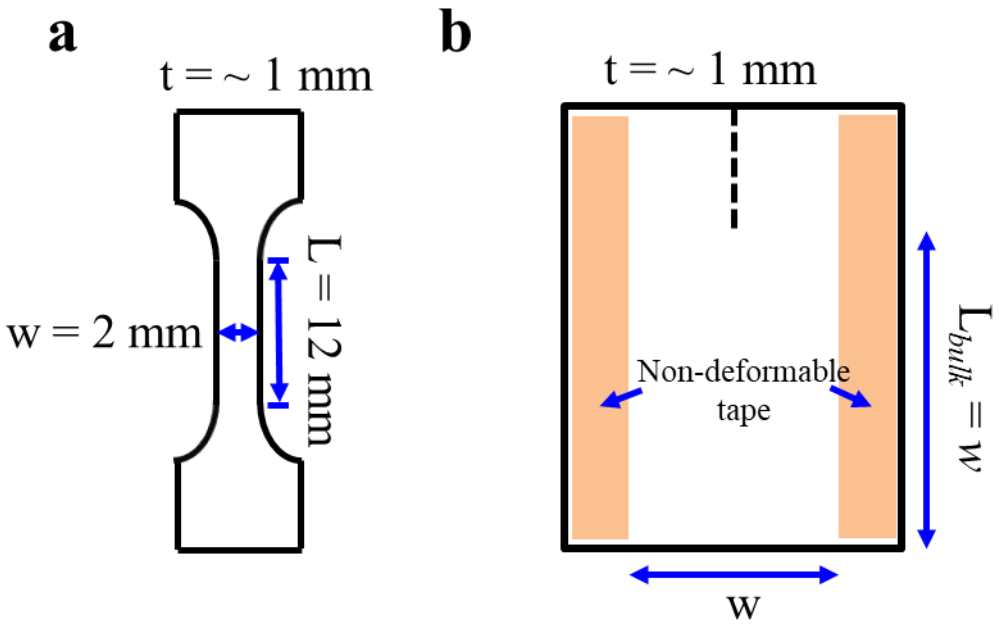

Figure 3.9. Elastomer sample geometries for tensile and tearing tests. (a) Dumbbell sample for tensile test. (b) Notched sample for tearing test.

Tables

Table 3.1. Monomer structures that make up the viscoelastomer matrices. Each matrix is produced from copolymerizing a soft segment (ethylene glycol phenyl ether acrylate (PEA), benzyl acrylate (BZA), or di(ethylene glycol) ethyl ether acrylate (DEEA)) with a hard segment (isobornyl acrylate (IBA)). The molar fraction of the hard segment is defined as *f*.

Matrix code	M1-*f*	M2-*f*	M3-*f*
Soft segment	PEA 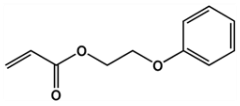	BZA 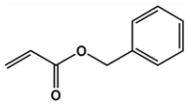	DEEA 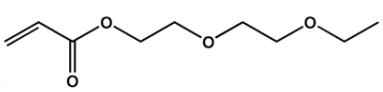
Hard segment	IBA 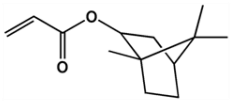	$f = \frac{M_{IBA}}{M_{IBA} + M_{Soft}}$	

Table 3.2. Summary of mechanical properties of the viscoelastomer matrices at different testing velocities. The properties are tensile fracture stress (σ_m), fracture strain (ε_m), Young's modulus (E_m), work of extension (W_m), and tearing energy (T_m). Each sample was tested $N \geqslant 3$ times to obtain the average value. The shear modulus μ_m of the matrix is 1/3 of the Young's modulus.

Sample code	Testing velocity (mm min^{-1})	Strain rate (s^{-1})	f	σ_m (MPa)	ε_m (%)	E_m (MPa)	W_m (MJ m^{-3})	T_m (kJ m^{-2})
M1-*f*	5	0.7	0.25	2.20 ± 0.28	1133 ± 24	1.71 ± 0.15	7.76 ± 0.28	20.66 ± 1.26
			0.3	3.20 ± 0.06	1082 ± 25	2.07 ± 0.23	10.57 ± 0.59	21.91 ± 1.55
	50	0.07	0.1	1.57 ± 0.08	1225 ± 6.4	0.80 ± 0.03	6.43 ± 0.16	14.84 ± 1.22
			0.15	1.96 ± 0.45	1101 ± 16	0.84 ± 0.07	7.27 ± 0.74	17.26 ± 4.92
			0.2	2.24 ± 0.23	1030 ± 18	1.72 ± 0.30	8.49 ± 0.93	19.03 ± 1.68
			0.25	3.20 ± 0.16	961 ± 45	2.23 ± 0.49	12.55 ± 3.81	25.39 ± 1.16
			0.3	5.44 ± 0.18	905 ± 40	4.39 ± 0.61	19.34 ± 2.15	33.96 ± 3.65
	500	0.007	0.1	3.27 ± 0.34	1063 ± 37	2.58 ± 0.28	13.22 ± 1.80	23.48 ± 1.38
			0.15	4.11 ± 0.64	868 ± 24	3.51 ± 0.88	14.52 ± 1.28	32.06 ± 1.83
			0.2	5.26 ± 0.32	752 ± 12	4.64 ± 1.21	14.72 ± 0.45	63.79 ± 1.27
			0.25	6.40 ± 0.02	634 ± 60	30.45 ± 4.21	22.80 ± 1.22	81.77 ± 3.80
			0.3	6.89 ± 0.42	538 ± 30	105.31 ± 11.58	29.65 ± 0.99	89.69 ± 9.44
M2-*f*	50	0.07	0.15	6.20 ± 0.04	1041 ± 56	3.96 ± 0.56	23.34 ± 2.74	37.65 ± 0.88
M3-*f*	50	0.07	0.6	1.86 ± 0.25	1391 ± 18	0.34 ± 0.05	8.29 ± 1.84	9.18 ± 1.00

Table 3.3. Structural parameters of the three plain weave fiber fabrics used in this work. Parameters include fabric area density (ρ_a), fabric thickness (t), cross-sectional perimeter of a fiber bundle (S), cross-sectional area of a fiber bundle (A_f), effective distance between adjacent fiber bundles (d), width of a fiber bundle (h), single fiber radius (r).

Fabrics	ρ_a (g m^{-2})	t (mm)	S [a)] (mm)	A_f [a)] (mm^2)	d [a)] (mm)	h [a)] (mm)	r (μm)
CF	200	0.30	3.8	0.204	0.361	1.705	5
GF	590	0.59	4.5	0.403	0.216	2.048	7
AF	320	0.55	4.2	0.396	0.184	1.812	8

a) These parameters were estimated from the SEM images of the corresponding composites.

Table 3.4. Summary of mechanical properties of fabrics and corresponding fiber bundles. The properties include tensile fracture force (F_f) and nominal stress (σ_f), fracture strain (ε_f), Young's modulus (E_f), work of extension (W_f), and tearing energy (T_f). Each sample was tested $N \geqslant 3$ times to obtain the average value. The testing velocity was 50 mm min^{-1}.

Sample code	F_f [a)](N)	σ_f(MPa)	ε_f (%)	E_f (GPa)	W_f (MJ m^{-3})	T_f (kJ m^{-2})
CF fabric	744 ± 54	496 ± 23	8.8 ± 0.2	6.6 ± 0.3	20.3 ± 3.8	2.5 ± 0.2
CF fiber bundle	183 ± 32	895 ± 41	6.8 ± 0.1	21.8 ± 1.6	39.0 ± 4.2	—
GF fabric[b)]	1210 ± 67	410 ± 22	5.7 ± 0.6	7.4 ± 1.0	14.3 ± 1.5	10.2 ± 1.1
GF fiber bundle[b)]	228 ± 16	565 ± 40	4.7 ± 0.4	17.7 ± 0.7	16.4 ± 2.1	—
AF fabric	1774 ± 85	645 ± 31	10.6 ± 0.4	7.8 ± 1.3	37.0 ± 2.3	17.0 ± 1.0
AF fiber bundle	430 ± 23	1085 ± 58	9.1 ± 0.3	17.3 ± 1.4	55.8 ± 3.4	—

a) Fabric is in a rectangle shape with a width of 5 mm.

b) Data of soaked GF sample in **Fig. S2** is employed.

Chapter 4-Mechanical Performance of Tough Fiber Reinforced Polymers

4.1. Introduction

Conventional fiber-reinforced thermosetting plastics usually demonstrate high strength, modulus, and low density, which are widely employed in industry as metal substitutes. However, it has long been a great challenge to fabricate fiber-reinforced polymers that incorporate both strength and toughness since these two mechanical properties are usually mutually conflicting.[19] The attainment of both strength and toughness is an essential requirement for most structural materials. They have little use as bulk structural materials if they do not show proper toughness even if the strength is high. In fact, it is materials with lower strength yet higher toughness that find general use in the most safety-critical applications, where failure is unacceptable.

In common rigid FRPs, the improvement of crack resistance has usually been a compromise between extrinsic toughening and intrinsic toughening.[76] Intrinsic toughening acts to inhibit damage mechanisms, such as fracture or debonding processes, and is primarily associated with plasticity. That is, it is effective against the initiation and propagation of cracks. On the other hand, with extrinsic toughening, the material's inherent crack resistance is unchanged. Instead, mechanisms such as crack

deflection and bridging act mainly on the wake of the crack to shield the local stress/strain experienced at the crack-tip. By operating principally in the crack wake, extrinsic toughening is only effective in resisting crack growth. Furthermore, this effect relies on crack size. Natural materials commonly show both toughening mechanisms, which is the major factor underlying their high crack resistance. However, a critical difference between natural structural materials and artificial composites is that natural materials generally comprise hard and soft phases arranged in complex hierarchical architectures.[1, 77-81] The soft, viscoelastic phases shear dramatically upon loading, effectively transfer the load to the hard phases in a considerably large area. As a result, the materials can release stored energy in a large energy dissipation zone, demonstrating relatively high fracture energy compared with rigid FRPs.

The lesson from nature has inspired the creation of soft/rigid composite materials, which show highly improved crack resistance compared with rigid FRPs. For instance, by introducing viscoelastic hydrogels that are adhesive, soft, and tough into strong and rigid fabric phases, extremely crack-resistant soft FRPs have been developed.[27-31] The FRPs overcome the conflict between strength and toughness, which show high strength comparable to traditional rigid FRPs yet superior toughness that is 100 times higher than rigid ones. Moreover, due to the high biocompatibility, the hydrogel-based FRPs hold great potential in biological applications.

On the other hand, however, the hydrogel-based FRPs are not suitable for industrial applications since water evaporation occurs inevitably during use, which largely weakens their life span. This explains the reason that we develop the viscoelastic elastomers as the matrices for FRPs. The adhesive, soft, and tough elastomers show comparable properties with the hydrogel, while they are water-free, highly enhancing the weather resistance.[32]

In this chapter, we investigate and discuss the mechanical performance of fiber-reinforced viscoelastomers. By tuning the molar fraction of monomers, the modulus of the energy-dissipative elastomers varies from hundreds of kilopascals to tens of megapascals, which is conducive to adjust relevant toughness of composites. Based on this consideration, we develop tough FRPs from various soft viscoelastomers/rigid woven fiber fabrics combinations. The resultant composites demonstrate extraordinarily high intrinsic toughness (up to 2500 kJ m^{-2}) that is far superior to any best-in-class tough materials. Meanwhile they show high strength (~700 MPa) as well as low density (~1 g cm^{-3}), which is a rarely achieved integration. Our work produces the toughest composites at present and puts forward a universal design criterion for novel tough structural materials.

4.2. Results and Discussion

4.2.1. Fabrication of tough fiber-reinforced polymers

Soft FRPs from are produced via a one-step random radical copolymerization of monomers in a mold where the fabric is sandwiched in the middle (**Figure 4.1a**). Here, FRP from M1-0.1 and CF is shown as an example. As the monomer liquid is hydrophobic and has low viscosity, it can wet the CF fabric and permeate easily into fiber bundles during monomer injection. As a result, the composites formed have an interlocking structure between the two components, with the matrix strongly bonded to the fibers, as seen by SEM observation (**Figure 4.1b**). The fabric can be seen in the soft FRP due to the optical transparency of the viscoelastomer matrix (**Figure 4.2**).

4.2.2. Mechanical properties of tough fiber-reinforced polymers

The fabricated FRPs are highly anisotropic, which are extremely resistant to stretching yet highly flexible to bending or twisting (**Figure 4.2**). Tensile tests and three-point bending tests reveal that the soft composite has a tensile modulus three orders of magnitude higher than the bending modulus (**Figure 4.3**), due to the fabric phase lying nominally along the neutral axis during bending. Moreover, the soft FRP demonstrates an incredibly high crack resistance. A soft FRP sample (w = 80 mm) with two long precut

cracks (30 mm) can hold 35 kg of hanging mass without crack propagation (**Figure 4.4**).

Uniaxial tensile tests are conducted to measure the load-bearing properties. Sample geometries and corresponding stress-strain curves are shown in **Figure 4.5**. The matrix is soft and highly stretchable, sustaining merely 1.5 MPa prior to failure and showing a work of extension of 6 MJ m^{-3} (inset of **Figure 4.5**). On the contrary, the neat carbon fiber fabric is very stiff and strong (490 MPa) but brittle, which fails at a strain of 8.8% and having a work of extension of 20 MJ m^{-3}. Interestingly, when the fabric is integrated with the matrix, the resulting composite shows a similar stiffness to the neat fabric, but it is much stronger (700 MPa) and breaks at a higher strain (12.5 %) than the neat fabric. The enhanced tensile behavior of soft FRPs compared to neat fabrics can be understood by a mechanism proposed by Hui et al, which highlights the role of modulus disparity.[70] The extreme fiber/matrix modulus ratio means that the soft matrix can effectively transfer the lost load of the broken fiber to neighboring fibers by dramatically deforming in shear, resulting in a considerable overload region. Therefore, the lost load is carried by a broad region of adjacent fiber segments instead of being concentrated on a limited length scale, which delays the catastrophic failure of fibers. Tensile properties of all FRPs are shown in **Figure 4.6** and summarized in **Table 4.1**.

Trouser tearing tests are performed to quantitatively measure the crack

resistance of the material (Experimental Section).[27-29, 82-84] As shown in **Figure 4.7**, the composite achieves an extraordinarily high tearing force, which reaches a maximum value of 940 N mm^{-1}, much higher than 3.7 N mm^{-1} of the neat fabric and 13.3 N mm^{-1} of the neat matrix. The composite has a tearing toughness (T) as high as 1400 kJ m^{-2}, which is several orders of magnitude greater than both individual neat components (3.0 kJ m^{-2} for the neat fabric and 9.5 kJ m^{-2} for the neat matrix). The toughness of this composite is also much higher than any of the current best-in-class materials.[12, 25, 26, 85-87] Tearing properties of all FRPs are shown in **Figure 4.8**.

4.2.3. Comparison with common tough materials

The soft FRPs developed here demonstrate an efficient combination of multiple properties compared with common tough materials.[2, 19, 88-91] **Figure 4.9** first gathers the tensile modulus of the soft FRPs as a function of density, with other industrial materials for comparison. Together with PA gel/fiber composites, the soft FRPs show lower tensile modulus than ceramics, metallic glasses, CFRP and GFRP, metals and alloys but higher tensile modulus than engineering polymers and elastomers, filling the gap between soft materials and traditional rigid materials. Figure **4.10** illustrates the fracture energy as a function of density for materials. The soft FRPs show an overwhelming advantage over common industrial

structural materials in terms of fracture energy, exceeding those of traditional rigid materials (CFRP and GFRP, metals and alloys, metallic glasses, and ceramics) by orders of magnitude. Yet the soft FRPs exhibit low density, which is comparable with engineering polymers and elastomers, and even woods. The soft FRPs also show a high tensile strength of 400 to 700 MPa, which are stronger than engineering polymers and elastomers, and rival conventional CFRP and GFRP (**Figure 4.11**). "Specific" mechanical quantities, which are the quantities divided by the density of the materials, are frequently used for the selection of lightweight but strong materials.[92, 93] **Figure 4.12** plots the specific fracture energy of materials as a function of specific strength. The soft FRPs are located in the upper-right corner of the plot, indicating an excellent combination of high toughness and strength with low weight. The superior performance of the soft FRPs beats all the best-in-class industrial materials at present and even exceeds the extremely tough PA gel/fiber composites. The soft FRPs developed in this work overcome the conflict between toughness and weight and should have bright application prospects in industry. Summarized mechanical properties of materials are shown in **Table 4.2**.

4.2.4. Temperature resistance

To investigate if the soft FRPs are usable at different temperatures, tearing test were conducted on M1-0.2 composites from 24 to 150 °C。Tearing

results are shown in **Figure 4.13**, as the testing temperature is increased, both the tearing force and corresponding energy are decreased. Taking a look at the tearing behavior of those composites in **Figure 4.14**, it is obvious to figure out that detachment of matrix from fabric occurs at high temperature, which leads to a poor force transmission from the matrix to the fabric due to the undesirable interface. The matrix is viscoelastic at room temperature, however, viscidity of it may vanish at relatively high temperature, making it behave as a highly elastic elastomer. Therefore, the interfacial bonding is deteriorated, resulting in the delamination and corresponding poor mechanical performance. However, one can still fabricate tough FRPs at high temperature by choosing viscoelastic matrices that show high glass-transition temperature.

4.2.5. The universality of the methodology to fabricate tough composites from varied matrices and fabrics

To further verify if the proposed method is universal to fabricate tough fiber-based soft composites from varied matrices and fabrics, more monomers are selected to prepare fiber-reinforced polymers (**Figure 4.15**). Specially, monomers for soft segment in the matrix are divided in four types depending on their structures (BZA, PEA, PDEA in a group, 2-MTA, DEEA in a group, LA, ISTA in a group, THFA itself in a group). The toughness of the resultant composites is tested in **Table 4.3**, with that of

neat elastomers or neat fabrics as a comparison. As indicated in **Table 4.3**, compared with neat elastomers and fabrics, all resultant composites are much tougher, with toughness several orders of magnitude higher than that of individual component. This encouraging result suggests that the preparation method can be further extended to fabricate tough soft composites from diverse matrices and fabrics as long as the precursor solution of monomers can permeate through the fabric to form an interlocking structure, which opens the bright prospect of their applications in many fields.

4.2.6. Fiber-reinforced polymers from thermal initiation

In the above context, FRPs are all prepared by thermal initiation. Here, FRPs with varied molar ratio of matrix (from $f = 0.3$ to 0.1) are fabricated to further examine the availability of thermal initiation. To prepare FRPs from thermal initiation, same dosage of azodiisobutyronitrile (AIBN) was employed to activate the polymerization at 70 °C instead of benzophenone (BP). Other experimental conditions are the same. Results of tearing test for composites from thermal polymerization are gathered in **Figure 4.16a-e** with composites from UV initiated photopolymerization as comparisons. Apparently, thermal initiation is an effective method to prepare tough soft composites as all newly made composites also show high tear resistance compared with those from photopolymerization. From the force-

displacement curves and corresponding L_{bulk} of composites, tear energy of composites is presented in **Figure 4.16f**. All thermal-polymerized composites are tougher than photopolymerized composites in terms of tearing resistance.

Matrices PEA-co-IBXA (f = 0.3 to 0.1) were also prepared and tested, whose mechanical properties are shown in **Figure 4.17** and **Figure 4.18** in comparison with those fabricated by photopolymerization. Unexpectedly, elastomers from different polymerization methods demonstrate dramatically different mechanical performance. With quite many elastomers prepared by thermal polymerization, it is realized that oxygen plays a much bigger role in affecting the mechanical performance of elastomers. The content of residual oxygen in oven is several thousand times higher than that in glovebox, which may result in products with much lower molecular weight and corresponding less desirable mechanical performance. In industrial production, repeatability is believed to be much better as long as the oxygen concentration can be well controlled.

4.3. Conclusions

In this chapter, we investigate a series of mechanical properties of tough fiber-reinforced polymers. The premise of the high-performance composites is a strong interface, resulting from the permeation of low-viscosity monomer solution into fabrics. The prepared composites are

highly anisotropic, which are extremely resistant to stretch but quite flexible under bending or twisting. Due to the extreme modulus ration of fiber to matrix, the FRPs show much improved tensile strength and tearing toughness compared with neat fabric and matrix. During loading, the soft matrix shears dramatically, which effectively transfer the force to a broad area in the FRP, which benefits the load bearing property and energy dissipation of FRPs in three ways. First, the effective force transfer brings about a considerable energy dissipation zone, enabling components to dissipate energy in a large area. Second, the tough matrix itself in the energy dissipation zone can dissipate large amounts of energy. Third, fibers in the energy dissipation zone are broken instead of pulled out, which fully releases the stored elastic energy by deformation. Therefore, the soft FRPs show an efficient combination of multiple fantastic properties, which is rarely achieved by other materials. On the other hand, the tearing performance of FRPs are significantly influenced by temperature, which decreases as temperature goes up. This shortcoming can be solved by utilizing matrix that has high glass transition temperature. Various FRPs from thermal initiation or different combinations prove the feasibility. In summary, the FRPs in this study show a combination of several desirable properties and beat all the best-in-class materials in present, and the preparation method can be easily extended to other systems, which hold great potential in industry applications.

4.4. Experimental Section

4.4.1. Materials

Plain weave carbon fiber fabric (CF), glass fiber fabric (GF), and aramid fiber fabric (AF) were purchased from Marukatsu Co., Ltd., Japan. All fabrics were used as received. Acrylate monomers, ethylene glycol phenyl ether acrylate (PEA), benzyl acrylate (BZA), 2-(2-phenoxyethoxy)ether acrylate (PDEA), ethylene glycol methyl ether acrylate (MEA), di(ethylene glycol) ethyl ether acrylate (DEEA), lauryl acrylate (LA), isooctadecyl acrylate (ISTA), Tetrahydrofurfuryl acrylate (THFA), isobornyl acrylate (IBA), and *tert*-butyl acrylate (TBA) were provided by Osaka Organic Chemical Industry Ltd, Japan. Ultraviolet initiator benzophenone (BP) and thermal initiator azodiisobutyronitrile (AIBN) were purchased from KANTO Chemical Co., Inc and used without further purification.

4.4.2. Methods

Preparation of fiber-reinforced viscoelastomers. Samples were prepared by placing two 0.5 mm spacers on both sides of the fabric, which was inserted between two hydrophobic films supported by glass plates to form a reaction mold. Subsequently monomers containing initiator (0.1 mol% of the total monomer molar concentration) were injected into the mold. The random copolymerization was allowed to proceed under an

argon atmosphere via ultraviolet irradiation (UVP lamp Toshiba-FL15BLB, wavelength 365 nm, light intensity 4 mW cm^{-2}) for 10 h. Neat elastomers were also prepared as controls.

Uniaxial tensile tests. For composites and fabrics, rectangular-shaped samples (10 mm wide and 80 mm length) were prepared with the fibers aligned parallel or perpendicular to the length direction. Tests were performed on a commercial tensile tester (Autograph AG-X, Shimadzu Co., Japan) equipped with a 20 kN load cell in the open atmosphere at room temperature. The initial length of the sample between grips was 20 mm. Since the fracture for the composite samples occurs at a small strain, and the load supported by the soft matrix at this strain is extremely low, the fracture strength of the composites is calculated from the maximum load divided by the cross-sectional area of neat fabric before loading (the width, w, multiplied by the fabric thickness, t) for both the neat fabric and the composite. The work of extension is defined as the area below the obtained stress-strain curve. The crosshead velocity was 50 mm min^{-1}, unless otherwise stated. For viscoelastomers, the tensile tests were carried out by using the same commercial tensile tester equipped with a 100 N load cell at 50 mm min^{-1} crosshead velocity in air. Before the tests, the viscoelastomers were cut into a dumbbell shape standardized as JIS-K6251-7 (2 mm in inner width, 12 mm in gauge length) with a cutting machine (Dumb Bell Co., Ltd.).

Trouser tearing tests. The tearing fracture energy of the samples was evaluated by trouser tearing tests. The tensile tester (Autograph AG-X, Shimadzu Co., Japan) equipped with a 20 kN load cell was employed to perform the tearing tests. A sample with a prescribed width *w* and length *w* + 30 mm was prepared. An initial notch of 30 mm was made in the middle of the sample along the length direction with a laser cutter. For neat elastomer samples, to prevent elongation of the legs during tests, stiff and thin tape was glued on both sides of the samples before testing. During testing, one leg of the sample was clamped to the base, and the other was clamped to the crosshead, which was displaced at a velocity of 50 mm min^{-1} at room temperature in the open atmosphere. After testing, the tearing force-displacement curves were obtained to calculate the tearing energy of samples by the following equation:[27-29]

$$T = \frac{\int_0^L F\, dL}{t \cdot L_{bulk}} \quad (4.1),$$

where *F* is the tearing force, *t* is the sample thickness, *L* is the displacement, and L_{bulk} is the projected crack length.

Three-point bend tests. The flexibility of the composites was examined by three-point bend tests using a tensile tester (Tensilon RTC-1150A, Orientec Co., Japan) equipped with a 100 N load cell in the open atmosphere. The sample width was 10 mm and the length between bottom points was 20 mm. The testing velocity was 30 mm min^{-1}.

Scanning electron microscopy. Microscale observation was carried out by scanning electron microscopy (SEM) (JEOL JSM-6010LA, Tokyo, Japan). Samples were gold-coated in an ion-sputtering machine (E-1010, Hitachi, Tokyo, Japan) before observation. The acceleration voltage varied from 15 to 20 kV.

Figures

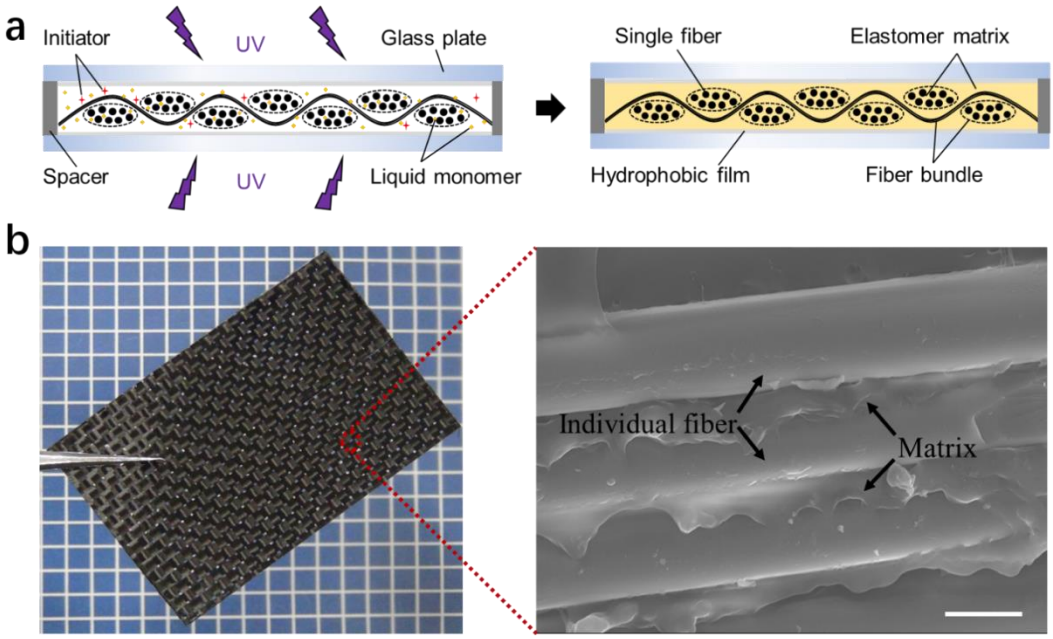

Figure 4.1. A typical procedure to prepare soft fiber-reinforced viscoelastomers. (a) Illustration of the preparation method. The low-viscosity monomers can easily permeate the fabric, leading to the formation of a strong interface and interlocking structure. (b) The appearance of the as-prepared soft FRP and enlarged view of the local area by SEM. The viscoelastomer matrix is M1-0.1. Individual fibers are fully wetted by the viscoelastomer matrix, suggesting a complete permeation of liquid monomers into fiber bundles and the formation of strongly bonded interface. The length of a lattice is 5 mm. The scale bar represents 5 μm.

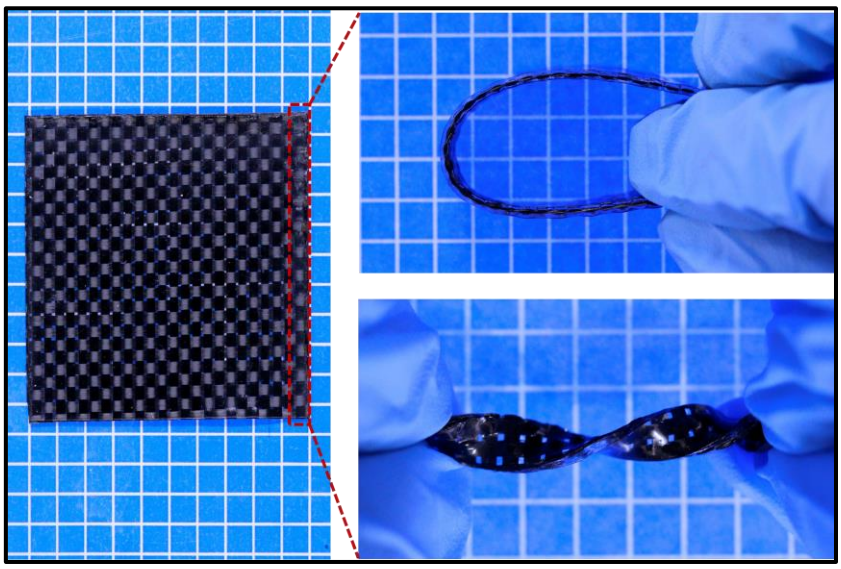

Figure 4.2. Demonstration of the superior mechanical properties of soft FRPs. The fabric is visible because the matrix is optically transparent. A strip of the composite is cut to clearly show its flexibility under bending or twisting. The length of a lattice is 5 mm.

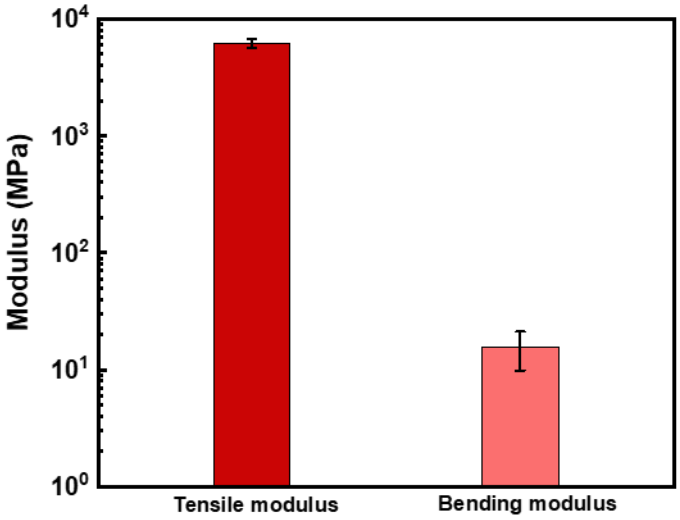

Figure 4.3. Anisotropy of soft fiber-reinforced polymer (FRP) from M1-0.1 and CF. The tensile modulus approaches 10 GPa while the bending modulus is about 10 MPa, indicating that the composite is highly stiff upon stretching but flexible under bending. The strain rates of tensile and bending tests were 0.07 mm min^{-1} and 0.042 mm min^{-1}, respectively. The velocity of tensile and bending tests were 50 mm min^{-1} and 30 mm min^{-1}, respectively.

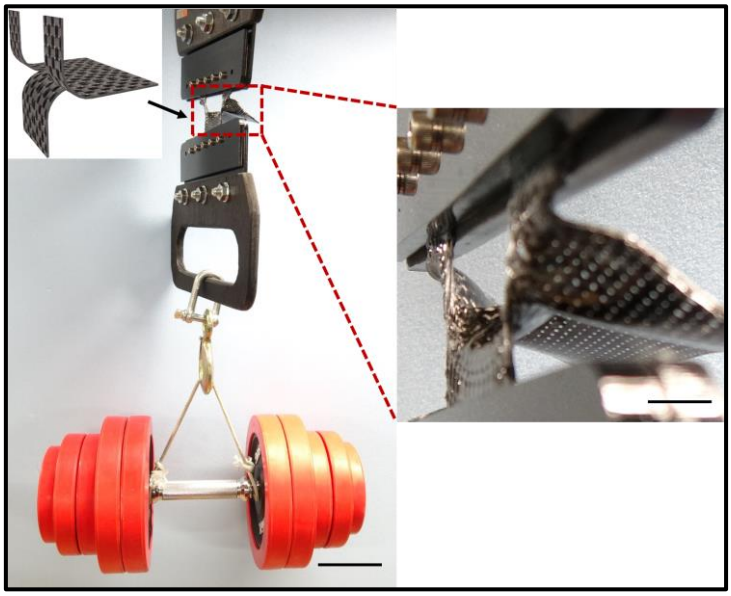

Figure 4.4. The extraordinary crack resistance of the composite. A composite specimen with two cracks can sustain 35 kg of weight without crack propagation. The scale bars represent 10 cm.

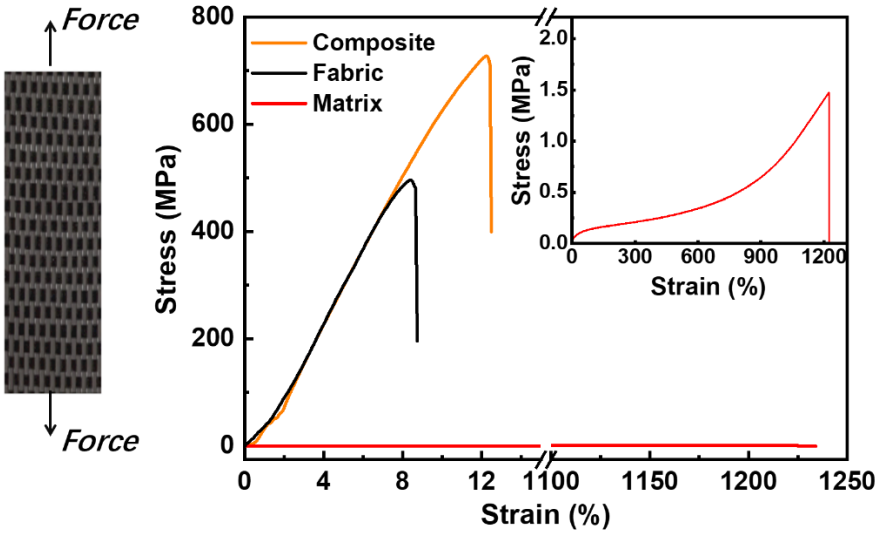

Figure 4.5. Tensile tests on the composite, neat fabric, and neat matrix, with 10 mm sample width, measured at strain velocity and strain rate of 50 mm min^{-1} and 0.07 s^{-1}, respectively. The composite shows improved strength and work of extension in comparison to the neat fabric.

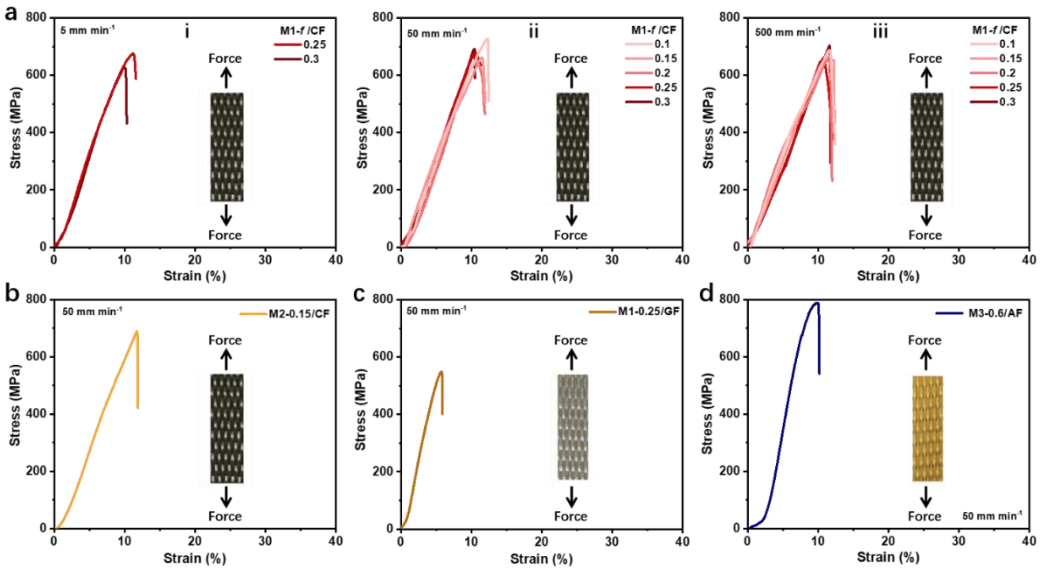

Figure 4.6. Tensile properties of soft FRPs using different combinations (a) The composites M1-*f* /CF with varied *f* are tested at tensile velocities of 5 mm min^{-1}, 50 mm min^{-1}, and 500 mm min^{-1} (a-i, a-ii, and a-iii), respectively. (b) Tensile property of M2-0.15/CF. (c) Tensile property of M1-0.25/GF. (d) Tensile property of M3-0.6/AF. Sample width and gauge length are 10 mm and 20 mm, respectively.

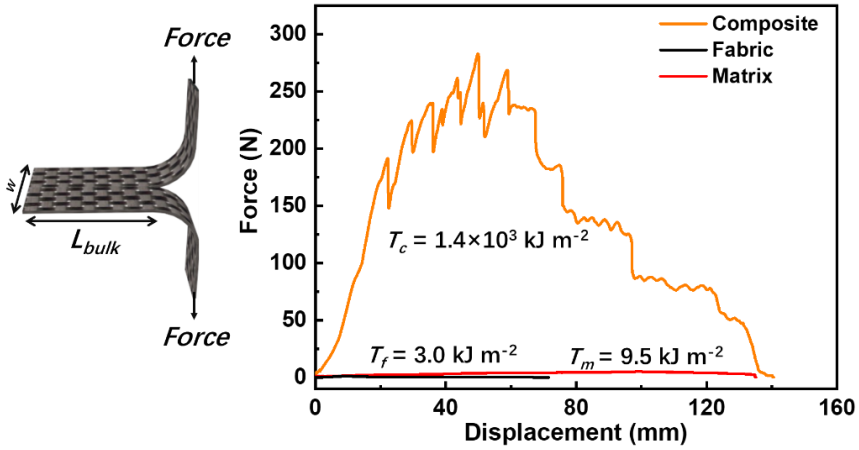

Figure 4.7. Trouser tearing tests on the composite, neat fabric and neat matrix. Samples are prepared with a width (w) of 50 mm, and a length of 80 mm. A pre-notch of 30 mm is made in the middle of the sample to make the projected length of tear (L_{bulk}) equal to width. Force-displacement curves show that the composite has much higher tearing strength and energy than the neat fabric and matrix. The tearing velocity was 50 mm min^{-1}.

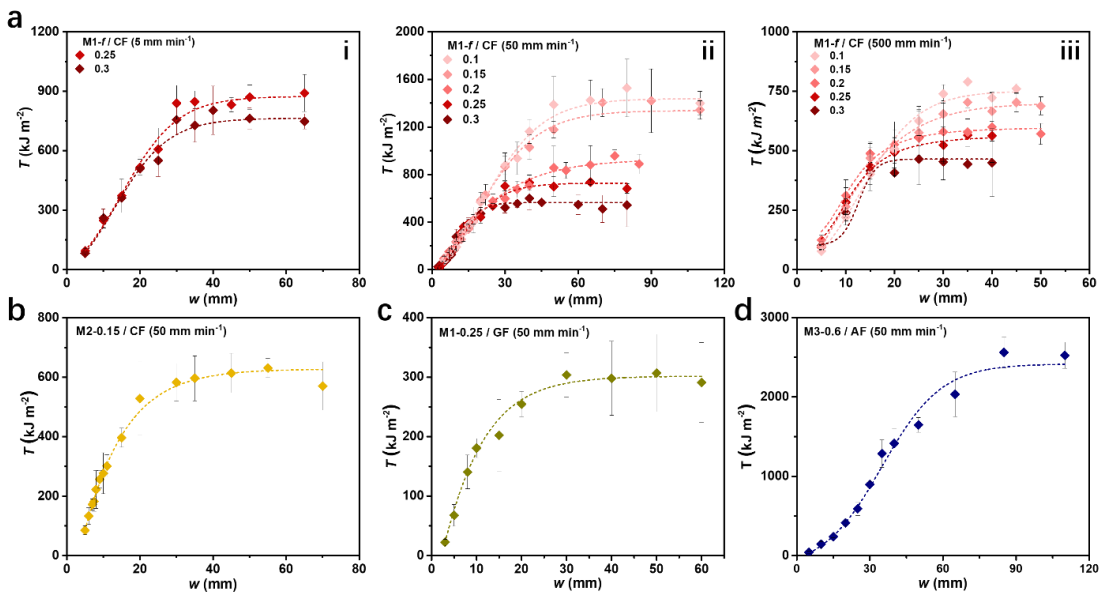

Figure 4.8. Sample size dependence of toughness as measured by tearing energy, T, for all composites fabricated in this work. (a) Tearing energy, T, as a function of sample width, w, for soft FRPs from M1-*f* and CF at testing velocities of 5 mm min^{-1} (i), 50 mm min-1 (ii), and 500 mm min^{-1} (iii), respectively. Since the elastomer matrices are viscoelastic, their mechanical behaviors are strain rate dependent. The inherent viscoelasticity of the matrices permits us to change mechanical behavior by changing the deformation rate. As expected, soft FRPs made from M1-*f* and CF show different w_2 and saturation T at different tearing velocities. (b) (c) (d) T as a function of w for soft FRPs from other combinations of matrix and fabrics. Two other series of viscoelastomers, P(BZA-co-IBA) and P(DEEA-co-IBA), denoted by M2-*f* and M3-*f*, respectively, are used in addition to M1-*f*. Also, glass fiber fabric (GF) and aramid fiber fabric (AF) are used in addition to CF. All fabrics have the same plain weave pattern to avoid difference in geometry. The results indicate that all composites show sample-size-dependent toughness. The saturation tearing energy is adopted as fracture energy Γ.

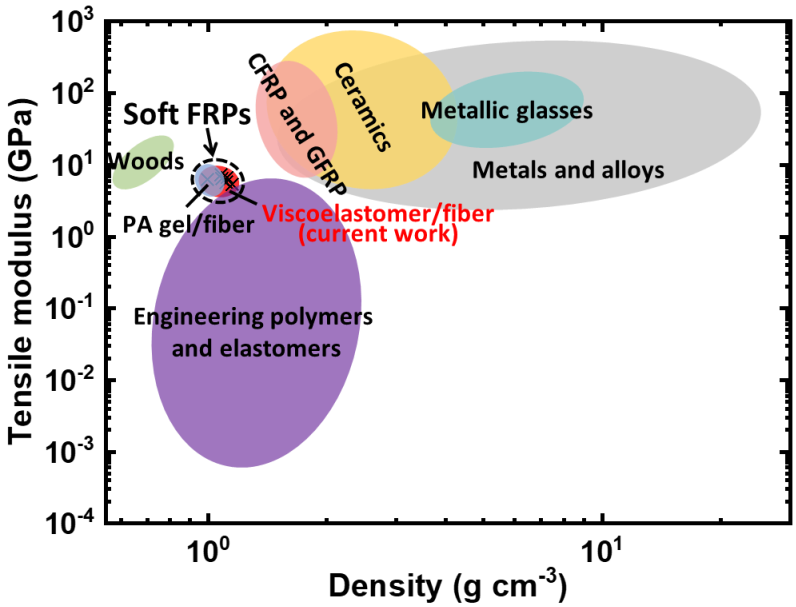

Figure 4.9. Tensile modulus (E) versus density (ρ) of various materials.

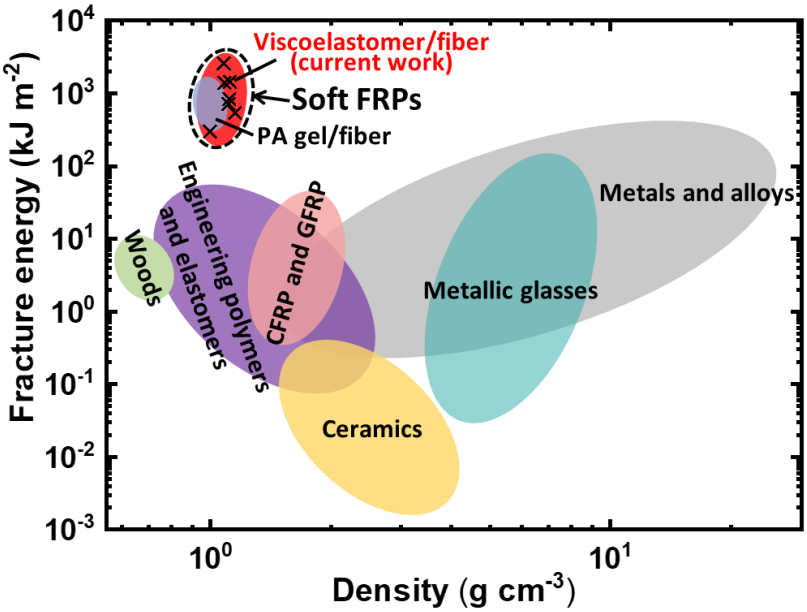

Figure 4.10. Fracture energy (Γ) versus density of various materials. Fracture energies of various materials were determined by trouser tearing tests (for soft FRPs), essential work of fracture (EWF) tests (for engineering polymers and elastomers), double cantilever beam or crack opening three point bend tests (for CFRP and GFRP, metallic glasses, metals and alloys, ceramics, and woods), respectively.

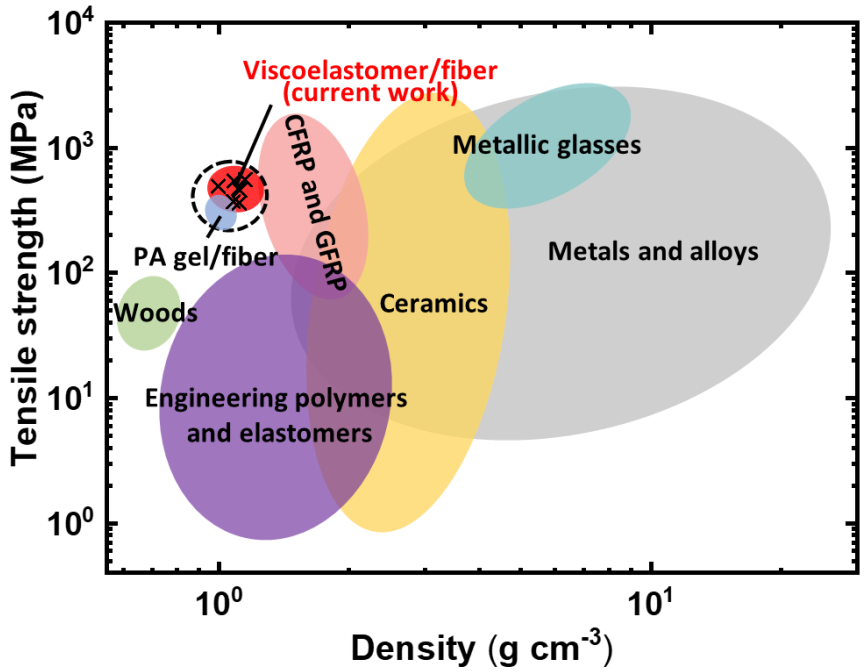

Figure 4.11. Tensile strength (σ) versus density of various materials.

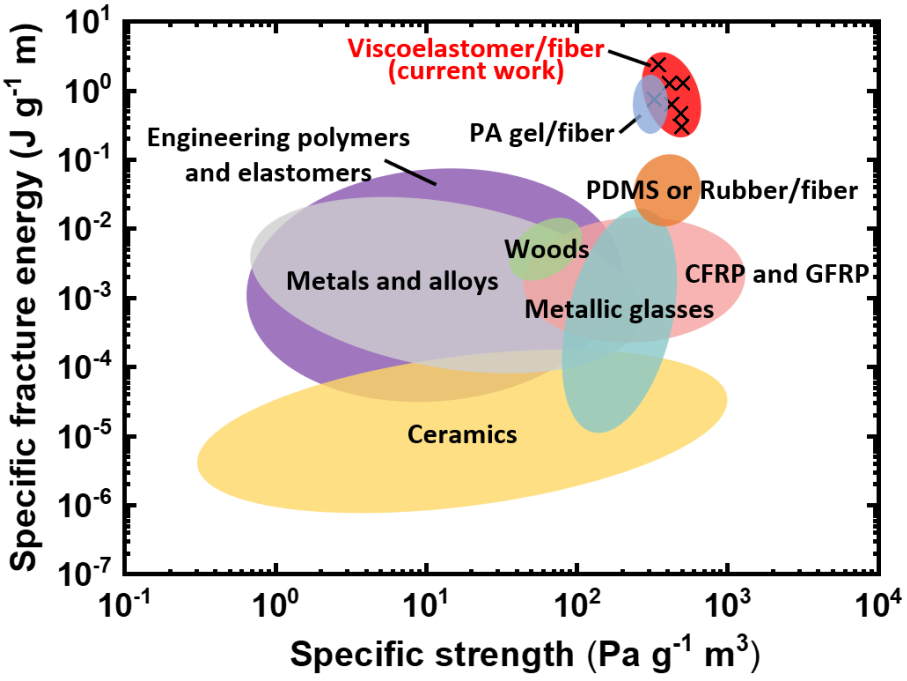

Figure 4.12. Specific fracture energy (Γ/ρ) versus specific strength (σ/ρ) of various materials.

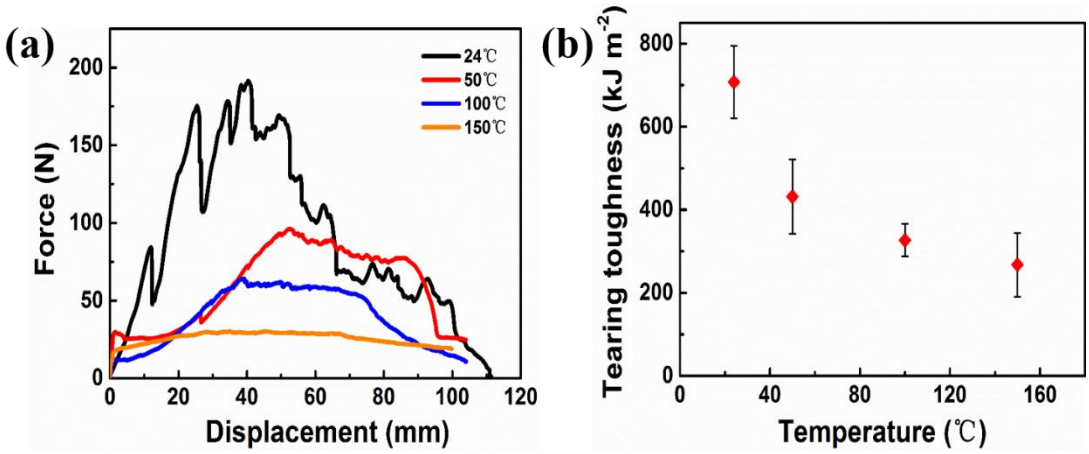

Figure 4.13. (a) Force-displacement curves of M1-0.2/CF composites (width = L_{bulk} = 40 mm) at different temperatures. (b) Corresponding tearing energy of composites.

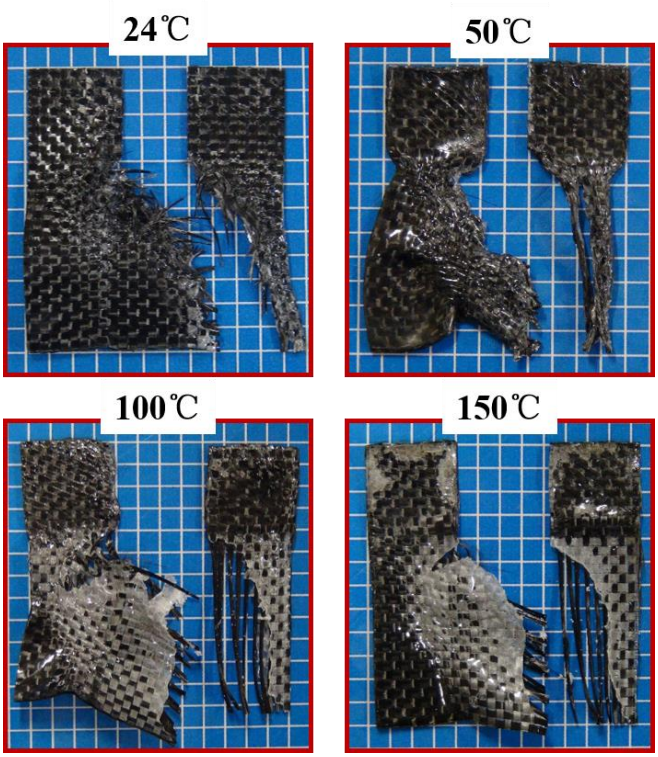

Figure 4.14. Photographs of M1-0.2/CF after tearing at different temperatures.

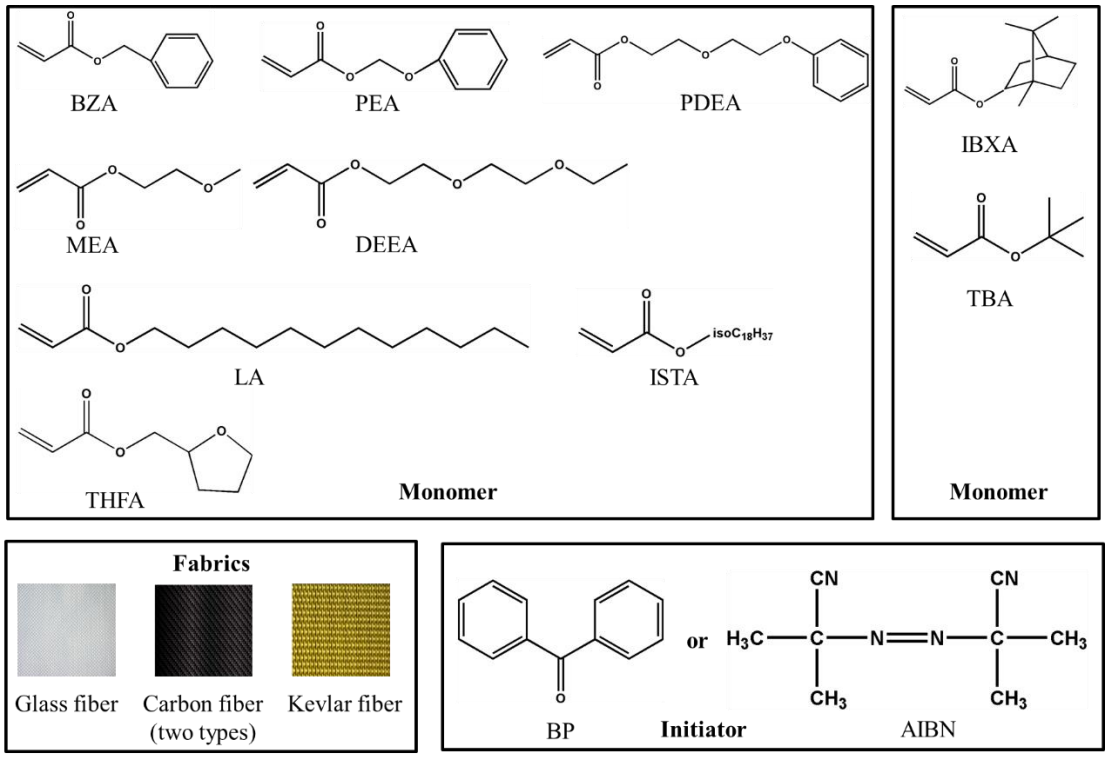

Figure 4.15. The selection of monomers, initiator and fabrics for fabricating various fiber-reinforced polymers.

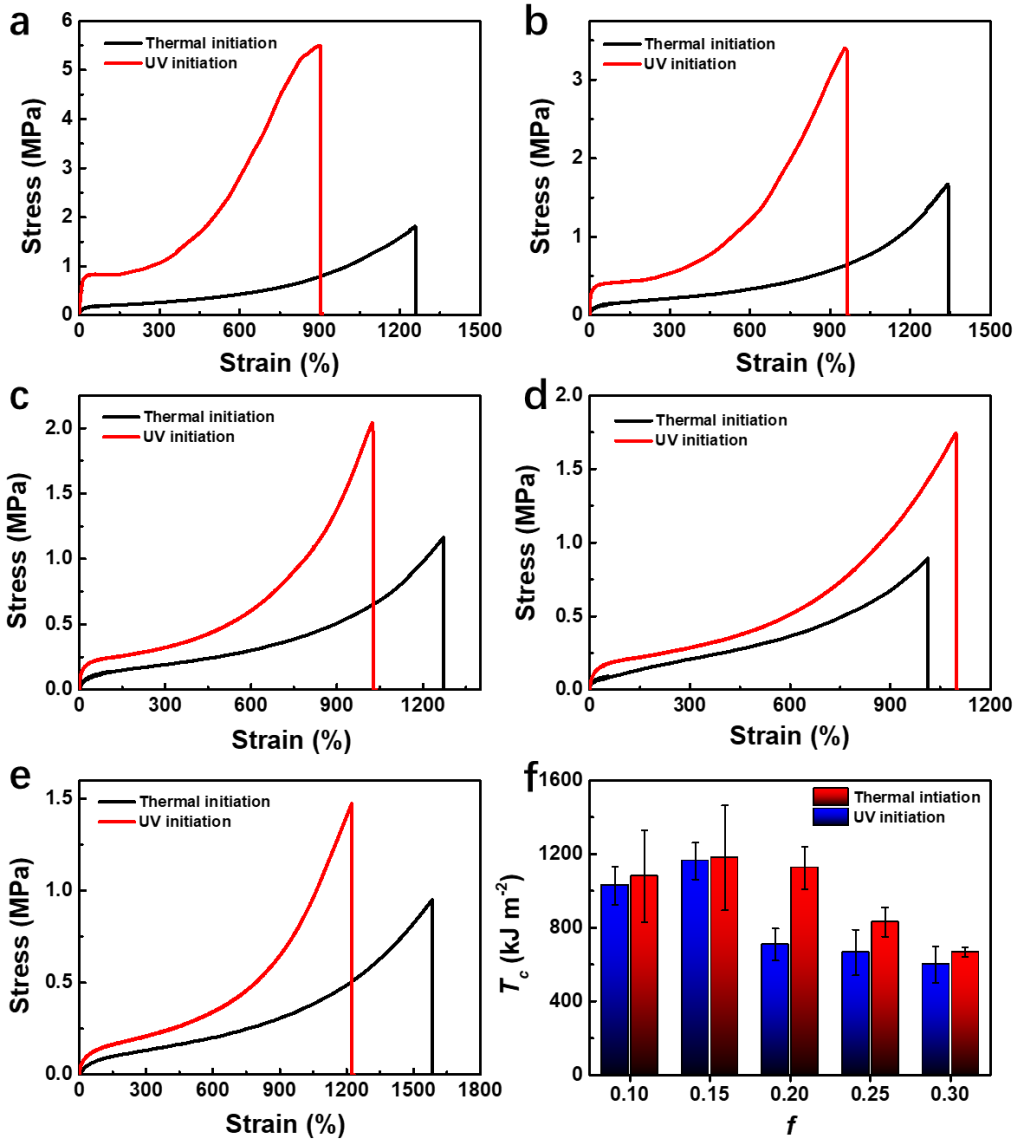

Figure 4.16. Force-displacement curves of PEA-co-IBXA composites (width = L_{bulk} = 40 mm) (a) f = 0.3, (b) f = 0.25, (c) f = 0.2, (d) f = 0.15, (e) f = 0.1 polymerized from thermal or UV initiation and corresponding tearing energies of them (f).

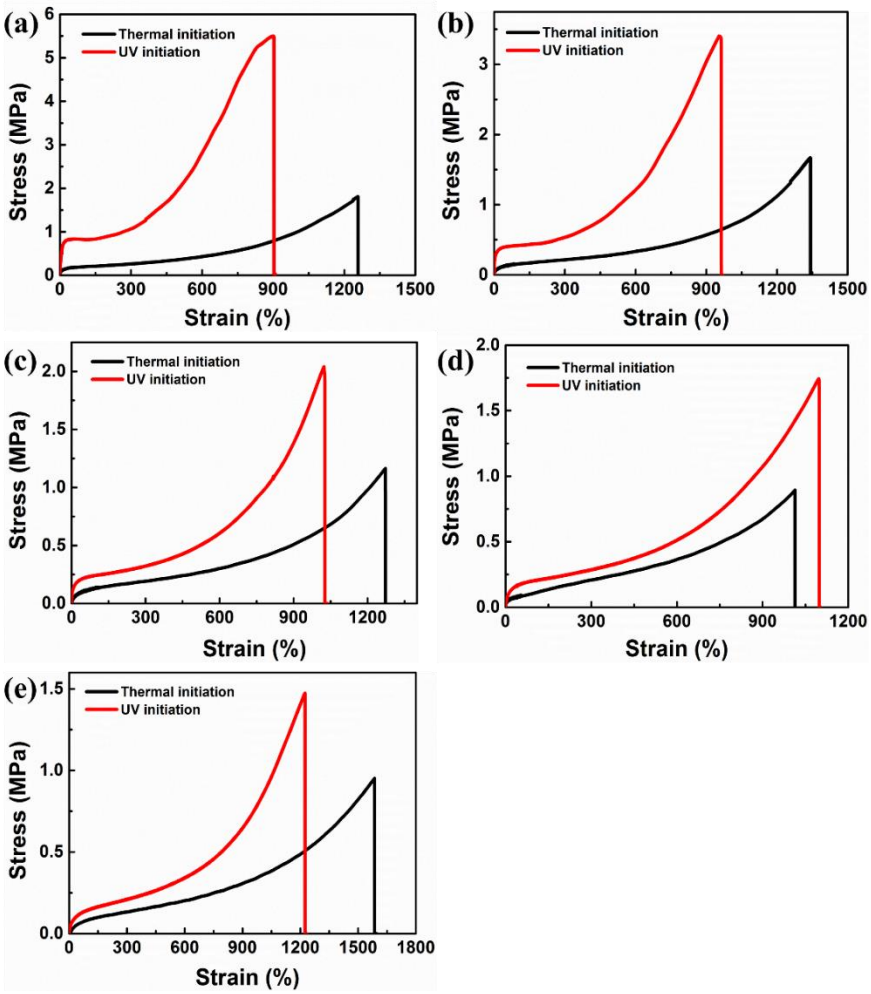

Figure 4.17. Stress-strain curves of PEA-co-IBXA elastomers (width = 2 mm, thickness = 1 mm, gauge length = 12mm) (a) $f = 0.3$, (b) $f = 0.25$, (c) $f = 0.2$, (d) $f = 0.15$, (e) $f = 0.1$ polymerized from thermal or UV initiation.

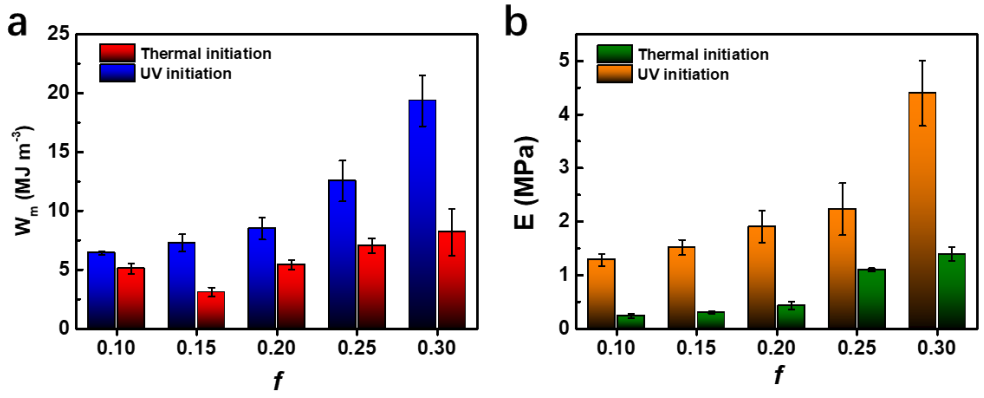

Figure 4.18. Strain energy density (a) and modulus (b) of matrices from thermal- and UV-initiated polymerization.

Tables

Table 4.1. Summary of mechanical properties of varied composites at different testing velocities. The properties include tensile fracture stress (σ_c), fracture strain (ε_c), Young's modulus (E_c), tensile work of extension to fracture the composites (W_c), the volume weighed average of the work of extension of the fiber bundle and the matrix at fracture (W_{eff}), and tearing energy (T_c). Each sample was tested $N \geqslant 3$ times to obtain the average value. Sample width and gauge length are 10 mm and 20 mm, respectively.

Sample code	Testing velocity (mm min^{-1})	f	σ_c (MPa)	ε_c (%)	E_c (MPa)	W_c (MJ m^{-3})	W_{eff} (MJ m^{-3})	T_c (kJ m^{-2})
M1-f/CF	5	0.25	667 ± 58	11.06 ± 0.93	6.67 ± 0.71	40.49 ± 2.97	23.36 ± 2.26	856 ± 24
		0.3	618 ± 45	10.45 ±1.28	6.52 ± 0.35	34.75 ± 3.61	24.77 ± 2.42	760 ± 28
	50	0.1	730 ± 65	12.36 ± 0.88	6.43 ± 0.50	44.18 ± 3.15	22.70 ± 2.20	1390 ± 41
		0.15	652 ± 59	11.86 ± 0.43	6.23 ± 1.11	42.23 ±1.92	23.12 ± 2.49	1435 ± 64
		0.2	645 ± 31	11.81 ± 1.33	6.72 ± 0.47	37.74 ± 3.62	23.73 ± 2.59	883 ± 46
		0.25	678 ± 56	11.26 ± 1.62	6.57 ± 0.41	39.83 ± 3.73	26.76 ± 4.03	712 ± 26
		0.3	691 ± 67	10.52 ± 0.9	6.51 ± 0.62	35.28 ± 2.01	29.15 ± 3.20	548 ± 29
	500	0.1	687 ± 55	12.15 ± 0.58	6.66 ± 0.26	46.37 ± 4.15	26.09 ± 3.02	750 ± 34
		0.15	665 ± 60	12.26 ± 0.73	6.36 ± 0.30	45.48 ± 2.88	26.74 ± 2.76	682 ± 25
		0.2	654 ± 49	11.91 ± 1.21	6.92 ± 0.69	40.63 ± 3.29	26.84 ± 2.35	576 ± 15
		0.25	662 ± 31	11.66 ± 1.53	6.44 ± 1.37	40.82 ± 3.82	30.89 ± 2.73	552 ± 20
		0.3	692 ± 41	11.71 ± 1.46	6.57 ± 0.87	43.66 ± 3.24	34.31 ± 2.62	453 ± 9
M2-f/CF	50	0.15	688 ± 65	12.04 ± 0.77	6.85 ± 0.39	38.37 ± 3.96	30.04 ± 2.38	597 ± 24
M1-f/GF	50	0.25	515 ± 33	6.12 ± 0.51	7.24 ± 1.22	19.76 ± 3.10	15.46 ± 2.58	300 ± 7
M3-f/AF	50	0.6	771 ± 56	11.27 ± 1.83	7.88 ± 1.70	37.50 ± 2.03	32.02 ± 0.92	2543 ± 26

Table 4.2. Summary of mechanical properties of various materials. The mechanical properties are tensile modulus (E), tensile strength (σ), fracture energy (Γ), density (ρ), specific strength (σ/ρ), specific fracture energy (Γ/ρ).

Material		E (GPa)	σ (MPa)	Γ (kJ m^{-2})	ρ (g cm^{-3})	σ/ρ (Pa g^{-1} m^{3})	Γ/ρ (J g^{-1} m)
Soft FRPs	Viscoelastomer/fiber	5.2-7.9	480-770	300-2500	0.9-1.2	310-670	0.3-2.4
	PA gel/fiber	5.0-7.6	240-340	400-1000	≈1.0	240-340	0.4-1.0
Hard FRPs	CFRP and GFRP	12.9-162	98-1275	0.36-20	1.4-2.0	50-860	4.3×10^{-4}-1.1×10^{-2}
	Metals and alloys	16.6-346	18-1525	0.6-190	1.6-22	0.9-200	9.4×10^{-5}-8.6×10^{-3}
	Metallic glasses	30.3-137	660-1800	0.003-340	3.9-8.3	100-294	1.8×10^{-5}-1.2×10^{-2}
	Ceramics	7.0-545	5-1970	0.02-0.05	1.7-4.0	0.5-620	1.0×10^{-6}-1.3×10^{-4}
Engineering polymers and elastomers		0.3-4.1	0.2-104	0.3-29.7	0.9-1.4	0.7-80	5.3×10^{-5}-2.4×10^{-2}
	Woods	6.8-17.1	31-60	2.4-5.9	0.6-0.8	45-85	3.2×10^{-3}-9.2×10^{-3}

Table 4.3. Tearing toughness of neat elastomers, neat fabrics, and resultant composites from various combinations.

Fabric \ Matrix	None	PDEA	PDEA-co-IBXA (*f*=0.5)	MEA	MEA-co-IBXA (*f*=0.4)	PEA	PEA-co-IBXA (*f*=0.25)	BZA	BZA-co-IBXA (*f*=0.15)
None		~4.4	~7.5	~5.5	~8.4	~9.6	~25.3	~15.1	~38.6
CF(thick)	~3	~420	~719	~323	~1182	~822	~731	~1109	~839
CF(thin)	~23	~826	~1307	~1143	~1504	~1554	~679	~1778	~660
GF	~9	~239	~326	~367	~739	~797	~202	~832	~491
KF	~17	~289	~1229	~299	~1337	~1089	~1291	~1054	~1374

Fabric \ Matrix	None	PDEA-co-TBA (*f*=0.5)	DEEA	DEEA-co-IBXA (*f*=0.6)	LA	LA-co-IBXA (*f*=0.4)	ISTA	ISTA-co-IBXA (*f*=0.4)	THFA	THFA-co-IBXA (*f*=0.3)
None		2.4	1.2	7.4	1.4	2.2	4.9	25.4	4.3	36.7
CF(thick)	3	652	145	808	153	280	846	739	884	538
CF(thin)	23	1607	366	1453	433	698	1088	1073	1661	983
GF	9	506	93	415	69	208	575	347	689	157
KF	17	468	74	1403	156	220	637	1341	579	1690

Chapter 5-Fracture Mechanism of Tough Fiber Reinforced Polymers

5.1. Introduction

Fracture is a common phenomenon in materials, while different materials demonstrate varied crack resistance or fracture process.[60, 94-96] Homogeneous materials are usually crack sensitive, which show significantly decrease in crack resistance when the size of crack grows above a material-specific length, defined by the ratio of the fracture energy measured in the large-cut limit and the work to rupture measured in the small-cut limit.[94] This length scale is usually called the size of energy dissipation zone. Composites are designed to be crack insensitive. One of the key points of their extraordinary crack resistance is that they commonly have a large size of energy dissipation zone, which enables the force to be transferred in a broad area among components, requiring far more energy to grow the crack compared to homogeneous materials.[79, 97-101] On the other hand, the energy dissipation in the area is also important for the crack resistance, which is usually decided by the intrinsic energy dissipation density of materials.[102-104] Generally, the crack resistance is characterized by fracture energy, which is influenced by two factors: 1) the length over which a material is deformed inelastically ahead of the advancing crack, known as the energy dissipation zone size, l_T, and 2) the energy dissipation

density of the dissipation zone when the crack advances, *W*. Theoretically, for composites consisting of a hard phase embedded into a soft matrix, the energy density generates from the contribution of both components, while the size of the energy dissipation zone is related to the force transfer length that is determined by the modulus ratio of hard to soft phase as well as the geometric parameters.[70, 74] Therefore, the fabrication of a crack-resistant composite can be theoretically achieved by combining a rigid and energy dissipative skeleton and a soft and energy dissipative matrix.

To fabricate a tough composite, another important factor should be taken into account. For traditional composites composed of rigid/rigid components, interface is critical for the energy dissipation.[105-107] Delamination occurs frequently when the components have poor interfacial interaction, and consequently the composites fail before reaching the theoretical size of energy dissipation zone, sharply limiting the energy dissipation and resulting crack resistance.[108-110] Surface treatment then becomes necessary for the production of rigid composites, which, is time- and cost-ineffective.

To overcome the challenges of conventional rigid composites, recently, fiber-reinforced soft composites are developed from polyampholyte hydrogels and glass fiber fabrics.[27-29] The soft, de-swelling, and viscoelastic PA gel, with multiple ionic bonds in the network, demonstrates a self-adjustable adhesion to either positively or negatively charged

surfaces,[30, 31] which forms good adhesion with negatively charged glass fibers. On the other hand, the fiber/matrix modulus ratio in this composite system achieves ~10^3 to 10^4, which greatly facilitates the force transfer between components. As a result, the PA/GF composites, with energy-dissipative components (strain energy density above 4 MJ m^{-3}) and a considerable force transfer length (critical width above 45 mm), exhibit high intrinsic toughness (~1000 kJ m^{-2}), strength (~300 MPa), and tensile modulus (~600 MPa), which fill the gap between soft materials and traditional rigid materials.

Similarly, we employ viscoelastic elastomers that are adhesive, soft, and tough to construct tough fiber-reinforced polymers (FRPs), which also demonstrate an efficient combination of multiple mechanical properties. In this chapter, we investigate the fracture mechanism of tough FRPs. By systematically tuning the chemistry and the composition of the viscoelastomer in the FRPs, we experimentally demonstrated that 1) the energy dissipation density W is related to the volume weighed average of work of extension at fracture of the viscoelastomer and the fiber bundles, W_{eff}, and 2) the size of the energy dissipation zone, l_T, is proportional to the square root of the fiber/matrix modulus ratio, $l_T \sim (\frac{E_f}{\mu_m})^{\frac{1}{2}}$, where E_f and μ_m are the Young's modulus of the fiber and shear modulus of the matrix, respectively. As W_{eff} is the maximum energy density that could be dissipated, this result indicates that our soft FRPs take full advantage of the

energy dissipation density in the dissipation zone, owing to the strong interface and high toughness of the matrices.

Our findings show that a combination of high strength fibers and soft, tough viscoelastomers maximizes the toughness (Γ). By using specifically formulated viscoelastomers and aramid fiber fabrics, soft FRPs with extraordinarily high Γ of 2500 kJ m^{-2} are developed for the first time. The toughness is far superior to any best-in-class tough materials, including metals and alloys. The soft FRPs also show high strength (700 MPa) as well as low density ($\approx$ 1 g cm^{-3}), comparable to traditional FRPs. This work provides a clear strategy for developing robust and lightweight soft FRPs for critical, load-bearing structural applications.

5.2. Results and Discussion

5.2.1. The importance of strong interface

The viscoelastic elastomers are highly adhesive, which forms a strong interface with rigid fabrics. The firm bonding between the matrix and fibers enables the full energy dissipation of components. However, not all elastomers can satisfy the requirements of strong bonding. To verify the importance of interface for tough FRPs, we prepare two sets of carbon-fiber reinforced polymers from M1-0.1 and polydimethylsiloxane (PDMS), respectively. Tearing behaviors of both FRPs are shown in **Figure 5.1**. FRP from PDMS exhibits apparent delamination of matrix from the fabric,

indicating a poor interfacial bonding between components. SEM observations further verify the debonding phenomenon. **Figure 5.2** shows that M1-0.1 matrix is significantly deformed yet strongly bonded to fibers after tearing, whereas no residual PDMS matrix is observed on fiber surfaces. Trouser tearing tests also reveal that M1-0.1/CF composite is much tougher than PDMS/CF composite with the same geometry (**Figure 5.3**). Interestingly, the energy dissipation density (W_m) of PDMS is ~8.39 MJ m^{-3}, which is comparable to that of M1-0.1. On the other hand, the modulus of PDMS is ~1.18 MPa, which is lower than that of M1-0.1. Therefore, according to the theory we proposed to quantify composite toughness, PDMS/CF composite should have a higher energy dissipation density as well as a larger force transfer length. This abnormal result indicates the importance of a strong interface to construct tough FRPs. Although M1-0.1/CF is highly deformed and fractured into two pieces, either part from it remains an intact composite without separation of matrix from fabric. However, detachment of matrix from fabric occurs for PMDS/CF during tearing test due to the difficult penetration of PDMS into fabric during preparation. This gives a reasonable explanation for the low toughness of PDMS/CF system. Namely, a large proportion of matrix detached from fabric during tearing, which contributes little to the composite toughness. This is essentially different from the energy dissipation mechanism of the concept “soft composite” we propose.

Following this point of view, the PDMS/CF system is, strictly speaking, not a soft composite but a soft compound. This result enhances our view that a strong interface plays a great role in toughening the composite.

5.2.2. Fracture behaviors of varied FRPs at the same width

First, we investigate the fracture behavior of FRPs from the same fabric but varied matrices at the fixed width. P(PDEA-co-IBA) with different *f* is used as the matrix. The matrix is defined as M4-*f* for simplicity. Mechanical properties of neat elastomers are shown in **Figure 5.4**. Obviously, higher concentration of hard segment (IBXA) gives rise to harder and tougher elastomer. Detailed parameters are summarized in **Table 5.1**. According to the difference in tensile modulus, we define the elastomer with the lowest modulus as soft elastomer, the one with the highest modulus as hard elastomer. FRPs are fabricated from these matrices with the same fabric. The tearing toughness is shown in **Figure 5.5**. With decreased *f*, the elastomer toughness decreases monotonously. The composite toughness, however, reaches a peak and then falls off, indicating that energy dissipation of matrix is not the only factor that determines the composite toughness. Direct evidence is obtained from tearing behaviors. As clearly demonstrated in **Figure 5.6**, energy dissipation zones differ significantly among composites. Softer matrix gives larger deformed zone of the resultant composite, indicating both matrix property and energy dissipation

zone play roles in affecting the composite toughness. Further understanding about the roles of matrix property and energy dissipation zone is realized by comparing how both factors work differently in the soft-matrix composite as well as the hard-matrix composite. As indicated in **Figure 5.7**, mechanical properties such as modulus and tearing energy, improve obviously for both composites as the testing velocity increases. Tearing energy of the soft-matrix composite also follows the same trend with that of elastomer (**Figure 5.8**a1 and b1). When it comes to the hard-matrix composite, it is surprising that tearing energy of the composite falls off as that of the elastomer increases (**Figure 5.8**a2 and b2). Explanations can be figured out from the different tearing behaviors between two kinds of composites. As illustrated in **Figure 5.9**, increasing the tearing velocity does not reduce energy dissipation zone of the soft-matrix composite since it has a quite large process zone. In this case, although the size of process zone is decreasing due to higher modulus of the matrix at high velocity, it is still larger than the sample geometry, enabling the composite to dissipate energy thoroughly during test. That is, matrix property is the key factor that influences the composite toughness in this situation. On the contrary, the energy dissipation zone of the hardest-matrix composite shrinks dramatically with increased modulus at high velocity, giving rise to a very limited energy dissipation zone during test (**Figure 5.10**). Even matrix can dissipate much more energy at higher testing velocity, the composite

toughness is highly restricted by the energy dissipation zone where allows matrix to contribute.

5.2.3. Size-dependent fracture behaviors of FRPs

The tradeoff between matrix property and energy dissipation zone triggers us to investigate the size-dependent fracture behaviors of FRPs, by which we can figure out the intrinsic influence of energy dissipation zone and matrix property. Here, M1-0.1/CF tested at 50 mm min^{-1} is taken as an example (**Figure 5.11a**). The plot of T versus w is divided into three regions by different fracture behaviors of the soft FRP. In region I ($0<w<w_1$), fracture occurs due to fiber pull-out and matrix failure, and T increases with increasing width, w (**Figure 5.11b**). In region II ($w_1 \leq w<w_2$), fracture occurs due to both fiber pull-out and fiber fracture, and T also increases with increasing w (**Figure 5.11c**). The width where the fiber starts to fracture is defined as the onset width of fiber fracture, w_1. In region III ($w \geq w_2$), fiber failure is the primary fracture mechanism, and T reaches the saturate toughness, Γ (**Figure 5.11d**). The width where the tearing energy starts to saturate is defined as the transition width, w_2, which reflects the process zone size of soft FRPs. The transition width, w_2, is attained by the crossover point of the two linear fitting lines for region I and II, and for region III, respectively. The conceptual illustration of size-dependent fracture behaviors is demonstrated in **Figure 5.12**.

5.2.4. An empirical method to determine characteristic width w_1 of FRPs

As discussed above, FRPs in this work possess two characteristic widths, w_1 and w_2. These two widths are crucial to divide the crack behaviors of FRPs into different regions. w_2 can be attained by the crossover point of the two linear fitting lines for region I and II, and for region III, respectively. Here, we introduce an experimental method to determine w_1 for FRPs. Huang et al. has verified the failure mode transition condition of a composite system, which indicates that as long as an intact fiber bundle fractures, energy dissipation zone can be deemed partially saturated in a composite.[28, 29] This understanding opens the possibility of acquiring the exact w_1 for a given composite by comparing its tearing behaviors at different widths. Taking the composite M1-0.25/CF as an example here (**Figure 5.13**), it is easy to figure out that under width of 14 mm, tearing behavior of the composite is entirely expressed as fiber pullout. As the width increases to 14 mm, fiber fracture appears, indicating that some parts of the process zone are saturated in the composite. Therefore, 14 mm is regarded as the critical width of this composite. Using the same method, we can also obtain the critical width of composites with other molar ratios (9 mm for M1-0.3/CF, 18 mm for M1-0.2/CF, 23 mm for M1-0.15/CF, 24 mm for M1-0.1/CF).

5.2.5. Model equation for determining the toughness of FRPs

To have a thorough understanding of the composite system and generalize the rule to fabricate composites from varied matrices and fabrics, mathematic factors that determine the composite toughness should be revealed. Looking into the tearing test, the total work to destroy the composite can be acquired from the area under the force-displacement curve, which equals the product of the energy density of composite and the volume of process zone. Namely,

$$Work = \int_0^L FdL = W \cdot V \quad (5.1),$$

where F is the tearing force, L is the displacement during test, W is the energy density, V is the volume of energy dissipation zone. While V is related to the geometry of composite:

$$V \sim l_T \cdot t \cdot L_{bulk} \quad (5.2),$$

Where l_T is the force transfer length, t is thickness of the composite, L_{bulk} is the length of the tearing path, hence we can establish the relationship between *Work* and sample parameters. On the other hand, composite toughness can be calculated from W and sample geometry:

$$T = \frac{Work}{t \cdot L_{bulk}} \quad (5.3),$$

where T is the composite toughness. Therefore, combining equation (5.1), (5.2) and (5.3), one can figure out the relationship between T and $W \cdot l_T$:

$$T \cong W \cdot l_T \quad (5.4).$$

It should be noted that the above situation assumes that the energy

dissipation zone is saturated. For composites with unsaturated energy dissipation zone, since the size of the process zone is restricted by the width, the equation (5.4) is modified as

$$T \cong W \cdot width \quad (5.5).$$

5.2.6. Fracture mechanism of FRPs in region I

In the case of samples with a width smaller than w_1, the failure mode is dominated by fiber pullout and matrix failure, as suggested in **Figure 5.11b**. According to the model equation (5.5), the tearing toughness of FRPs should be related to the energy dissipation density as well as sample size. Hence, what determines the energy dissipation density becomes extremely important for the tearing toughness. Theoretically, for composites consisting of parallel fibers embedded in a soft matrix, the energy dissipation density by fiber pullout is given as:[70]

$$W_{pullout} = 2\rho_f T_m wr \quad (5.6),$$

where ρ_f is the number of fibers per unit volume, T_m is the fracture toughness of the soft matrix, w is the sample width, r is the fiber radius. This equation takes account of matrix fracture surrounding individual fibers and well explains that the mechanical performance of fibers does not contribute to the energy dissipation since they are pulled out instead of fractured, whereas the geometric parameters of fibers influence the frequency of matrix fracture. Substituting equation (5.6) into (5.5), the

tearing toughness of FRPs in the given mechanism of fiber pullout is found to be:

$$T = 2\rho_f r T_m w^2 \quad (5.7).$$

Using α to represent the geometric parameters of fibers, equation (5.7) can be simplified as:

$$T = \alpha T_m w^2 \quad (5.8).$$

Therefore, three variables are influencing the tearing toughness of FRPs. Namely, geometric parameters of fiber, fracture toughness of matrix, and bulk sample size. By fixing the fabric or matrix, respectively, we can quantitively verify the role of fibers and matrix in affecting the tearing toughness of FRPs.

At first, we use the same matrix M1-0.2 to fabricate FRPs to verify the role of fiber parameters on tearing toughness. Two kinds of carbon fiber fabrics (thin and thick) are employed, they are defined as t-CF and CF, respectively. Images of both fabrics used here are shown in **Figure 5.14**. Geometric and mechanical parameters are summarized in **Table 5.2**. FRPs are tested at varied widths to obtain the size-dependent tearing energy. As exhibited in **Figure 5.15**, tearing energies of FRPs from CF and t-CF are both proportional to w^2, while the slopes are different. Since both FRPs are from the same matrix with constant T_m, according to equation (5.8), it is α that leads to the variance of slopes. The geometric parameter α of both fabrics is shown in the inset of **Figure 5.15**. The t-CF possesses a larger α

than that of CF, which is consistent with the difference of slopes.

Next, we change the matrix while keeping fabric the same. We employ M1-0.1 and M1-0.2 as matrices to fabricate FRPs. Since the matrix is highly viscoelastic, we also change the testing velocity to tune their mechanical properties and investigate the influence on tearing energy of FRPs. Results in **Figure 5.16** also indicate that tearing energies of all FRPs are proportional to w^2, while the variance in T_m leads to their different slopes because α is constant. The inset further verifies that the slope increases as the tearing energy of matrix goes up.

A systematic result is shown in **Figure 5.17**, where both fiber geometry α and tearing energy of matrix T_m are changing simultaneously. Tearing energy of FRPs, T_c, is found to be equal to $W_{pullout} \cdot w$, suggesting both fibers and matrix contribute to the energy dissipation even though fibers do not fail. The geometry of fibers determines the amount and frequency of matrix failure during fiber pullout, this is also verified in **Figure 5.18**, which shows that the tearing energy of FRPs, T_c, is systematically higher than $T_m \cdot w$, indicating matrix is not the only factor that facilitates the energy dissipation during composite failure.

5.2.6. Fracture mechanism of FRPs in region III

Fracture of FRPs in region II is rather complicated since it involves both fiber pullout and fracture. On the other hand, this middle region is not as

important as region I and III to understand the intrinsic fracture mechanism of FRPs. Therefore, the fracture mechanism of region II is not discussed in this thesis. Instead, the fracture mechanism of region III is discussed here since it reflects the intrinsic tearing properties of FRPs. As indicated in equation (5.4), when the sample size reaches or is beyond the intrinsic energy dissipation zone, the tearing energy becomes constant, which gives the intrinsic, size-independent tearing energy, Γ of the composites.

To understand what determines the energy dissipation density and force transfer length in equation (5.4) and reveal the correlation between the mechanical properties of the viscoelastic matrices and the crack resistance of the soft FRPs, we further compare the behavior of soft FRPs by varying the mechanical properties of the matrix, P(PEA-*co*-IBA), by tuning *f*. The M1-0.3 viscoelastomer demonstrates relatively high modulus, fracture stress, work of extension, and tearing toughness when compared to M1-0.1 (**Figure 3.3** in chapter 3). The fiber/matrix modulus ratio (E_f/μ_m) of the f=0.3 composite is approximately 1.5×10^4, while the f=0.1 composite approaches 8.0×10^4. The force-displacement curves of the tearing tests are compared in **Figure 5.19**. Both composites are sufficiently large (w =70 mm) to ensure that there is no size-dependent effect and the failure behavior is primarily fiber fracture. Interestingly, the f=0.1 composite with high E_f/μ_m is much more crack-resistant than the f=0.3 composite with low E_f/μ_m even though the former has a softer, weaker and less tough matrix.

The f=0.1 composite exhibits a much higher tearing force, which brings about a tearing toughness of 1400 kJ m^{-2}, outperforming the f=0.3 composite (550 kJ m^{-2}) by 150%.

Inset images in **Figure 5.19** show the composites after tearing. In clear contrast with the limited distortion of the f=0.3 composite ($E_f/\mu_m = 1.5\times10^4$), the f=0.1 composite ($E_f/\mu_m = 8.0\times10^4$) undergoes significant deformation after tearing (highlighted by dashed white regions), indicating a large energy dissipation zone on the centimeter scale. This result demonstrates that high E_f/μ_m significantly facilitates force transfer over a large distance, allowing extensive energy dissipation throughout this region.

The large, macroscale energy dissipation zone suggested by **Figure 5.19** allows us to investigate the sample size dependence on the tearing behavior, from which we can accurately determine the force transfer length. When the sample width (w) is decreased to a value less than the force transfer length, the tearing resistance starts to decrease with w and the failure behavior of the composites also changes.[27-29] **Figure 5.20** shows the influence of sample size on tearing energy, T, for the f=0.1 and f=0.3 composites. They are tested from w = 5 mm to increasingly large w until T saturates. Similar to PA hydrogel/glass fabric composites,[29] two characteristic sample widths, w_1 and w_2, are observed. Fiber fracture starts to occur at w_1 and becomes the main fracture mode at w_2. The tearing energy increases with the sample width w, and saturates at w_2,

$$T = k \cdot w, \ w < w_2 \quad (5.9a),$$

$$T = k \cdot w_2, \ w \geq w_2 \quad (5.9b).$$

The proportional constant k has a unit of energy dissipation density (J m^{-3}). Equation (2) states that the tearing energy T is balanced by the release of stored strain energy in the crack tip zone of length w for samples with width $w < w_2$ or w_2 for samples with width $w \geq w_2$. The saturation T at $w \geq w_2$ gives the intrinsic, size-independent tearing energy, Γ of the composites. Therefore, the parameters k and w_2 can be associated with the energy dissipation density, W, and the energy dissipation zone size, l_T, as $W = k$ and $l_T = w_2$, respectively, for the relationship shown in equation (5.4).

The f=0.1 composite achieves $\Gamma \approx$ 1400 kJ m^{-2} at w_2 = 60 mm. In comparison, the f=0.3 composite attains $\Gamma \approx$ 550 kJ m^{-2} at w_2 = 21 mm. The f=0.1 composite needs a larger w_2 to reach Γ, which indicates a larger force transfer length, in comparison with the f=0.3 composite. These results are consistent with the observation of the dissipation area of samples that undergo tearing (**Figure 5.19**).

To quantitatively understand the parameters k (or W) and w_2 (or l_T), we further investigated the correlation between these two quantities and the mechanical properties of the soft FRPs from different combinations of viscoelastomer matrices and fibers in chapter 3. For simplicity, samples are denoted as Mi-f/xF for composites made from matrix Mi-f (i=1,2,3) and fiber fabrics xF (xF =CF, GF, and AF), where CF, GF, and AF stand for

carbon fiber, glass fiber, and aramid fiber fabric, respectively. As indicated in **Figure 4.8** in chapter 4, the tearing energies of all composites measured at different tearing velocities show similar sample width dependence as those in **Figure 5.20**. Summarized w_2 and fiber/matrix property ratios for all composites at different tearing velocities are shown in **Table 5.3**.

As shown in **Figure 5.21**, the log-log plot of w_2 versus E_f/μ_m for different combinations of fibers and soft matrices at varied tearing velocities shows a linear correlation with a slope of 0.5 for $E_f/\mu_m > 10^4$, following a scaling equation,

$$w_2(mm) = 0.19\,(\frac{E_f}{\mu_m})^{\frac{1}{2}} \qquad (5.10).$$

Positive correlations between w_2 and fracture stress ratio, fracture strain ratio, and fracture energy ratio of fiber to matrix (**Figure 5.22**) also exist, but the strongest correlation is observed with modulus ratio. These results suggest that the modulus ratio is the most relevant quantity to determine the load transfer length.

For unidirectional fiber reinforced composites with parallel fibers perfectly bonded to a soft elastic matrix, Hui et al have found theoretically that the force transfer length is proportional to the square root of the fiber/matrix modulus ratio.[70] The scaling relation $w_2 \sim (\frac{E_f}{\mu_m})^{\frac{1}{2}}$ is in good agreement with this theoretical relationship. Furthermore, the pre-factor 0.19 mm in Equation (5.10) is very close to the theoretical values (0.201~0.208 mm), estimated from the geometry of the composites.

In **Figure 5.21** we observe that the two data points with $E_f/\mu_m < 10^4$ show an upward deviation of w_2 from the scaling relation $w_2 \sim (\frac{E_f}{\mu_m})^{\frac{1}{2}}$, which means the force transfer length is greater than predicted from the scaling relation of Equation (5.10). These data are tested at a high velocity of 500 mm min^{-1}, corresponding to a strain rate of 0.7 s^{-1} in tensile tests. At such high strain rate, the matrices M1-0.3 and M1-0.25 of the composites show high modulus and obvious yielding behavior (**Figure 3.3** in chapter 3). Therefore, debonding at the interface occurs easily, and the force transfer is due to topological interlocking between the fabric and the matrix, which needs a wider sample size to reach the critical force for fiber fracture. In fact, SEM observation on the fracture surface of the composite with E_f/μ_m of 6.0×10^2 reveals that no residual matrix remains on the surface of the broken fibers (**Figure 5.23-i**), indicating interfacial debonding during tearing. On the contrary, for the composite with E_f/μ_m of 1.5×10^4, the matrix is still strongly bonded to the fibers even though it undergoes dramatic shear deformation (**Figure 5.23-ii**). These results demonstrate that a soft matrix favors strong bonding to the fabric. With the premise of a strong interface, the force transfer length of FRPs is proportional to the square root of modulus ratio.

Next, we discuss what determines the energy dissipation density W. For tough homogeneous materials, W is related to the work of extension at fracture of the material.[44, 94, 111, 112] Since our soft, inhomogeneous

composites have very large force transfer lengths on the cm scale, tensile tests on specimens with conventional cm size should give higher strength and work of extension than the intrinsic values.[70] Therefore, it is not proper to use experimentally obtained tensile data (**Figure 4.6** in chapter 4) to determine W. When the composite undergoes tearing, fiber breaking and matrix failure during fiber pullout both contribute to energy dissipation. For the composites studied here, the energy dissipated by the soft, tough matrices can be significant and is on the same order of magnitude as the energy dissipated by fiber breaking (**Table 3.2, 3.4** in chapter 3). Hence, we introduce an effective work of extension, W_{eff}, which is the volume weighed average of the work of extension of the fiber bundle, W_f, and the matrix, W_m, at fracture.

$$W_{eff} = W_f \cdot V_f + W_m \cdot (1 - V_f) \quad (5.11),$$

where V_f is the volume fraction of fiber in the composites (50% in this work). W_{eff} is found to be systematically smaller than the work of extension at fracture of the composites W_c estimated by testing specimens with a gauge length of 20 mm. Since the load transfer length is equal to w_2, $l_T = w_2$, we investigated the correlation between the tearing energy Γ and the product of $W_{eff} \cdot w_2$. As seen in the plot of Γ versus $W_{eff} \cdot w_2$ for varied soft FRP systems at varied deformation rates (**Figure 5.24**), all of the data falls on the straight line of $\Gamma = W_{eff} \cdot w_2$. This result suggests that W_{eff} reflects the energy dissipation density ($W=W_{eff}$). It is also worth noting that the

composites with low E_f/μ_m (< 10^4) also conform to the correlation although their force transfer length, due to interfacial debonding, does not obey the square root relation with the modulus ratio. This is because even though debonding occurs at the interface, the force transfer by the interlocking structure of the composites also results in fiber breaking, instead of pulled out from matrix, leading to the full energy release of components.

The analysis above demonstrates that maximizing the values of the two important parameters, W and l_T, facilitates the design of extremely tough soft FRPs. This is realized by combining a matrix P(DEEA-*co*-IBA) (M3-0.6) that is adhesive, soft (μ_m = 0.11 MPa), and tough (W_m = 8.3 MJ m^{-3}), with AF fabric that is extremely rigid (E_f = 17 GPa) and strong (σ_f = 1085 MPa, W_f = 56 MJ m^{-3}). W is maximized through the high energy dissipation density of the fiber while l_T is maximized by the extremely high modulus ratio (E_f/μ_m=1.5×10^5). The resulting soft FRP, possessing both high W (W_{eff} = 32 MJ m^{-3}) and l_T (w_2 = 84 mm), achieves a tearing toughness as high as 2500 kJ m^{-2} (**Figure 5.24**), which exceeds that of metals as well as recently developed tough PA gel/fiber composites.[27-29]

The force transfer length or the size of the energy dissipation zone of a material is usually expressed by a plot of fracture energy, Γ, versus the work of extension at fracture, W.[89] The slope of the plot reflects the size of the energy dissipation zone, l_T, according to Equation (5.4). Here, we show the plot of Γ versus W for various material systems, from soft to rigid

in **Figure 5.25**. We used W_{eff} for our soft FRPs. It is obvious that the soft fiber-reinforced polymers (soft FRPs) containing a viscoelastic matrix, no matter whether the matrix is polyampholyte (PA) hydrogel or viscoelastomer, show energy dissipation zones approaching 100 mm, which is higher than any common material system.[2, 19, 88-91] In contrast, the traditional rigid carbon-fiber and glass-fiber reinforced polymers, known as CFRP and GFRP, respectively, can barely achieve energy dissipation zones above 1 mm. Even though W of soft FRPs and some rigid FRPs are quite close, the significant difference in the size of the energy dissipation zone leads to variance in their toughness.

5.3. Conclusions

In this chapter, we investigate the fracture mechanism of tough soft FRPs from soft elastomers and stiff fabrics. We show that the tearing toughness of FRPs can be divided into three regions depending on tearing behavior. Fiber pullout occurs first (region I), afterwards fiber fracture starts, along with fiber pullout (region II), at last fiber fracture (region III) is the main failure mechanism of composites. Tearing toughness is size-dependent in region I and II, and becomes size-independent in region III. For tearing toughness in region I, we demonstrate that it is related to the energy dissipation density by fiber pullout and sample width, where the energy dissipation density is determined by fiber geometry, matrix toughness, and

sample width. For tearing toughness in region III, to generate FRPs with high saturation toughness (Γ), both energy dissipation density ($W = k$) and process zone size ($l_T = w_2$) should be optimized. We show that the energy dissipation density is related to the additive of the component energy dissipation density (W_{efff}) while the process zone size is proportional to the square root of modulus ratio (E_f/μ_m) of fiber bundle to matrix, $l_T \sim (\frac{E_f}{\mu_m})^{\frac{1}{2}}$. These findings give a guidance to design and develop strong and tough composites, by utilizing adhesive, soft yet tough matrix as well as rigid but strong fiber. Based on this strategy, we demonstrate how new soft FRP composites from combination of viscoelastic elastomers and fabrics can reach unprecedented levels of crack resistance even beyond the toughest known materials. An important premise of producing tough FRPs is a strong interface, which enables components to fully release stored energy.

5.4. Experimental Section

5.4.1. Materials

Plain weave carbon fiber fabric (CF), glass fiber fabric (GF), and aramid fiber fabric (AF) were purchased from Marukatsu Co., Ltd., Japan. Acrylate monomers, ethylene glycol phenyl ether acrylate (PEA), benzyl acrylate (BZA), di(ethylene glycol) ethyl ether acrylate (DEEA), and isobornyl acrylate (IBA) were provided by Osaka Organic Chemical Industry Ltd, Japan. Ultraviolet initiator benzophenone (BP) was

purchased from KANTO Chemical Co., Inc.

5.4.2. Methods

Preparation of fiber-reinforced viscoelastomers. Samples were prepared by placing two 0.5 mm spacers on both sides of the fabric, which was inserted between two hydrophobic films supported by glass plates to form a reaction mold. Subsequently monomers containing initiator (0.1 mol% of the total monomer molar concentration) were injected into the mold. The random copolymerization was allowed to proceed under an argon atmosphere via ultraviolet irradiation (UVP lamp Toshiba-FL15BLB, wavelength 365 nm, light intensity 4 mW cm^{-2}) for 10 h. Neat elastomers were also prepared as controls.

Uniaxial tensile tests. For composites and fabrics, rectangular-shaped samples (10 mm wide and 80 mm length) were prepared with the fibers aligned parallel or perpendicular to the length direction. Tests were performed on a commercial tensile tester (Autograph AG-X, Shimadzu Co., Japan) equipped with a 20 kN load cell in the open atmosphere at room temperature. The initial length of the sample between grips was 20 mm. The work of extension is defined as the area below the obtained stress-strain curve. The crosshead velocity was 50 mm min^{-1}, unless otherwise stated. For viscoelastomers, the tensile tests were carried out by using the same commercial tensile tester equipped with a 100 N load cell at 50 mm

min^{-1} crosshead velocity in air. Before the tests, the viscoelastomers were cut into a dumbbell shape standardized as JIS-K6251-7 (2 mm in inner width, 12 mm in gauge length) with a cutting machine (Dumb Bell Co., Ltd.).

Trouser tearing tests. The tearing fracture energy of the samples was evaluated by trouser tearing tests. The tensile tester (Autograph AG-X, Shimadzu Co., Japan) equipped with a 20 kN load cell was employed to perform the tearing tests. A sample with a prescribed width *w* and length *w* + 30 mm was prepared. An initial notch of 30 mm was made in the middle of the sample along the length direction with a laser cutter. For neat elastomer samples, to prevent elongation of the legs during tests, stiff and thin tape was glued on both sides of the samples before testing. During testing, one leg of the sample was clamped to the base, and the other was clamped to the crosshead, which was displaced at a velocity of 50 mm min^{-1} at room temperature in the open atmosphere. After testing, the tearing force-displacement curves were obtained to calculate the tearing energy of samples by the following equation:[27-29]

$$T = \frac{\int_0^L F\, dL}{t \cdot L_{bulk}} \qquad (5.12),$$

where F is the tearing force, t is the sample thickness, L is the displacement, and L_{bulk} is the projected crack length.

Scanning electron microscopy. Microscale observation was carried out

by scanning electron microscopy (SEM) (JEOL JSM-6010LA, Tokyo, Japan). Samples were gold-coated in an ion-sputtering machine (E-1010, Hitachi, Tokyo, Japan) before observation. The acceleration voltage varied from 15 to 20 kV.

Figures

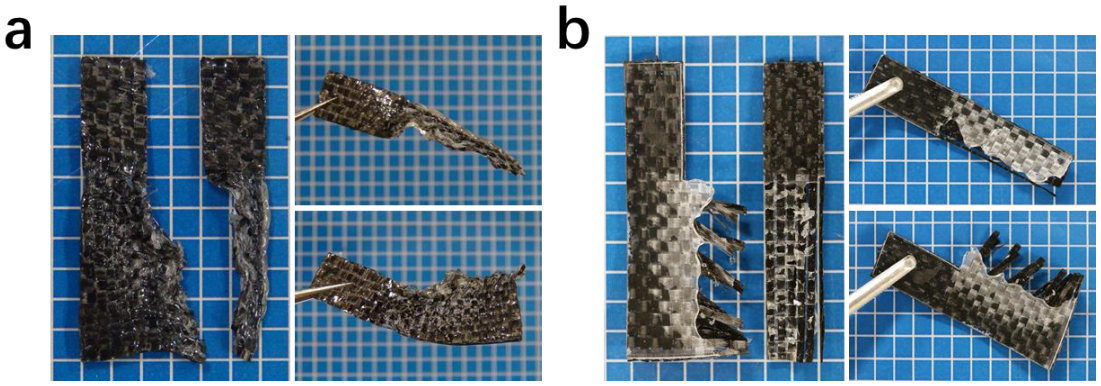

Figure 5.1. Tearing behaviors of carbon-fiber reinforced polymers from viscoelastic matrix M1-0.1 (a) and PDMS (b), respectively. Delamination of matrix from the fabric is easily observed in PDMS based composite.

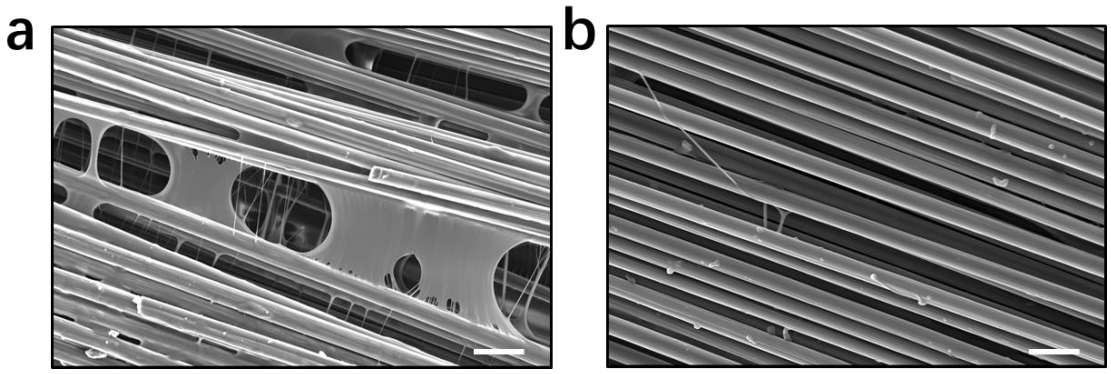

Figure 5.2. SEM observations of FRPs after tearing. (a) FRP from viscoelastic matrix M1-0.1. (b) FRP from PDMS matrix. The scale bars represent 20 μm.

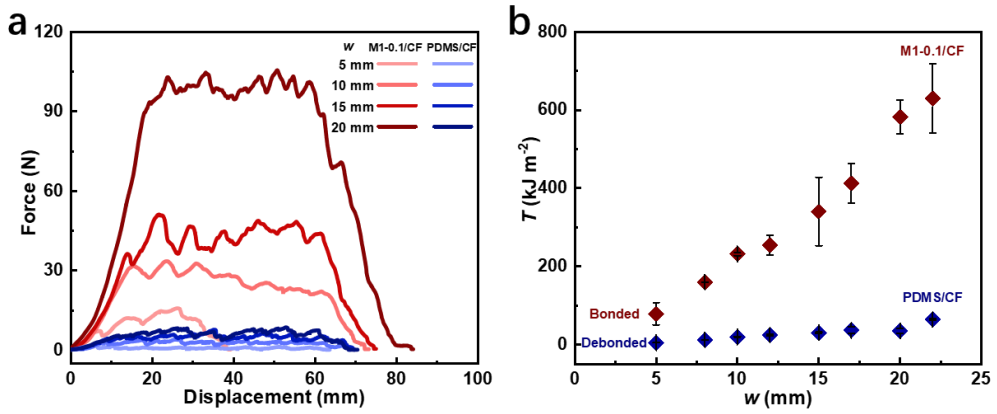

Figure 5.3. Tearing properties of FRPs from M1-0.1 and PDMS. (a) Force-displacement curves at varied width. (b) Tearing energy versus width.

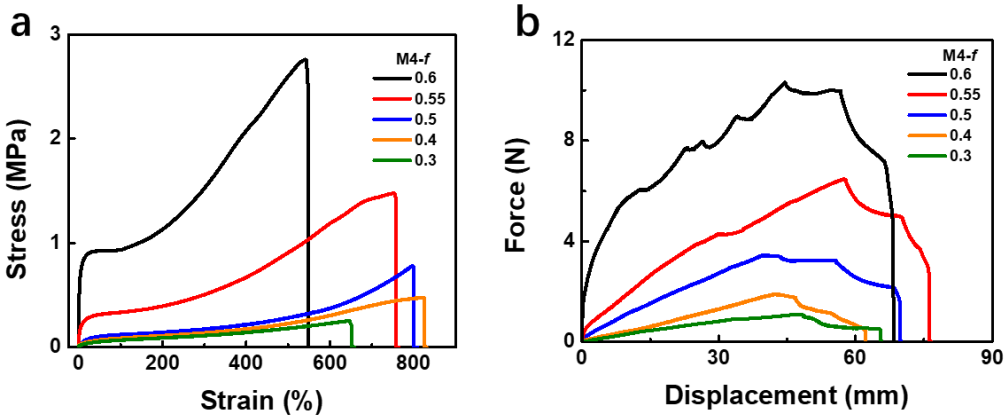

Figure 5.4. Mechanical properties of matrices. (a) Tensile properties. (b) Tearing properties.

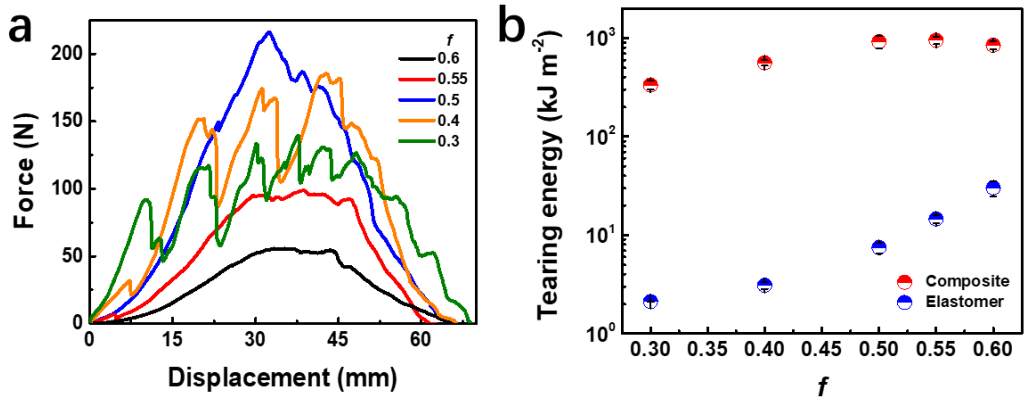

Figure 5.5. (a) Tearing results of composites with different molar ratios. (b) Tearing energies of composites (red) and elastomers (blue) as a function of *f*. The width of all composites is fixed at 30 mm.

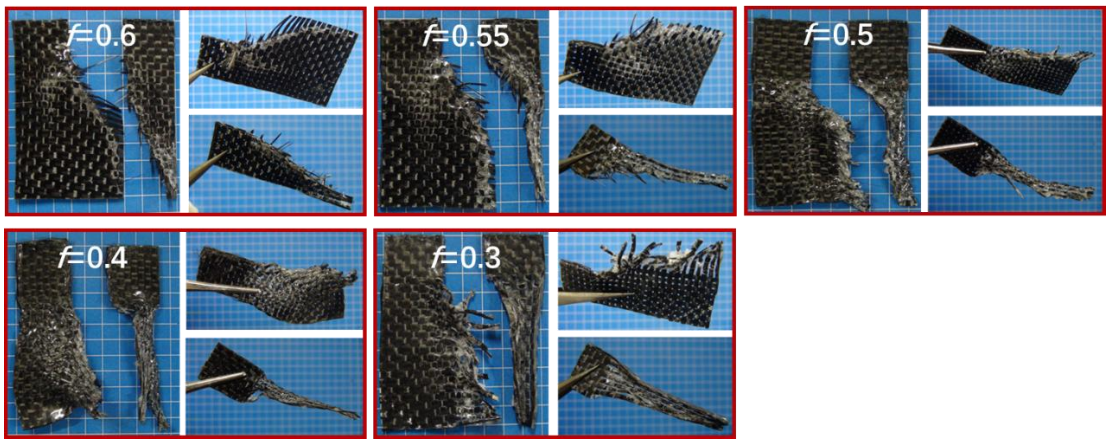

Figure 5.6. Tearing behaviors of M4-*f*/CF composites with varied *f*. The width of all composites is fixed at 30 mm.

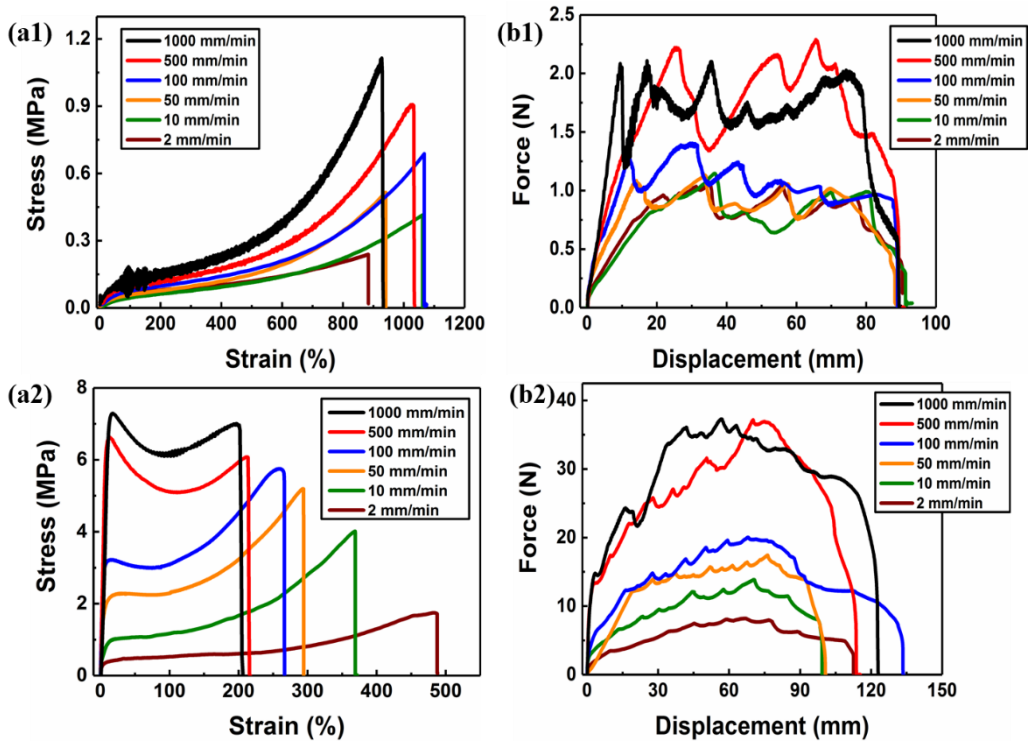

Figure 5.7. Tensile results of the soft elastomer (M4-0.3) (a1) and the hard elastomer (M4-0.6) (a2) at different velocities. Tearing results of the soft elastomer (M4-0.3) (b1) and the hard elastomer (M4-0.6) (b2) at different velocities.

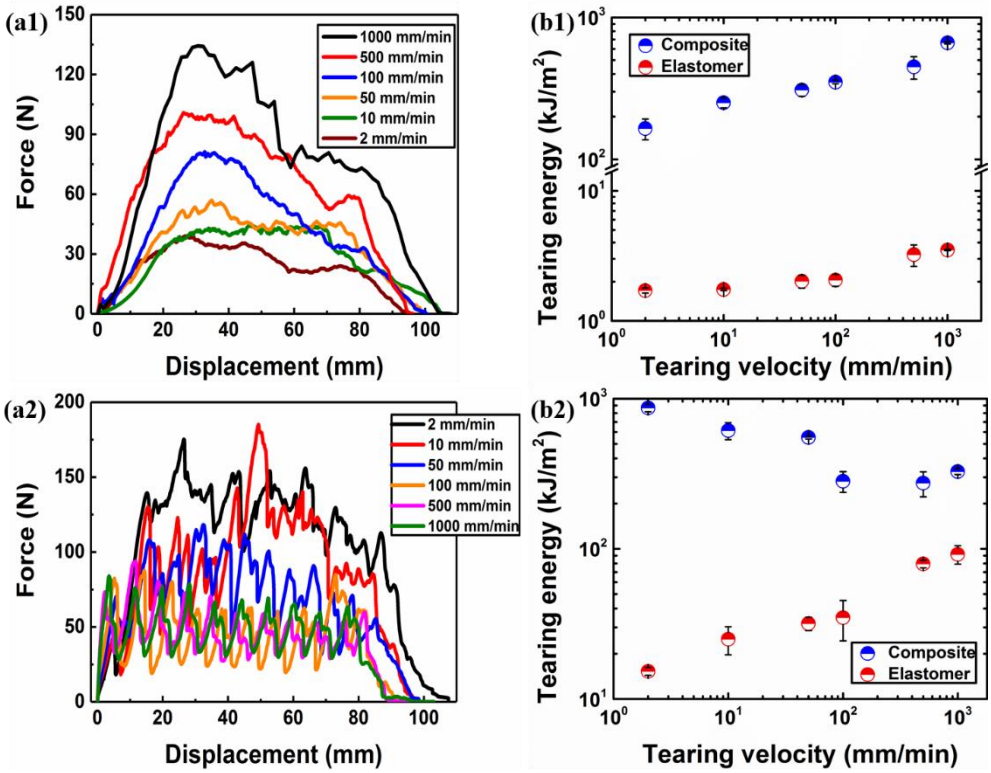

Figure 5.8. Tearing results of the soft-matrix composite (M4-0.3) (a1) and the hard-matrix composite (M4-0.6) (a2) at different velocities. Tearing energy of the soft elastomer and the corresponding composite (M4-0.3) (b1), the hard elastomer and the corresponding composite (M4-0.6) (b2) as a function of tearing velocity.

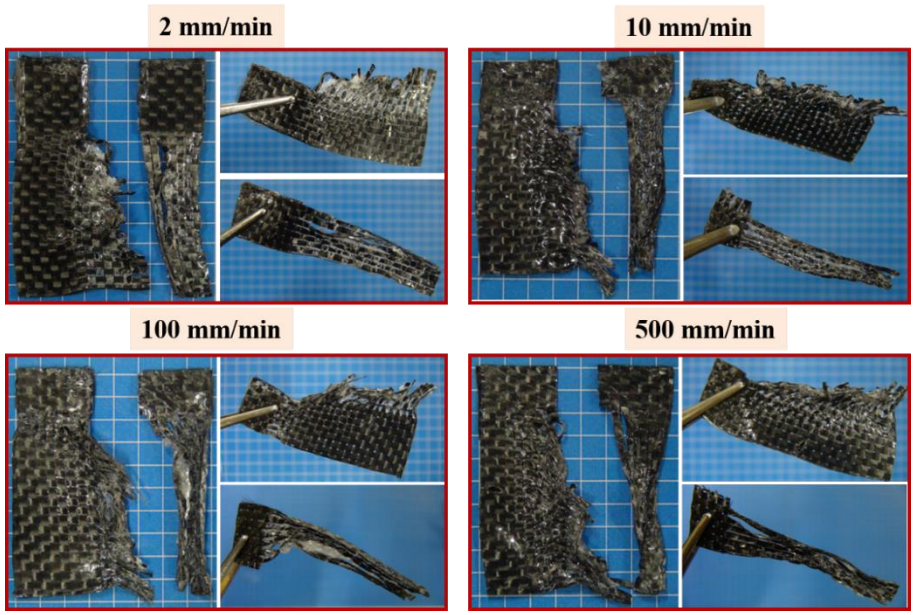

Figure 5.9. Tearing behaviors of the soft-matrix composite (width = 30 mm) at different velocities.

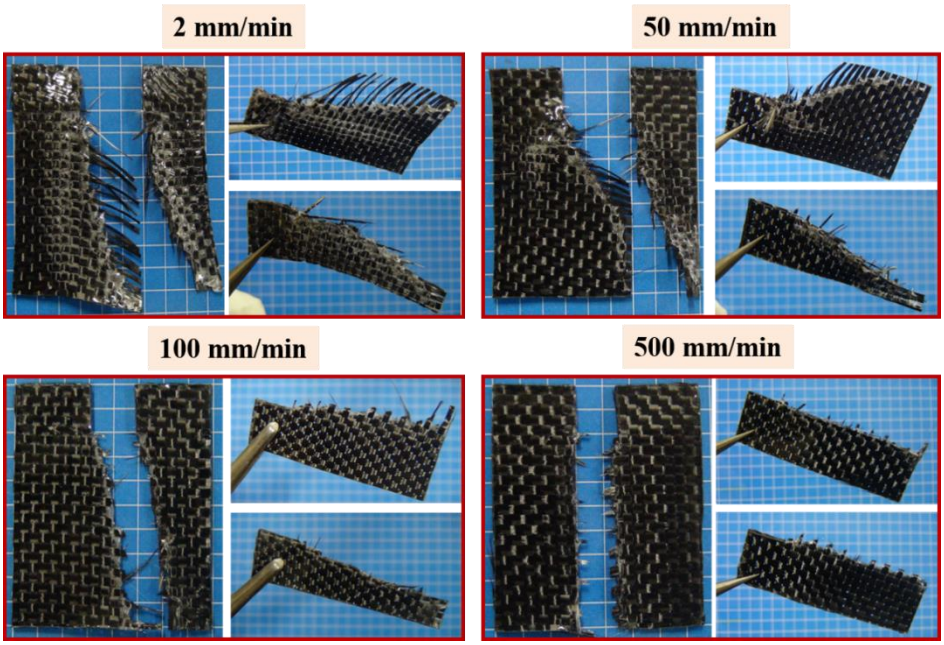

Figure 5.10. Tearing behaviors of the hard-matrix composite (width = 30 mm) at different velocities.

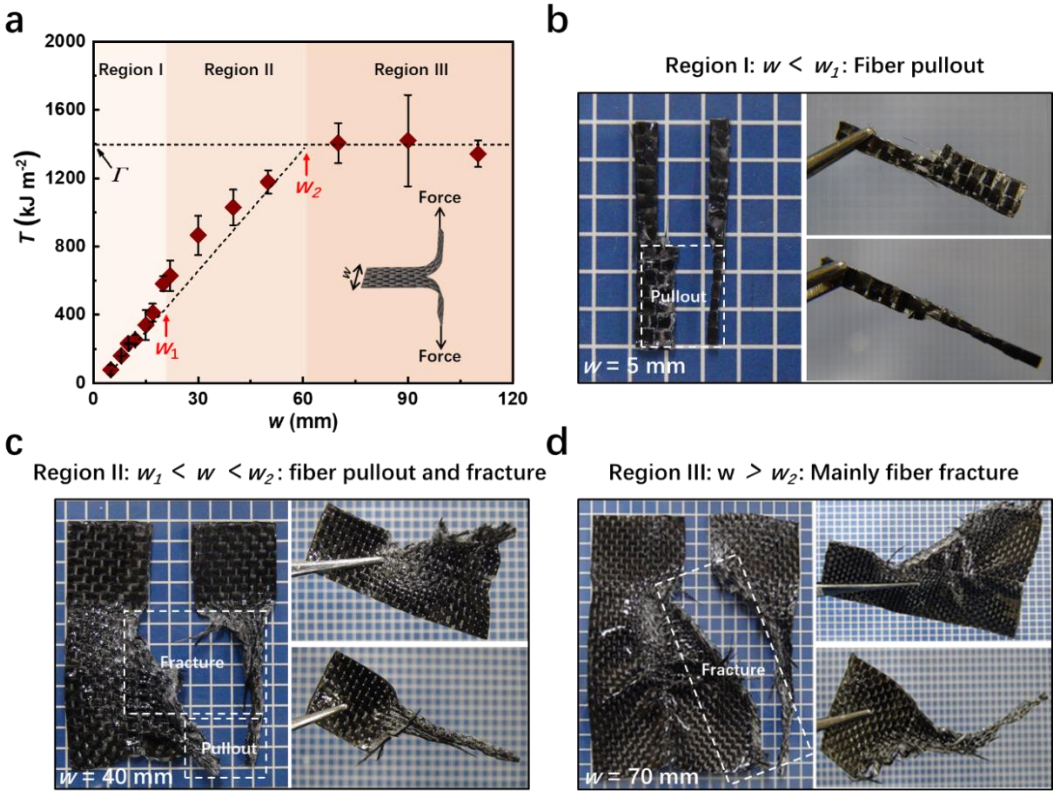

Figure 5.11. Determination of the onset width of fiber fracture, w_1, and transition width of fracture behavior, w_2, for soft FRPs by correlating their fracture behavior with the plot of T versus w in three regions.

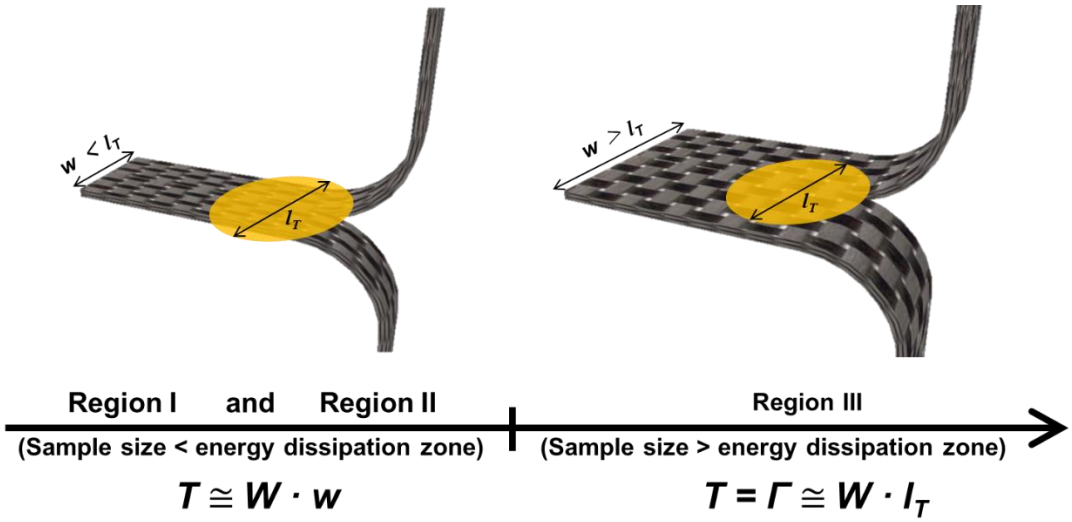

Figure 5.12. Conceptual illustration of size-dependent fracture behavior of FRPs.

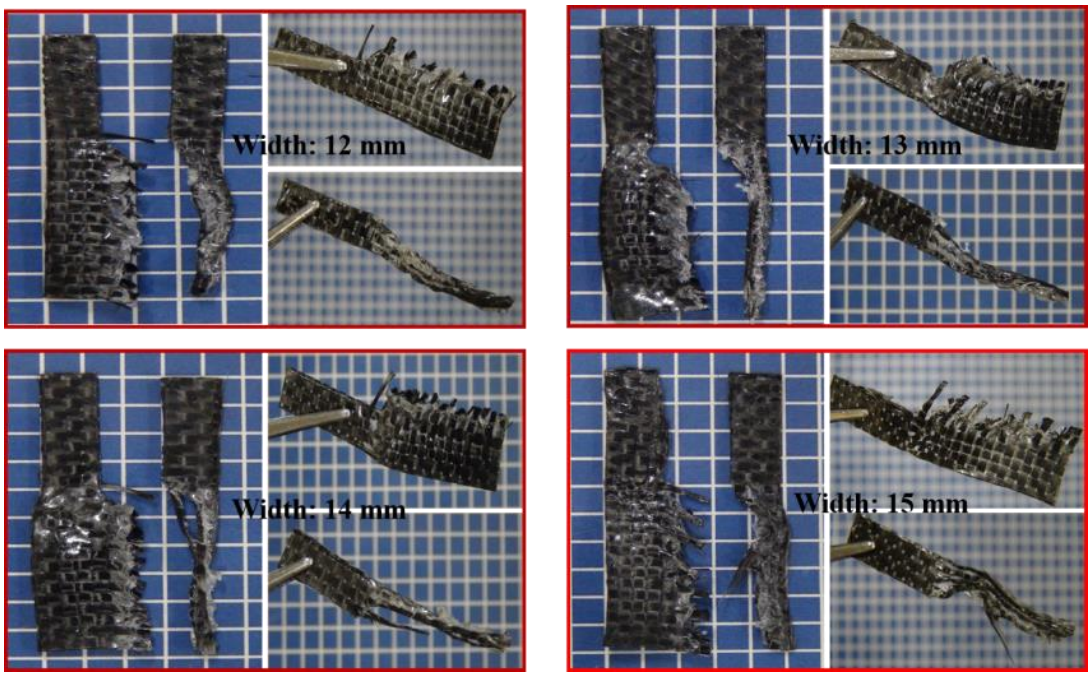

Figure 5.13. Determination of w_1 for the composite M1-0.25/CF by comparing the tearing behaviors at different widths.

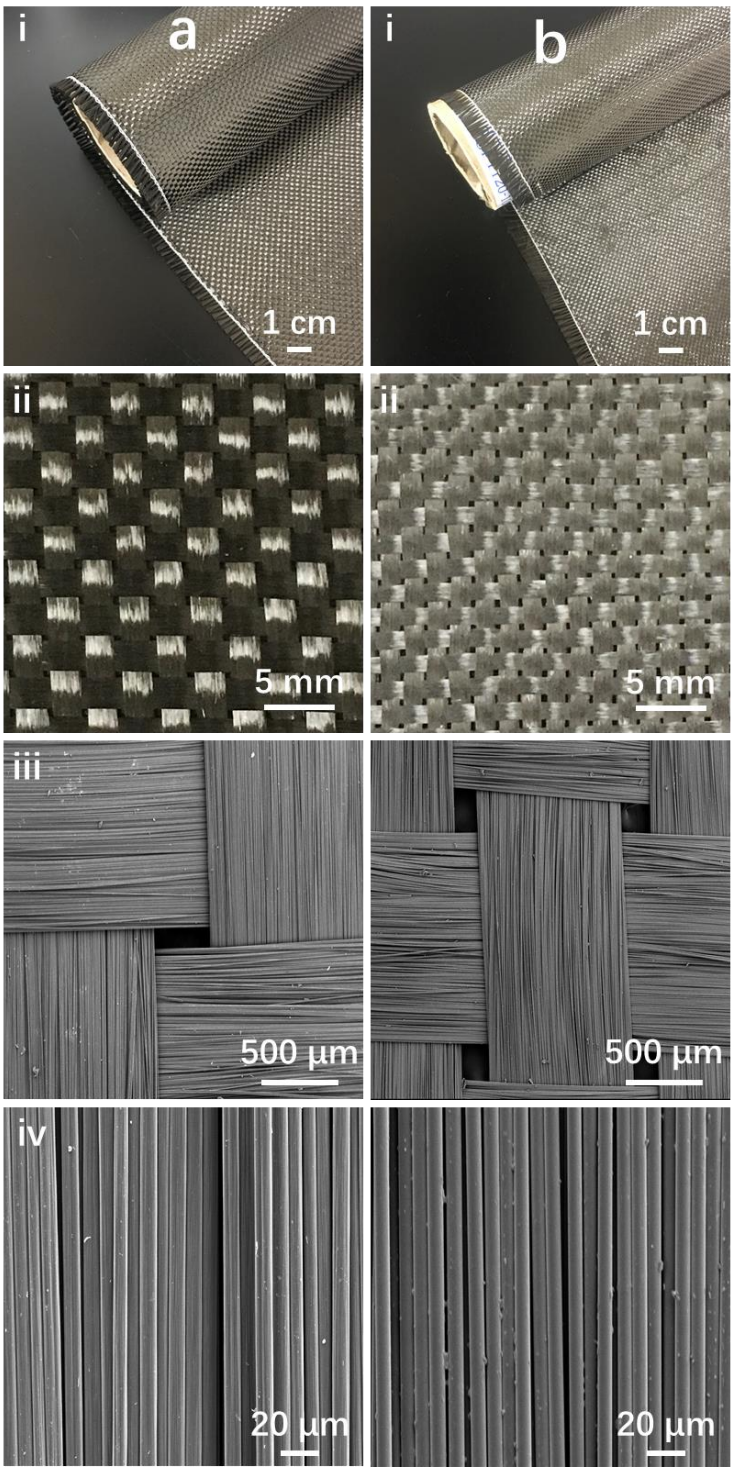

Figure 5.14. Macro- and micrographs of plain weave (a) carbon fiber (CF), (b) glass fiber (GF), and (c) aramid fiber (AF) fabrics used in this work. All fabrics are in a plane weave pattern of fiber bundles that contains thousands of individual thin fibers. (i) The macrographs of all fabrics. (ii) The plain weave structures. (iii) SEM micrographs of woven fiber bundles. (iv) Individual fibers.

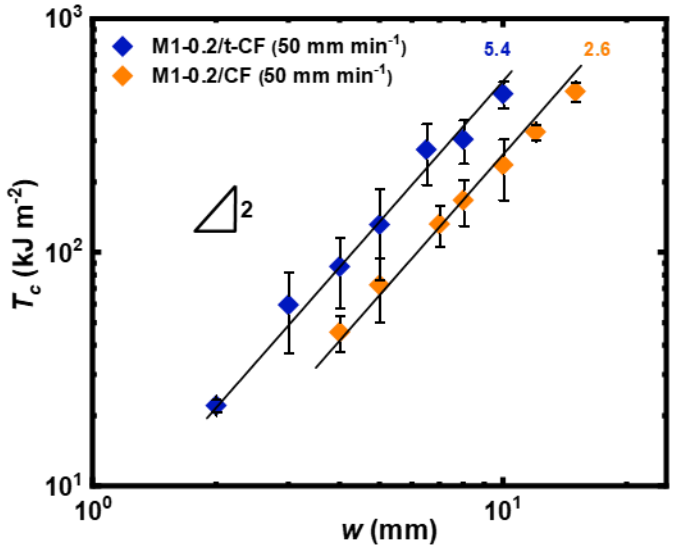

Figure 5.15. Tearing energy versus width of FRPs from same matrix and different fibers.

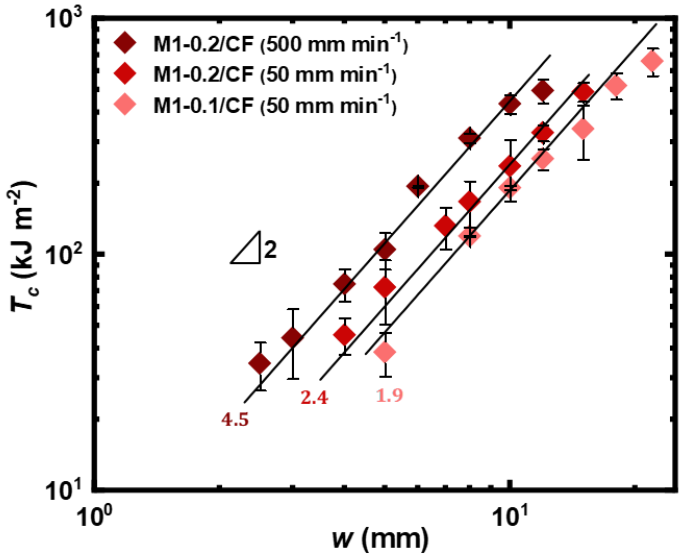

Figure 5.16. Tearing energy versus width of FRPs from same fabric and different matrices.

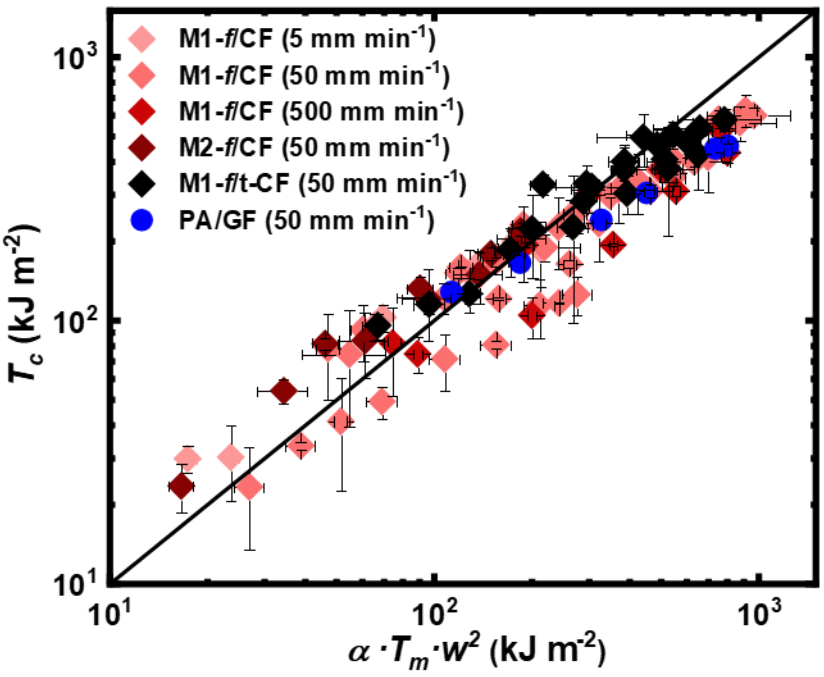

Figure 5.17. T_c versus $W_{pullout}$·w of FRPs from various fabrics and matrices.

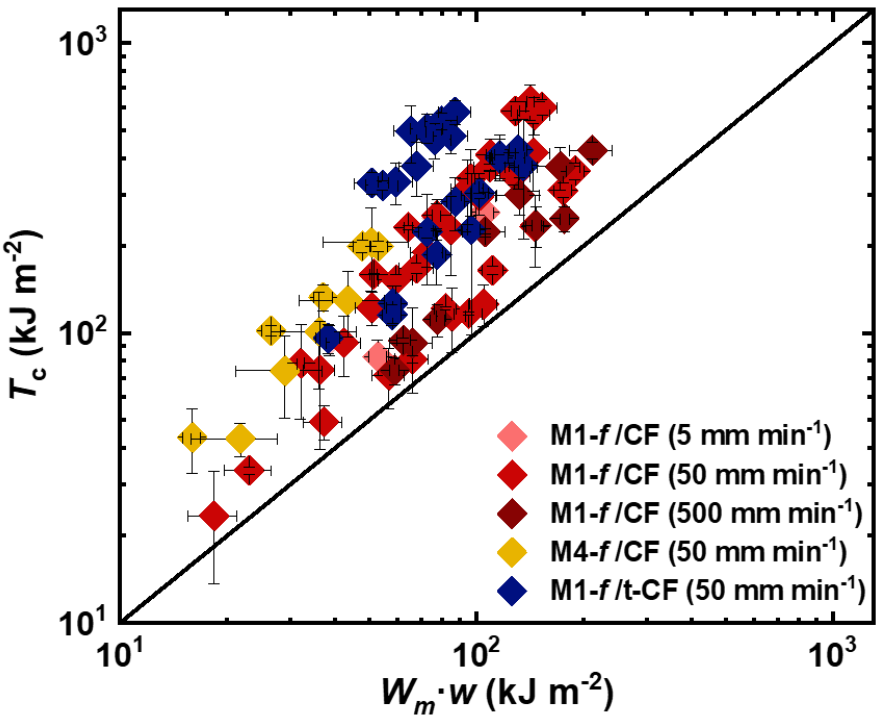

Figure 5.18. T_c versus W_m·w of FRPs from various fabrics and matrices.

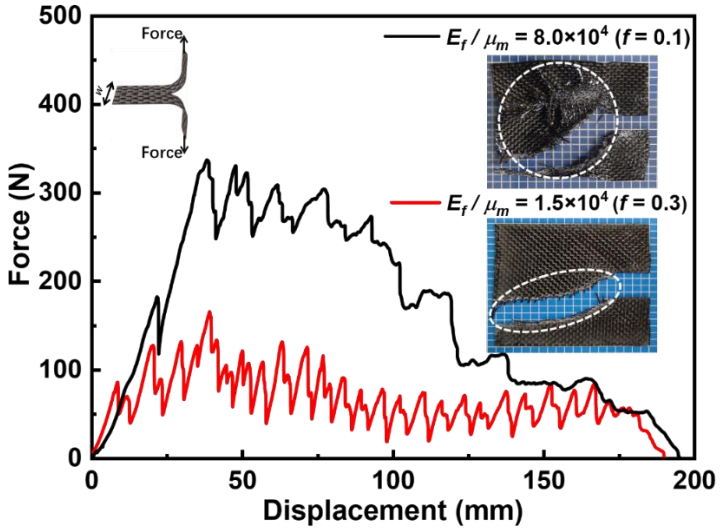

Figure 5.19. Representative force-displacement curves of trouser tearing tests on composites from CF and M1-*f* with different modulus ratios, E_f/μ_m. Comparing composites made from M1-0.3, composites made from M1-0.1 with high modulus ratio show a higher tearing force as well as a larger deformation zone indicated by the inset images, suggesting a larger force transfer length. Tearing velocity was 50 mm min^{-1}.

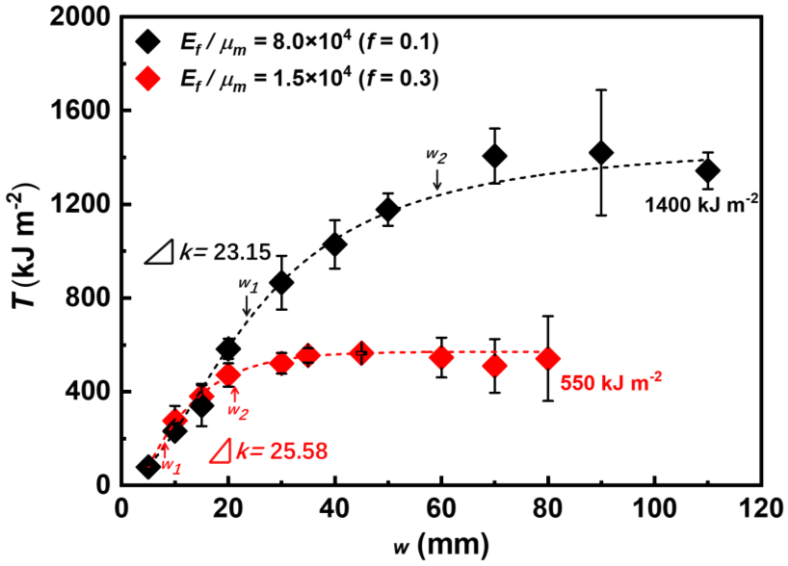

Figure 5.20. Composite toughness as measured by tearing energy, T as a function of sample size, w. T increases with w and reaches the saturation toughness $T = \Gamma$ at a critical size that is related to the size of energy dissipation zone of the composite, $w_2 = l_T$.[29] The composite with high modulus ratio reaches a higher saturation toughness at a larger w. Tearing velocity was 50 mm min^{-1}.

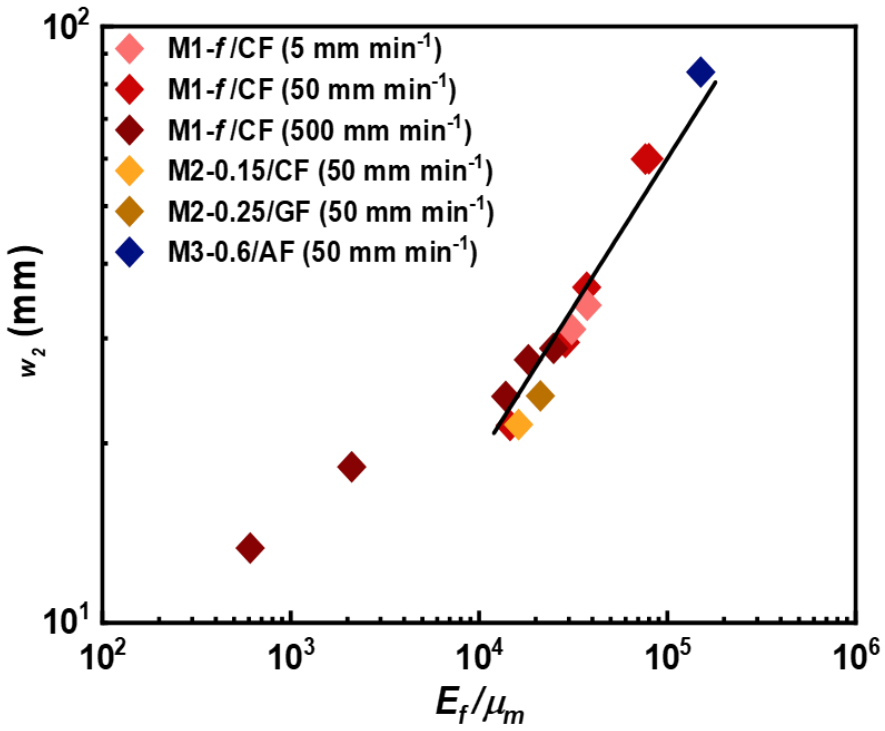

Figure 5.21. Correlation between the size of the energy dissipation zone, determined by w_2, and the modulus ratio for composites from various combinations of fabrics and matrices that are measured at different velocities. For composites with modulus ratio larger than 10^4, w_2 is proportional to the square root of the modulus ratio, w_2 (mm) = 0.19 $(E_f/\mu_m)^{1/2}$. CF, GF, and AF stand for carbon, glass, and aramid fiber fabrics, respectively.

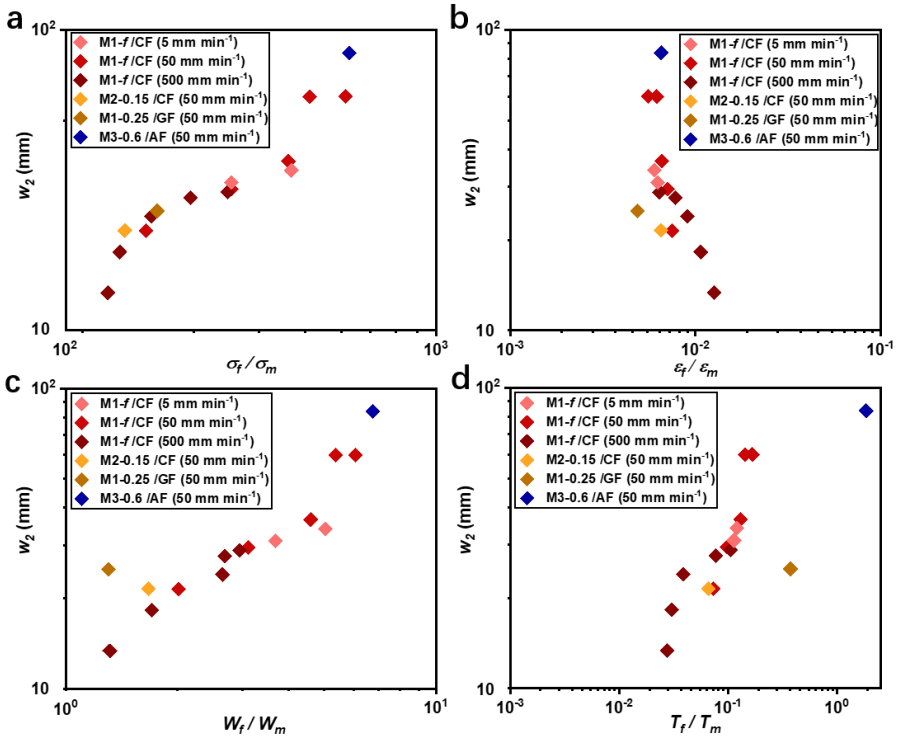

Figure 5.22. The relationship between w_2 and fiber/matrix property ratios for all soft FRPs in this work. (a) w_2 versus fiber/matrix fracture stress ratio, σ_f/σ_m; (b) w_2 versus fiber/matrix fracture strain ratio, $\varepsilon_f/\varepsilon_m$; (c) w_2 versus fiber/matrix work of extension ratio, W_f/W_m; (d) w_2 versus fabric/matrix tearing energy ratio, T_f/T_m.

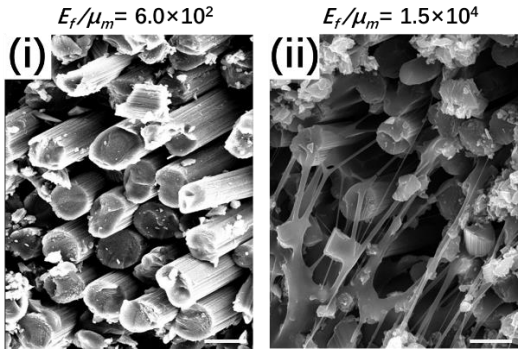

Figure 5.23. SEM images of fractured surfaces for composites shown in **Figure 5.21** by (i) and (ii). For composites made from the relatively rigid matrix (μ_m = 35.1 MPa) and having low modulus ratio, debonding occurs when fibers are fractured and pulled out (i). On the contrary, for composites from the soft matrix (μ_m = 1.5 MPa) and having high modulus ratio, the matrix is still strongly bonded when fibers are fractured and pulled out (ii). Scale bars represent 10 μm.

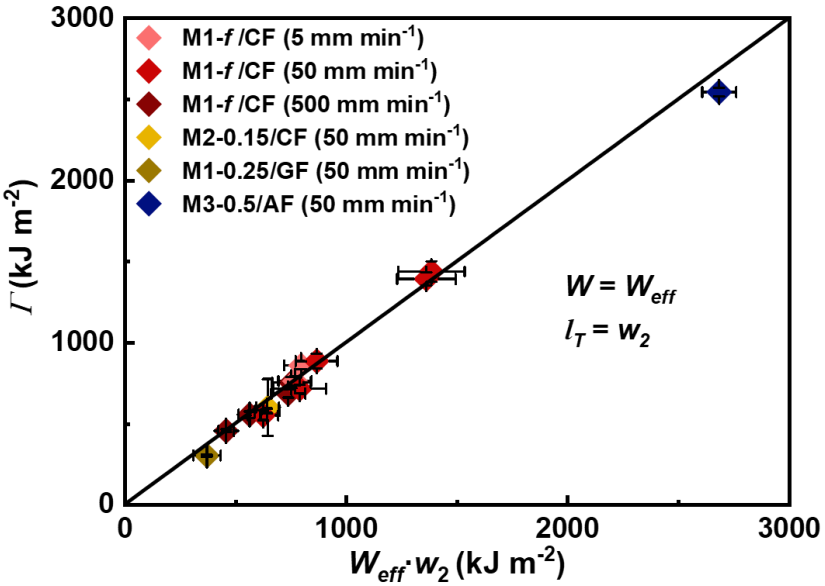

Figure 5.24. The experimentally determined saturation toughness, Γ of soft FRPs versus $W_{eff} \cdot w_2$, where W_{eff} is the volume weighed average of the work of extension of the fiber bundle and the matrix at fracture, and w_2 is the experimentally determined size of the energy dissipation zone (force transfer length). The validity of $\Gamma = W_{eff} \cdot w_2$ indicates the energy dissipation density W and the size of energy dissipation zone l_T shown in Equation (5.4) is related to W_{eff} and w_2, respectively.

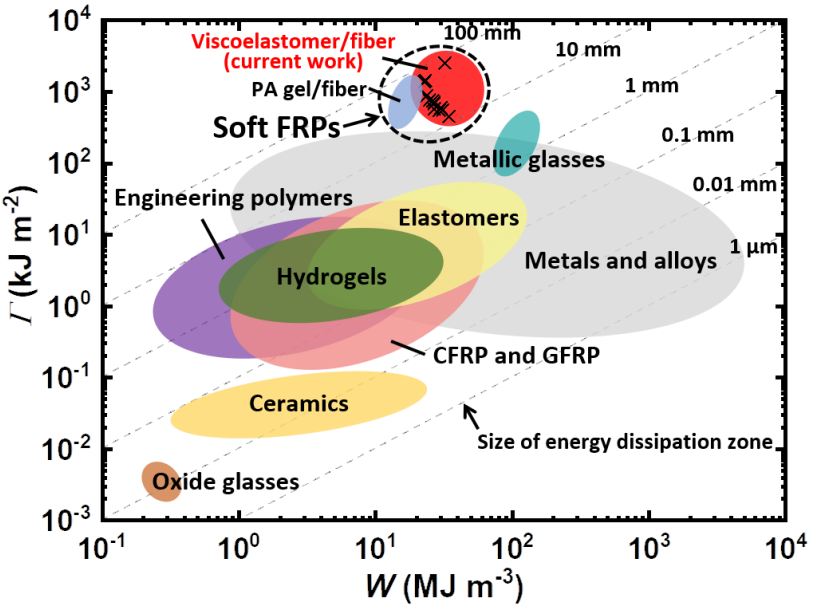

Figure 5.25. Γ of various materials versus energy dissipation density, W. The slopes shown by the dotted lines reflect the size of the energy dissipation zone of different materials.

Tables

Table 5.1. Tensile, tearing parameters and glass-transition temperatures of elastomers M4-*f*.

Property \ *f*	0.6	0.55	0.5	0.4	0.3
Tensile modulus (MPa)	50	10	0.55	0.21	0.08
Glass-transition temperature (℃)	16.62	15.35	9.82	0.38	3.53
Tearing toughness (kJ m^{-2})	30.15	14.55	7.46	3.10	2.11

Table 5.2. Geometric and mechanical parameters of CF and t-CF.

Fabric	Bundle sectional area (mm^2)	Bundle width (mm)	Mass (g/m^2)	Tensile stress (GPa)	Tensile strain (%)	Tensile modulus (GPa)	Strain energy density (MJ m^{-3})
CF	~0.204	~1.7	200	~0.894	~6.87	~21.38	~38.97
t-CF	~0.062	~0.98	120	~1.396	~5.3	~38.91	~44.85

Table 5.3. Summary of relevant ratios of fiber/matrix mechanical properties and experimentally observed force transfer length w_2 for different composite systems. The ratios include tensile fracture stress ratio (σ_f/σ_m), fracture strain ratio ($\varepsilon_f/\varepsilon_m$), Young's modulus /shear modulus ratio (E_f/μ_m), work of extension ratio (W_f/W_m), and tearing energy ratio (T_f/T_m). For comparison, the theoretical force transfer length l_T for a model composite consisting of parallel fibers embedded in a soft matrix is calculated from **Equation (S2)** using the structure parameters of fabrics shown in **Table S1** and the fiber/matrix modulus ratio of the composites.

Sample code	Testing velocity (mm min^{-1})	f	σ_f/σ_m ($\times10^2$)	$\varepsilon_f/\varepsilon_m$ ($\times10^{-3}$)	E_f/μ_m ($\times10^4$)	W_f/W_m	T_f/T_m ($\times10^{-2}$)	w_2 (mm)	l_T (mm)
M1-*f*/CF	5	0.25	4.07	6.00	3.75	5.03	12.00	34.10	40.26
		0.3	2.80	6.28	3.11	3.69	11.32	31.06	36.62
	50	0.1	5.70	5.55	7.99	6.07	5.12	60.03	58.73
		0.15	4.57	6.18	7.64	5.36	14.37	59.94	57.45
		0.2	4.00	6.60	3.73	4.59	13.03	36.53	40.13
		0.25	2.80	7.08	2.87	3.11	9.77	29.53	35.23
		0.3	1.65	7.51	1.46	2.02	7.30	21.43	25.11
	500	0.1	2.74	6.40	2.49	2.95	10.56	28.85	32.78
		0.15	2.18	7.83	1.83	2.69	7.74	27.62	28.10
		0.2	1.70	9.04	1.38	2.65	3.89	23.97	24.45
		0.25	1.40	10.73	0.21	1.71	3.03	18.26	9.54
		0.3	1.30	12.64	0.06	1.32	2.77	13.35	5.13
M2-*f*/CF	50	0.15	1.44	6.53	1.62	1.67	6.59	21.50	26.46
M1-*f*/GF	50	0.25	1.77	4.89	2.38	1.31	40.17	24.02	31.83
M3-*f*/AF	50	0.6	5.83	6.54	15.04	6.74	184.78	83.86	77.77

Chapter 6-Applying the Design Strategy to Develop Crack-resistant Hydrogel Composites

6.1. Introduction

Hydrogels, generally consisting of three-dimensional hydrophilic polymer network and abundance of water, have been widely applied in many field, such as stimuli response,[113-115] drug delivery,[116, 117] tissue engineering,[118] etc. However, a pivotal shortcoming that restricts the applications of hydrogels is their poor crack resistance.[119] Because of the lack of crack-resistant mechanism, common hydrogels merely show fracture energy on the order of 10^{-1}~10^{0} J m^{-2}.[120-122] The values are much lower than those of cartilages (10^{2}~10^{3} J m^{-2}) and rubbers (10^{3} J m^{-2}).[21] The weak, brittle mechanical characteristic of hydrogels hinders further extensive use of this material. Thus far, hydrogels have been limited to the usage where the mechanical properties are not highly concerned.[123, 124]

The crack resistance of a material, usually expressed by fracture energy, Γ (J m^{-2}), is theoretically determined by force transfer length, l_T (m) and energy dissipation density, W (J m^{-3}),[70]

$$\Gamma \cong l_T \cdot W \tag{6.1}$$

Common hydrogels intrinsically have both low l_T and W due to the absence of efficient crack-resistant mechanism. When a crack is initiated and the gel is stretched, the deformation is inhomogeneous. Namely, the polymer

chains ahead of the crack are much more stretched than chains elsewhere, only the chains ahead of the crack tend to break.[44] Therefore, the gel is notch-sensitive because energy dissipates over a highly localized region: only a tiny fraction of the chains in the network—those crossing the crack plane—participate in energy dissipation, leading to small l_T. On the other hand, only a trace amount of energy is required to break the polymer chains,[125-128] giving rise to a low W.

A successful method to enhance the crack resistance of hydrogels is to introduce the soft/rigid composite design. For composites consisting of a rigid phase embedded in a soft matrix, the l_T is related to the hard/soft modulus ratio and the W depends on the energy dissipation density of both components. Therefore, to enhance the crack resistance of hydrogels, a soft/hard composite design is widely recognized. For example, double network hydrogels demonstrate high fracture energy on the order of 10^3 J m^{-2}.[68, 69] The pre-stretched first network composed of polyelectrolytes has much higher modulus than the ductile, soft second network. The direct coupling of the two networks facilitates the efficient force transfer, results in polymer chains in a large zone being subjected to stress. Therefore, the resulting gels possess l_T on the order of millimeter scale and high fracture energy.[52, 129]

In this work, we develop an even more crack-resistant hydrogels by the soft/rigid design. Alginate hydrogels dried in confined condition (DCC) are

employed as the rigid skeleton,[130] and lightly cross-linked polyacrylamide hydrogels act as the soft matrix. The DCC method yields the skeleton high modulus on the order of 10^2 MPa, leading to an extremely high component modulus ratio, which facilitates the force transfer between two components (high l_T). Moreover, DCC-gels also show high energy dissipation density on the order of 10^1 MJ m^{-3}, giving rise to high W. Benefiting from both high l_T and W, the biocompatible composite gels, with a muscle-like structure, demonstrate fracture energy as high as 60 kJ m^{-2}, two orders of magnitude higher than that of cartilages and exceeding any tough hydrogels. This kind of extremely crack-resistant hydrogels hold great potential in biological applications, such as artificial ligaments, tendons, etc.

6.2. Results and Discussion

6.2.1. Preparation of DCC- and composite hydrogels

The composite gel is prepared by two steps. For the first step, initially, Na-alginate gel is cross linked by calcium ions (**Figure 6.1**). Afterwards DCC-alginate gel is fabricated by drying the calcium cross-linked alginate gel in confined condition (**Figure 6.2**). Second, the DCC-alginate gel is immersed in the monomer solution of 2M acrylamide in the presence of cross-linker and initiator. The polymerization is allowed to proceed in argon atmosphere under UV light for 10 h.

6.2.2. Morphology of DCC-gels

The DCC method yields alginate hydrogels with anisotropic aligned fibrous structure. During drying, the gel shrinks due to the evaporation of water. As its two ends are fixed, the width and thickness of the hydrogel will shrink, but not the length. Therefore, the gel experiences tensile stress in the length direction during drying, causing orientation of the polymer chains along the length direction. When dried, the polymer concentration increases and above a critical concentration the polymers form nanofibrils through supramolecular interactions. Further drying induces aggregation of nanofibrils to form thicker fibers. The process is repeated to form the hierarchical fibrous structure of the gel. The reswollen gel maintains the same structure due to the formation of stable supramolecular interactions. Therefore, the DCC-gel are endowed with high rigidness and strength, which is a good candidate as the skeleton of composites.

The morphology of DCC-gel is shown in **Figure 6.3**. The bulk gel shows a shrunken appearance in width and thickness dimension. SEM observation reveals that aligned fibrous structure is formed inside the gel, indicating the successful preparation of the rigid skeleton.

6.2.2. Swelling of DCC-gel in water and second monomer solution

To make a composite gel, double network method is employed. A premise to prepare a double network structure is that the second monomer can enter

the network structure of the first network. To verify the swelling properties of DCC-gel, we immerse the DCC-gel into water and second monomer, respectively. The results are shown in **Figure 6.4**. The DCC-gel show close swelling properties in water and monomer solution, indicating that the second monomer can permeate into the first network during swelling. This result suggests that double network method is applicable to produce composite hydrogels.

6.2.3. Mechanical properties of composite hydrogels

Tensile properties of composite hydrogels are shown in **Figure 6.5**, with DCC-alginate, Polyacrylamide gel (PAAm gel), and normally dried (ND) alginate gel as comparisons. The PAAm gel is soft and ductile, which is much more stretchable than other gels, showing a low modulus. ND-gel is much stiffer and stronger because of the chain aggregation during water evaporation. DCC-gel is even stronger and stiffer. As mentioned before, during drying of DCC-gel, strong hydrogen bonds are formed among polymer chains due to the increased polymer concentration. Therefore, breaking these bonds requires large amounts of energy, leading to a high strength and energy dissipation density of DCC-gel. Moreover, after introducing a soft matrix, the composite gel shows even higher strength and energy dissipation density. According to the theory raised by Hui et al., the soft matrix shears dramatically during loading, effectively transferring

the force to a broad area, which delays the catastrophic failure of the skeletons.[70]

6.2.4. Fracture in composite hydrogels

Single notch tests are employed to examine the fracture energy of hydrogels (**Figure 6.6**).[34, 44] Sample geometry is exhibited in **Figure 6.7**. The fracture energy Γ is calculated using the following equation:

$$\Gamma = \frac{6}{\sqrt{\lambda}} W(\lambda_c) c \qquad (6.2),$$

where $W(\lambda_c)$ is the strain energy density of an uncracked sample subjected to a uniaxial stretch λ_c. Fracture behaviors of composite gel is shown in **Figure 6.8**, with DCC-gel as a comparison. The composite gel shows an obvious crack blunting while the crack in DCC-gel propagates much more easily. Based on the fracture behavior, we can reasonably expect a high fracture energy of composite gels. **Figure 6.9** gathers the results of single notch tests for DCC and composite gels. According to equation (6.2), the fracture energy of DCC gel is 29.5 kJ m^{-2} while that of composite gel is twice higher (61.4 kJ m^{-2}), indicating the enhanced crack resistance by introducing soft matrix into DCC system.

Size effect on the fracture energy of hydrogels is also investigated. As is shown in **Figure 6.10**, both DCC and composite gels do not show apparent size-dependent fracture energy, which indicates that the sample size is beyond the intrinsic energy dissipation zone. That is, the energy

dissipation zone is saturated and the fracture energy reflects the intrinsic crack resistance of the gels. The composite gel shows fracture energy approximately twice that of DCC-gel. Since the energy dissipation density of composite gel is higher than that of DCC-gel, the increase in fracture energy should be attributed to the improvement of energy dissipation density instead of force transfer length, according to equation (6.1). As discussed before, the force transfer is related to both component modulus ratio and fiber geometric parameter. The introduction of soft matrix, on one hand, enhances the modulus ratio, on the other hand, however, may decrease the geometric parameter. This decrease neutralizes the improvement of modulus ratio and leads to the invariance of force transfer length.

6.2.5. Comparison with other tough hydrogels

The extraordinary crack resistance of composite gels stimulates us to have a systematic comparison with other hydrogel systems. As exhibited in **Figure 6.11**, both DCC and composite gels show much higher fracture energy and energy dissipation density compared with other hydrogels, even exceeding those of cartilages. The slopes reflect the size of energy dissipation zone or force transfer length. Both DCC and composite gels show close force transfer length to other hydrogels, proving that the increase of modulus ratio is neutralized. The extremely high crack

resistance and biocompatible compositions endow the composite hydrogels with great potential in biological fields.

6.3. Conclusions

In this chapter, we applied the design criterion of extremely tough fiber-reinforced polymers to fabricate crack-resistant hydrogels. Soft matrix polyacrylamide hydrogel is introduced into alginate hydrogel system that is dried in confined condition (DCC). The resulting composite hydrogels, possessing highly aligned fibrous network structure, show improved tensile stress, modulus, and energy dissipation density, without sacrificing ductility. Single notch tests reveal that the composite gels have a fracture energy of as high as 60 kJ m^{-2}, almost two orders of magnitude higher than the best-in-class hydrogels in present. The big increase in energy dissipation density is account for the high fracture energy. This work verifies the validity of the design criterion and produces extremely tough biocompatible hydrogels, which holds great potential to design other tough materials for various applications.

6.4. Experimental Section

6.4.1. Materials

Analytical grade Na-alginate (viscosity 80–120 cP, Wako Pure Chemical Industries Ltd., Japan), calcium chloride (Wako Pure Chemical Industries

Ltd., Japan), Acrylamide (Junsei Chemical), N,N'-Methylenebisacrylamide (MBAA) (Wako Pure Chemical Industries Ltd., Japan), 2-oxoglutaric acid (Wako Pure Chemical Industries Ltd., Japan) were used as received without further purification. All aqueous solutions were prepared using ultrapure deionized water.

6.4.2. Methods

Preparation of composite hydrogels. Composite hydrogels are prepared by introducing a soft second network in the DCC hydrogel system. First, the DCC gel is prepared. Alginate solution was prepared by dissolving 4 wt% Na-alginate in water and stirring overnight. To prepare Ca-alginate gel, reaction cell was first prepared by sandwiching two glass plates (10 mm × 10 mm), separated using a 2 mm spacer. The upper end was kept open for solution insertion. Half of the reaction cell was filled with 4 wt% Na-alginate solution. 0.5 M CaCl2 *aq.* solution was introduced from the upper empty part of reaction cell. Ca^{2+} ions diffused through the alginate solution. Ca-alginate gel started to form when alginate solution met Ca^{2+} ions. After complete gelation, Ca-alginate gel was taken out of the reaction cell and placed in 0.5 M *aq.* CaCl2 solution for 1 d to complete the cross-linking process. Finally, the gel was thoroughly washed with water to remove non-cross-linked salt and polymer. The Ca-alginate gel was used to prepare DCC-alginate gels. To apply DCC (drying in confined condition)

on Ca-alginate gel, both ends of a sample of ~1.5 mm thickness and 10 mm width were clamped. The distance between the two clamps was 30 mm. The gel was left in the atmosphere (temperature: 25 °C, humidity: 40–60%) to dry. After complete air drying, the gel was taken out of the device, the clamped part cut from both ends. Second, the DCC gel was immersed into the arylamide solution in the presence of initiator and cross-linker for two days. Afterwards, the gel was taken out and exposed to UV light for 10 h to allow the formation of second network.

Uniaxial tensile tests. Tests were performed on a commercial tensile tester (Autograph AG-X, Shimadzu Co., Japan) equipped with a 100 N load cell in the open atmosphere at room temperature. The initial length of the sample between grips was 12 mm. The crosshead velocity was 50 mm min^{-1}. Before the tests, the hydrogels were cut into a dumbbell shape standardized as JIS-K6251-7 (2 mm in inner width, 12 mm in gauge length) with a cutting machine (Dumb Bell Co., Ltd.).

Single notch tests. The tearing fracture energy of the samples was evaluated by single notch tests. The tensile tester (Autograph AG-X, Shimadzu Co., Japan) equipped with a 100 N load cell was employed to perform the tearing tests. A sample with a prescribed width (5 mm) and length (2.5 to 20 mm) was prepared. An initial notch of 1 mm was made in the middle of the sample along the width direction with a laser cutter. During testing, both ends of the sample were clamped to the base, one of

which was displaced at a velocity of 50 mm min^{-1} at room temperature in the open atmosphere. Samples without notch were also tested to calculated the fracture energy using equation (6.2).

Scanning electron microscopy. Microscale observation was carried out by scanning electron microscopy (SEM) (JEOL JSM-6010LA, Tokyo, Japan). Before observation, samples were treated with freeze drying method. Afterwards, Samples were gold-coated in an ion-sputtering machine (E-1010, Hitachi, Tokyo, Japan). The acceleration voltage varied from 15 to 20 kV.

Figures

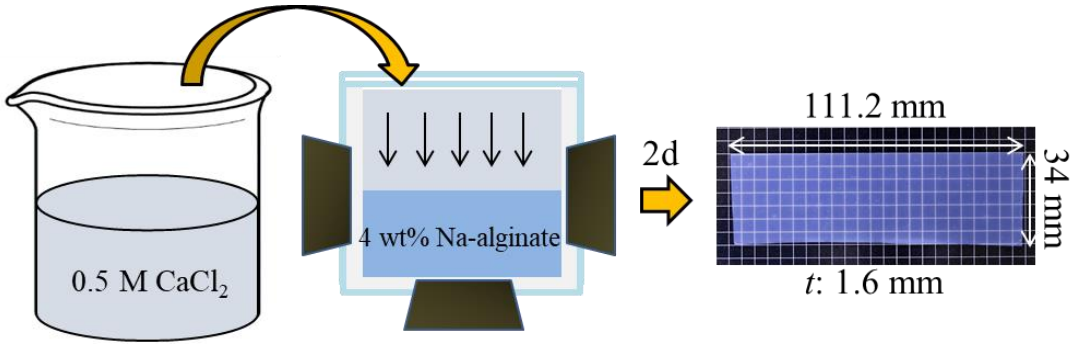

Figure 6.1. Preparation of calcium cross-linked alginate hydrogel.

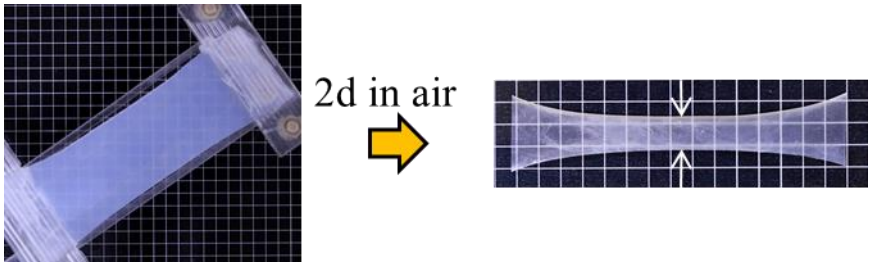

Figure 6.2. DCC method to fabricated DCC-alginate hydrogel.

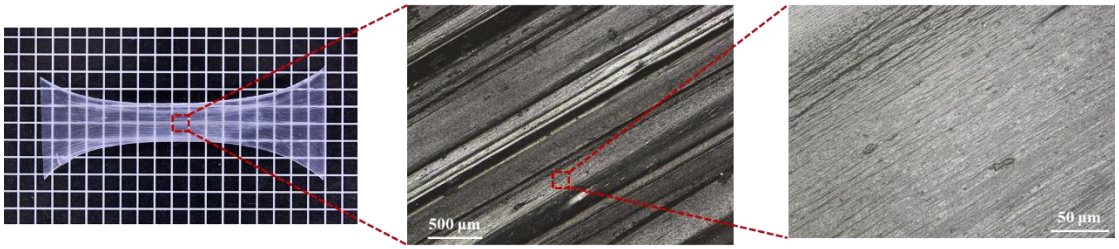

Figure 6.3. Appearance and SEM morphology of DCC-alginate hydrogel.

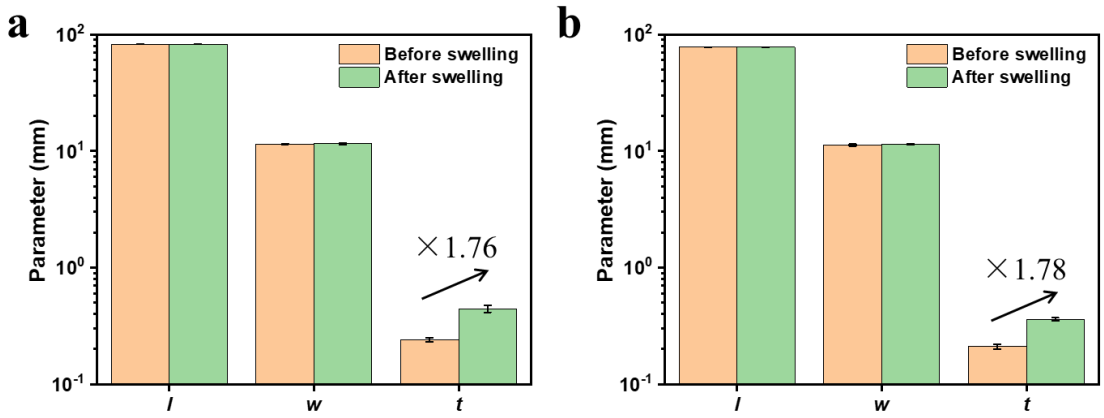

Figure 6.4. Swelling properties of DCC-gel in water (a) and acrylamide monomer solution (b).

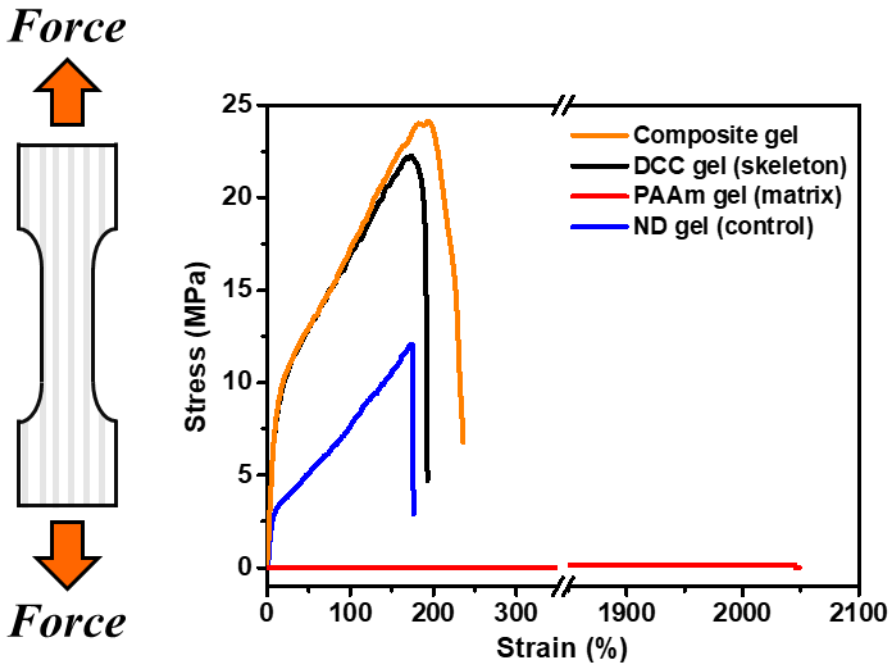

Figure 6.5. Tensile properties of hydrogels. For composite and DCC gels, the tension direction is parallel with the fiber alignment.

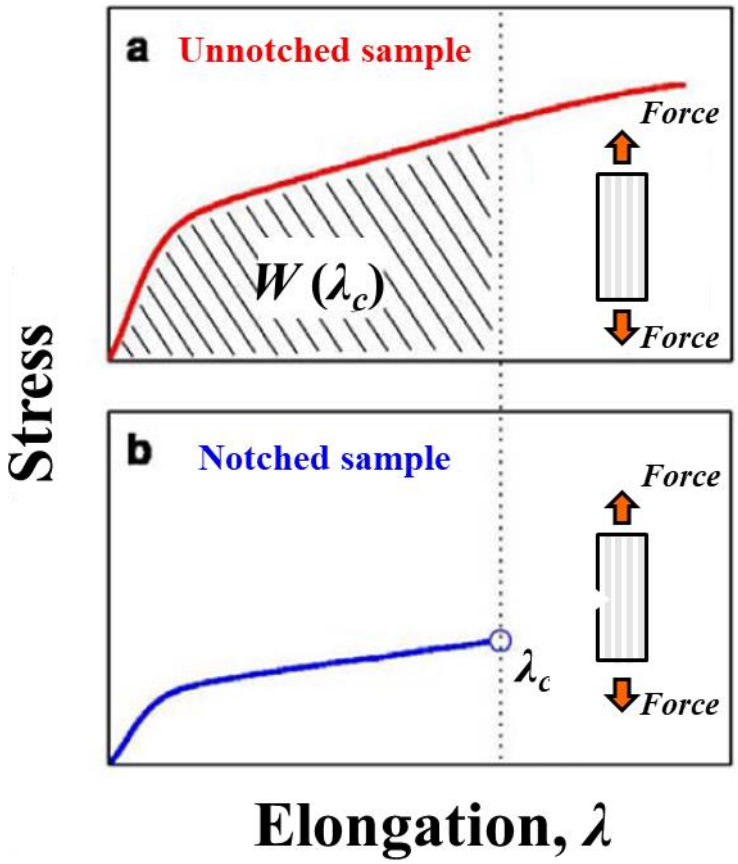

Figure 6.6. Single notch test to determine the fracture energy of hydrogels. Two samples of the same gel were tested in tension. One sample was unnotched, and the other sample was notched. The unnotched sample was used to measure the stress-strain curve. The area beneath the force-length curve gave the work done by the force to the unnotched sample. The notched sample was used to measure the critical distance between the clamps, , when the notch turned into a running crack.

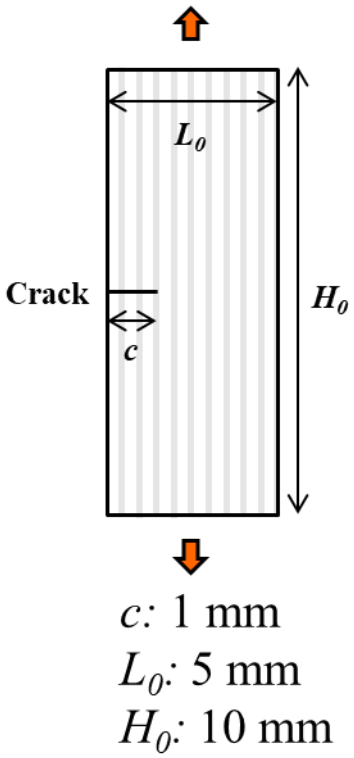

Figure 6.7. Sample geometry for single notch test.

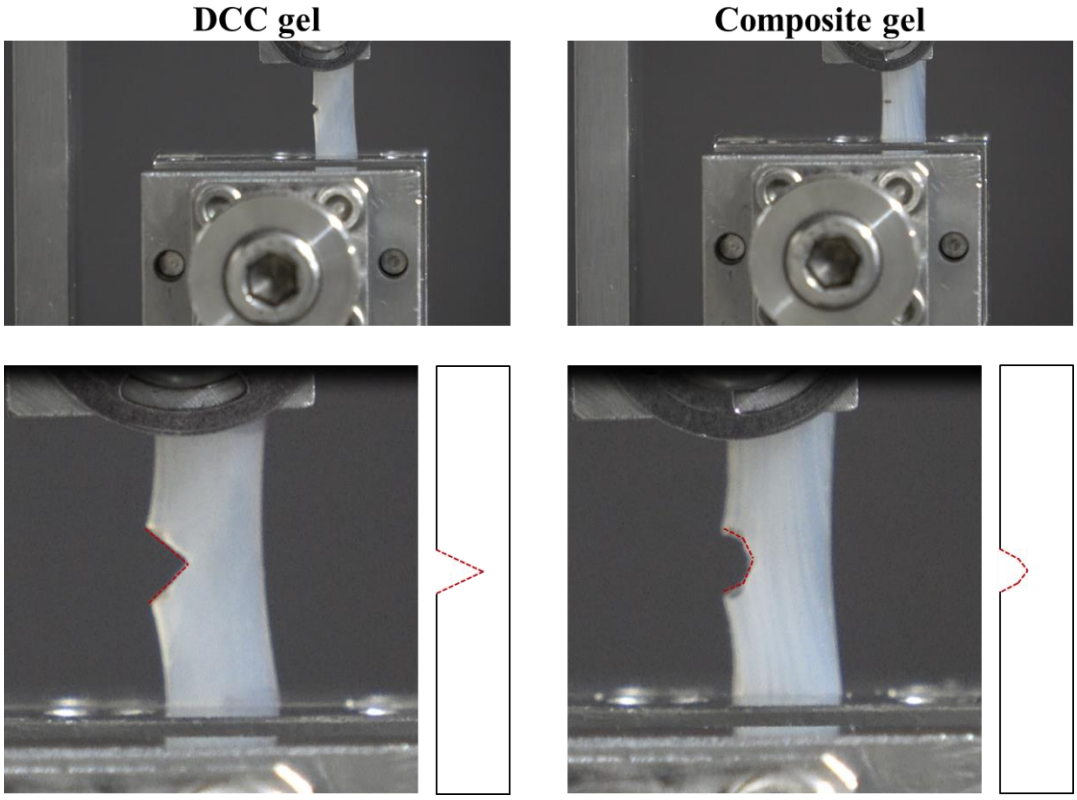

Figure 6.8. Fracture behaviors of DCC and composite gels.

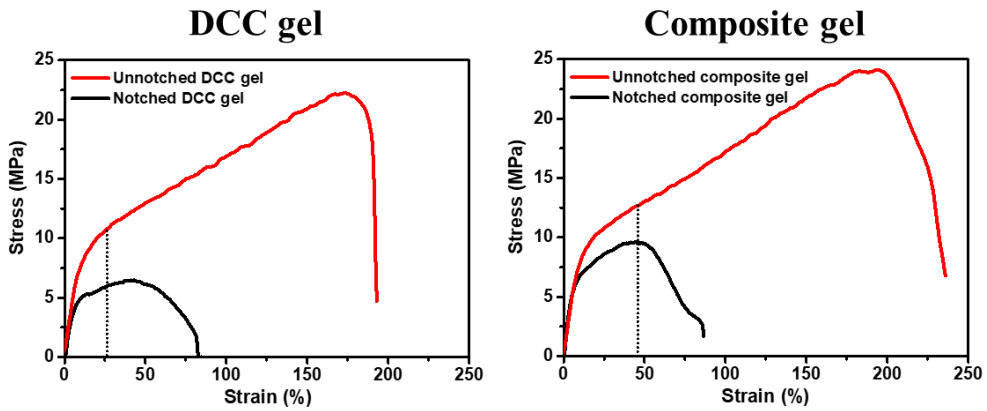

Figure 6.9. Results of single notch tests for DCC and composite gels.

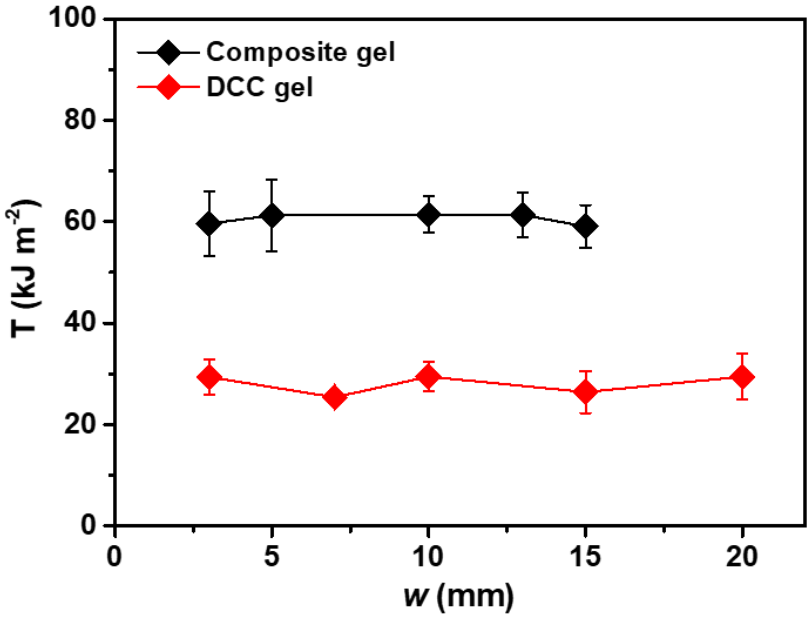

Figure 6.10. Size effect on fracture energy of DCC and composite gels.

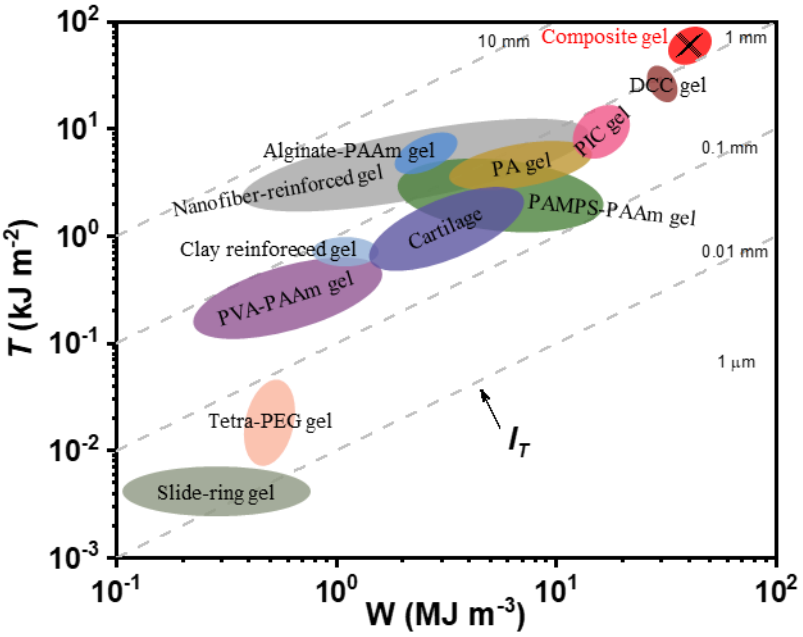

Figure 6.11. Fracture energy T, versus energy dissipation density, W, for various hydrogel systems. The slopes reflect the size of energy dissipation zone, according to equation (6.1).

Chapter 7-Conclusions

This dissertation proposed a universal design principle for developing extraordinarily crack-resistant structural materials: maximizing both energy dissipation density and energy dissipation zone by the combination of strong and rigid skeletons with soft, adhesive, and tough viscoelastic matrices. This principle is not limited to fabricate fiber-reinforced polymers, but can be extended to other soft material systems such as hydrogels. Conclusions of this dissertation are as follows.

In **Chapter 3**, the basic idea of design extremely crack-resistant fiber-reinforced polymers (FRPs) is illustrated. The key point of the idea is to use viscoelastic matrices that are adhesive, soft, and tough, which results in composites showing unique features that are totally different from traditional rigid FRPs: 1) the good adhesion between fibers and matrix enables a strong interface, which ensures both components to fully dissipate stored energy; 2) the softness of matrices gives extremely high fiber/matrix modulus ratio, leading to energy dissipation zones several orders of magnitude larger than common FRPs from rigid matrices; 3) the tough matrices show strain energy density comparable to fibers, highly enhancing the energy dissipation density of FRPs in the dissipation zone. Based on above considerations, a recently developed viscoelastic elastomers are employed to fabricate soft FRPs. The elastomers possess

low modulus yet high toughness and adhesion capacity, satisfying the requirements for making tough FRPs. The prepared FRPs have an interlocking structure with matrix strongly adhered to the fibers, which are expected to have a significant crack resistance.

In **Chapter 4**, the mechanical properties of as-prepared FRPs are examined. The prepared composites, with a strong component interface, are highly anisotropic, which are extremely resistant to stretch but quite flexible under bending or twisting. The FRPs also show much improved tensile strength and tearing toughness compared with neat fabric and matrix due to the extremely high modulus ratio of fiber to matrix. An efficient combination of multiple desirable properties is found in the soft FRPs, including high strength, high toughness, and low density, which is rarely achieved by other material systems. However, the tearing properties of FRPs are significantly affected by high temperature, which is expected to be solved by using matrix which has high glass transition temperature. Another advantage of the FRP system is that the material can be readily fabricated from either thermal initiation or UV initiation, and can be prepared from various matrix and fiber combinations. In summary, the soft FRPs show a combination of several desirable properties and beat all the best-in-class materials in present, and the preparation method can be easily extended to other systems, which hold great potential in industry applications.

In **Chapter 5**, the mechanism of the extremely high crack resistance of soft FRPs is clarified. By analyzing the size-dependent tearing energy of FRPs, the fracture behaviors of FRPs are divided into three regions according to two characteristic widths, w_1, and w_2. When the sample width is blow w_1, the fracture behavior of FRPs is fiber pullout as well as matrix fracture, which is defined as region I. In this region, fibers do not break or contribute to the elastic energy dissipation. However, the geometry of fibers influences the frequency of matrix destruction. The energy dissipation density by fiber pullout is found to be proportional to the product of fiber geometry, matrix toughness, and width, which is verified by several FRP systems. Region II is defined as the sample width is between w_1 and w_2. In this region, fibers are both pulled out and fractured, with matrix failure. Since the fracture behavior is complicated in this region and it does not reflect the intrinsic crack resistance of the FRPs, theoretical model is not launched. Finally, when the sample width is above w_2, the composite shows a size-independent tearing energy, which means that the energy dissipation zone is saturated. This region is defined as region III. In this region, fibers are mainly fractured, with matrix failed. The tearing energy is found to be related to the force transfer length and energy dissipation density. The force transfer length is decided by fiber geometry as well as component modulus ratio. The energy dissipation density generates from the volume weighed average work of extension of

components. These findings give a guidance to design and develop strong and tough composites, by utilizing adhesive, soft yet tough matrix as well as rigid but strong fiber. Based on this strategy, we demonstrate how new soft FRP composites from combination of viscoelastic elastomers and fabrics can reach unprecedented levels of crack resistance even beyond the toughest known materials.

In **Chapter 6**, we applied the learned strategy to hydrogel systems, aiming to develop a crack-resistant composite hydrogel. Alginate hydrogels that are dried in confined condition are selected as the skeleton since they show high tensile modulus and energy dissipation density, which is conducive for making composites with high modulus ratio and energy dissipation density. An extremely soft hydrogel system, polyacrylamide, is employed as the soft matrix. The resulting composite hydrogels, possessing highly aligned fibrous network structure, show improved tensile stress, modulus, and energy dissipation density, without sacrificing ductility. Single notch tests reveal that the composite gels have a fracture energy of as high as 60 kJ m^{-2}, almost two orders of magnitude higher than the best-in-class hydrogels in present. The big increase in energy dissipation density is account for the high fracture energy. This chapter verifies the validity of the design criterion and produces extremely tough biocompatible hydrogels, which holds great potential to design other tough materials for various applications.

References

1. F. Bouville, E. Maire, S. Meille, B. Van de Moortèle, A. J. Stevenson, S. Deville, Strong, tough and stiff bioinspired ceramics from brittle constituents. *Nat. Mater.* **13**, (2014) 508.
2. B. Gludovatz, A. Hohenwarter, D. Catoor, E. H. Chang, E. P. George, R. O. Ritchie, A fracture-resistant high-entropy alloy for cryogenic applications. *Science* **345**, (2014) 1153-1158.
3. Z. Li, K. G. Pradeep, Y. Deng, D. Raabe, C. C. Tasan, Metastable high-entropy dual-phase alloys overcome the strength–ductility trade-off. *Nature* **534**, (2016) 227.
4. J. N. Coleman, U. Khan, W. J. Blau, Y. K. Gun'ko, Small but strong: a review of the mechanical properties of carbon nanotube–polymer composites. *Carbon* **44**, (2006) 1624-1652.
5. J. Summerscales, N. Dissanayake, A. Virk, W. Hall, A review of bast fibres and their composites. Part 2–Composites. *Compos. Part A-Appl. S.* **41**, (2010) 1336-1344.
6. D. Miracle, Metal matrix composites–from science to technological significance. *Compos. Sci. Technol.* **65**, (2005) 2526-2540.
7. P. K. Mallick, Fiber-reinforced composites: materials, manufacturing, and design. CRC press, (2007).
8. H. Akil, M. Omar, A. Mazuki, S. Safiee, Z. M. Ishak, A. A. Bakar, Kenaf fiber reinforced composites: A review. *Mater. Design* **32**, (2011) 4107-4121.
9. W. Thomas, High Strength Glass Fibre-Resin Composites. *Nature* **242**, (1973) 455-456.
10. J. McLoughlin, New high temperature carbon fibre composite. *Nature* **227**, (1970) 701.
11. H. Ku, H. Wang, N. Pattarachaiyakoop, M. Trada, A review on the tensile properties of natural fiber reinforced polymer composites. *Compos. Part B-Eng.* **42**, (2011) 856-873.
12. D. C. Hofmann, J.-Y. Suh, A. Wiest, G. Duan, M.-L. Lind, M. D. Demetriou, W. L. Johnson, Designing metallic glass matrix composites with high toughness and tensile ductility. *Nature* **451**, (2008) 1085.
13. H. D. Wagner, A. Lustiger, Optimized toughness of short fiber-based composites: the effect of fiber diameter. *Compos. Sci. Technol.* **69**, (2009) 1323-1325.
14. T. Hsieh, A. Kinloch, K. Masania, J. S. Lee, A. Taylor, S. Sprenger, The toughness of epoxy polymers and fibre composites modified with rubber microparticles and silica nanoparticles. *J. Mater. Sci.* **45**, (2010) 1193-1210.
15. S.-Y. Fu, X.-Q. Feng, B. Lauke, Y.-W. Mai, Effects of particle size, particle/matrix interface adhesion and particle loading on mechanical properties of particulate–polymer composites. *Compos. Part B-Eng.* **39**, (2008) 933-961.
16. K. Kepple, G. Sanborn, P. Lacasse, K. Gruenberg, W. Ready, Improved fracture toughness of carbon fiber composite functionalized with multi walled carbon nanotubes. *Carbon* **46**, (2008) 2026-2033.
17. D. R. Bortz, E. G. Heras, I. Martin-Gullon, Impressive fatigue life and fracture toughness improvements in graphene oxide/epoxy composites. *Macromolecules* **45**, (2011) 238-245.
18. S. Lv, D. M. Dudek, Y. Cao, M. Balamurali, J. Gosline, H. Li, Designed biomaterials to mimic the mechanical properties of muscles. *Nature* **465**, (2010) 69.
19. R. O. Ritchie, The conflicts between strength and toughness. *Nat. Mater.* **10**, (2011) 817.
20. U. G. Wegst, H. Bai, E. Saiz, A. P. Tomsia, R. O. Ritchie, Bioinspired structural materials. *Nat. Mater.* **14**, (2015) 23.

21. K. Stok, A. Oloyede, Conceptual fracture parameters for articular cartilage. *Clin. Biomech.* **22**, (2007) 725-735.
22. W. Yang, V. R. Sherman, B. Gludovatz, E. Schaible, P. Stewart, R. O. Ritchie, M. A. Meyers, On the tear resistance of skin. *Nat. Commun.* **6**, (2015) 6649.
23. Y. A. Shin, S. Yin, X. Li, S. Lee, S. Moon, J. Jeong, M. Kwon, S. J. Yoo, Y.-M. Kim, T. Zhang, Nanotwin-governed toughening mechanism in hierarchically structured biological materials. *Nat. Commun.* **7**, (2016) 10772.
24. F. Libonati, G. X. Gu, Z. Qin, L. Vergani, M. J. Buehler, Bone-inspired materials by design: toughness amplification observed using 3D printing and testing. *Adv. Eng. Mater.* **18**, (2016) 1354-1363.
25. L.-B. Mao, H.-L. Gao, H.-B. Yao, L. Liu, H. Cölfen, G. Liu, S.-M. Chen, S.-K. Li, Y.-X. Yan, Y.-Y. Liu, Synthetic nacre by predesigned matrix-directed mineralization. *Science* **354**, (2016) 107-110.
26. L. Xu, X. Zhao, C. Xu, N. A. Kotov, Water-rich biomimetic composites with abiotic self-organizing nanofiber network. *Adv. Mater.* **30**, (2018) 1703343.
27. D. R. King, T. L. Sun, Y. Huang, T. Kurokawa, T. Nonoyama, A. J. Crosby, J. P. Gong, Extremely tough composites from fabric reinforced polyampholyte hydrogels. *Mater. Horiz.* **2**, (2015) 584-591.
28. Y. Huang, D. R. King, T. L. Sun, T. Nonoyama, T. Kurokawa, T. Nakajima, J. P. Gong, Energy-dissipative matrices enable synergistic toughening in fiber reinforced soft composites. *Adv. Funct. Mater.* **27**, (2017) 1605350.
29. Y. Huang, D. R. King, W. Cui, T. L. Sun, H. Guo, T. Kurokawa, H. R. Brown, C.-Y. Hui, J. P. Gong, Superior fracture resistance of fiber reinforced polyampholyte hydrogels achieved by extraordinarily large energy-dissipative process zones. *J. Mater. Chem. A* **7**, (2019) 13431-13440.
30. T. L. Sun, T. Kurokawa, S. Kuroda, A. B. Ihsan, T. Akasaki, K. Sato, M. A. Haque, T. Nakajima, J. P. Gong, Physical hydrogels composed of polyampholytes demonstrate high toughness and viscoelasticity. *Nat. Mater.* **12**, (2013) 932.
31. C. K. Roy, H. L. Guo, T. L. Sun, A. B. Ihsan, T. Kurokawa, M. Takahata, T. Nonoyama, T. Nakajima, J. P. Gong, Self-Adjustable Adhesion of Polyampholyte Hydrogels. *Adv. Mater.* **27**, (2015) 7344-7348.
32. L. Chen, T. L. Sun, K. Cui, D. R. King, T. Kurokawa, Y. SARUWATARI, J. P. Gong, Facile Synthesis of Novel Elastomers with Tunable Dynamics for Toughness, Self-healing and Adhesion. *J. Mater. Chem. A*, (2019).
33. J. W. Hutchinson, Z. Suo, in *Adv. Appl. Mech.* (Elsevier, 1991), vol. 29, pp. 63-191.
34. R. Long, C.-Y. Hui, Fracture toughness of hydrogels: measurement and interpretation. *Soft Matter* **12**, (2016) 8069-8086.
35. C. Creton, M. Ciccotti, Fracture and adhesion of soft materials: a review. *Rep. Prog. Phys.* **79**, (2016) 046601.
36. M. Thouless, H. Cao, P. Mataga, Delamination from surface cracks in composite materials. *J. Mater. Sci.* **24**, (1989) 1406-1412.
37. J. Holbery, D. Houston, Natural-fiber-reinforced polymer composites in automotive applications. *JOM* **58**, (2006) 80-86.
38. R. Malkapuram, V. Kumar, Y. S. Negi, Recent development in natural fiber reinforced

polypropylene composites. *J. Reinf. Plast. Compos.* **28**, (2009) 1169-1189.
39. H. Hargitai, I. Rácz, R. D. Anandjiwala, Development of hemp fiber reinforced polypropylene composites. *J. Thermoplast. Compos. Mater.* **21**, (2008) 165-174.
40. M. Rühle, A. G. Evans, High toughness ceramics and ceramic composites. *Prog. Mater Sci.* **33**, (1989) 85-167.
41. M. D. Thouiess, O. Sbaizero, L. S. Sigl, A. G. Evans, Effect of interface mechanical properties on pullout in a SiC-fiber-reinforced lithium aluminum silicate glass-ceramic. *J. Am. Ceram. Soc.* **72**, (1989) 525-532.
42. E. Bischoff, M. Rühle, O. Sbaizero, A. G. Evans, Microstructural studies of the interfacial zone of a SiC-fiber-reinforced lithium aluminum silicate glass-ceramic. *J. Am. Ceram. Soc.* **72**, (1989) 741-745.
43. P. Rao, T. L. Sun, L. Chen, R. Takahashi, G. Shinohara, H. Guo, D. R. King, T. Kurokawa, J. P. Gong, Tough hydrogels with fast, strong, and reversible underwater adhesion based on a multiscale design. *Adv. Mater.* **30**, (2018) 1801884.
44. J.-Y. Sun, X. Zhao, W. R. Illeperuma, O. Chaudhuri, K. H. Oh, D. J. Mooney, J. J. Vlassak, Z. Suo, Highly stretchable and tough hydrogels. *Nature* **489**, (2012) 133.
45. R. Rivlin, A. G. Thomas, Rupture of rubber. I. Characteristic energy for tearing. *J. Polym. Sci.* **10**, (1953) 291-318.
46. T. Baumberger, C. Caroli, D. Martina, Solvent control of crack dynamics in a reversible hydrogel. *Nat. Mater.* **5**, (2006) 552.
47. T. Baumberger, C. Caroli, D. Martina, Fracture of a biopolymer gel as a viscoplastic disentanglement process. *Eur. Phys. J. E* **21**, (2006) 81-89.
48. M. E. Seitz, D. Martina, T. Baumberger, V. R. Krishnan, C.-Y. Hui, K. R. Shull, Fracture and large strain behavior of self-assembled triblock copolymer gels. *Soft Matter* **5**, (2009) 447-456.
49. G. Miquelard-Garnier, D. Hourdet, C. Creton, Large strain behaviour of nanostructured polyelectrolyte hydrogels. *Polymer* **50**, (2009) 481-490.
50. M. A. Haque, T. Kurokawa, G. Kamita, J. P. Gong, Lamellar bilayers as reversible sacrificial bonds to toughen hydrogel: hysteresis, self-recovery, fatigue resistance, and crack blunting. *Macromolecules* **44**, (2011) 8916-8924.
51. Y. Tanaka, R. Kuwabara, Y.-H. Na, T. Kurokawa, J. P. Gong, Y. Osada, Determination of fracture energy of high strength double network hydrogels. *J. Phys. Chem. B* **109**, (2005) 11559-11562.
52. Q. M. Yu, Y. Tanaka, H. Furukawa, T. Kurokawa, J. P. Gong, Direct observation of damage zone around crack tips in double-network gels. *Macromolecules* **42**, (2009) 3852-3855.
53. M. A. Haque, T. Kurokawa, J. P. Gong, Super tough double network hydrogels and their application as biomaterials. *Polymer* **53**, (2012) 1805-1822.
54. H. Greensmith, Rupture of rubber. X. The change in stored energy on making a small cut in a test piece held in simple extension. *J. Appl. Polym. Sci.* **7**, (1963) 993-1002.
55. W.-C. Lin, W. Fan, A. Marcellan, D. Hourdet, C. Creton, Large strain and fracture properties of poly (dimethylacrylamide)/silica hybrid hydrogels. *Macromolecules* **43**, (2010) 2554-2563.
56. K. Mayumi, J. Guo, T. Narita, C. Y. Hui, C. Creton, Fracture of dual crosslink gels with permanent and transient crosslinks. *Extreme Mech. Lett.* **6**, (2016) 52-59.
57. H. Guo, N. Sanson, D. Hourdet, A. Marcellan, Thermoresponsive Toughening with Crack Bifurcation in Phase-Separated Hydrogels under Isochoric Conditions. *Adv. Mater.* **28**, (2016) 5857-5864.

58. A. Gent, Adhesion and strength of viscoelastic solids. Is there a relationship between adhesion and bulk properties? *Langmuir* **12**, (1996) 4492-4496.
59. M. W. Keller, S. R. White, N. R. Sottos, A self-healing poly (dimethyl siloxane) elastomer. *Adv. Funct. Mater.* **17**, (2007) 2399-2404.
60. K. J. Koester, J. Ager Iii, R. Ritchie, The true toughness of human cortical bone measured with realistically short cracks. *Nat. Mater.* **7**, (2008) 672.
61. R. O. Ritchie, Natural materials: armoured oyster shells. *Nat. Mater.* **13**, (2014) 435.
62. G. E. Fantner, T. Hassenkam, J. H. Kindt, J. C. Weaver, H. Birkedal, L. Pechenik, J. A. Cutroni, G. A. Cidade, G. D. Stucky, D. E. Morse, Sacrificial bonds and hidden length dissipate energy as mineralized fibrils separate during bone fracture. *Nat. Mater.* **4**, (2005) 612.
63. J. Behiri, W. Bonfield, Crack velocity dependence of longitudinal fracture in bone. *J. Mater. Sci.* **15**, (1980) 1841-1849.
64. H. Peterlik, P. Roschger, K. Klaushofer, P. Fratzl, From brittle to ductile fracture of bone. *Nat. Mater.* **5**, (2006) 52.
65. K. Piekarski, Fracture of bone. *J. Appl. Phys.* **41**, (1970) 215-223.
66. T. Matsuda, R. Kawakami, R. Namba, T. Nakajima, J. P. Gong, Mechanoresponsive self-growing hydrogels inspired by muscle training. *Science* **363**, (2019) 504-508.
67. S. Lin, J. Liu, X. Liu, X. Zhao, Muscle-like fatigue-resistant hydrogels by mechanical training. *Proc. Natl. Acad. Sci. USA* **116**, (2019) 10244-10249.
68. J. P. Gong, Y. Katsuyama, T. Kurokawa, Y. Osada, Double-network hydrogels with extremely high mechanical strength. *Adv. Mater.* **15**, (2003) 1155-1158.
69. J. P. Gong, Why are double network hydrogels so tough? *Soft Matter* **6**, (2010) 2583-2590.
70. C.-Y. Hui, Z. Liu, S. L. Phoenix, Size effect on elastic stress concentrations in unidirectional fiber reinforced soft composites. *Extreme Mech. Lett.*, (2019) 100573.
71. Z. Wang, C. Xiang, X. Yao, P. Le Floch, J. Mendez, Z. Suo, Stretchable materials of high toughness and low hysteresis. *Proc. Natl. Acad. Sci. USA* **116**, (2019) 5967-5972.
72. A. Thomas, Rupture of rubber. II. The strain concentration at an incision. *J. Polym. Sci.* **18**, (1955) 177-188.
73. K. Volokh, P. Trapper, Fracture toughness from the standpoint of softening hyperelasticity. *J. Mech. Phys. Solids* **56**, (2008) 2459-2472.
74. J. M. Hedgepeth, Stress concentrations in filamentary structures. (1961).
75. H. Cox, The elasticity and strength of paper and other fibrous materials. *Br. J. Appl. Phys.* **3**, (1952) 72.
76. R. Ritchie, Mechanisms of fatigue crack propagation in metals, ceramics and composites: role of crack tip shielding. *Materials Science and Engineering: A* **103**, (1988) 15-28.
77. U. G. Wegst, H. Bai, E. Saiz, A. P. Tomsia, R. O. Ritchie, Bioinspired structural materials. *Nat. Mater.* **14**, (2015) 23-36.
78. C. Ortiz, M. C. Boyce, Bioinspired structural materials. *Science* **319**, (2008) 1053-1054.
79. L. S. Dimas, G. H. Bratzel, I. Eylon, M. J. Buehler, Tough composites inspired by mineralized natural materials: computation, 3D printing, and testing. *Adv. Funct. Mater.* **23**, (2013) 4629-4638.
80. K. E. Tanner, Small but extremely tough. *Science* **336**, (2012) 1237-1238.
81. P. Song, Z. Xu, Y. Lu, Q. Guo, Bio-inspired hydrogen-bond cross-link strategy toward strong and tough polymeric materials. *Macromolecules* **48**, (2015) 3957-3964.

82. A. M. Hubbard, W. Cui, Y. Huang, R. Takahashi, M. D. Dickey, J. Genzer, D. R. King, J. P. Gong, Hydrogel/Elastomer Laminates Bonded via Fabric Interphases for Stimuli-Responsive Actuators. *Matter* **1**, (2019) 674-689.
83. E. Triki, P. Dolez, T. Vu-Khanh, Tear resistance of woven textiles–criterion and mechanisms. *Compos. Part B-Eng.* **42**, (2011) 1851-1859.
84. E. Triki, T. Vu-Khanh, P. Nguyen-Tri, H. Boukehili, Mechanics and mechanisms of tear resistance of woven fabrics. *Theor. Appl. Fract. Mec.* **61**, (2012) 33-39.
85. M. D. Demetriou, M. E. Launey, G. Garrett, J. P. Schramm, D. C. Hofmann, W. L. Johnson, R. O. Ritchie, A damage-tolerant glass. *Nat. Mater.* **10**, (2011) 123.
86. B. L. Smith, T. E. Schäffer, M. Viani, J. B. Thompson, N. A. Frederick, J. Kindt, A. Belcher, G. D. Stucky, D. E. Morse, P. K. Hansma, Molecular mechanistic origin of the toughness of natural adhesives, fibres and composites. *Nature* **399**, (1999) 761.
87. E. Munch, M. E. Launey, D. H. Alsem, E. Saiz, A. P. Tomsia, R. O. Ritchie, Tough, bio-inspired hybrid materials. *Science* **322**, (2008) 1516-1520.
88. Á. Kmetty, T. Bárány, J. Karger-Kocsis, Self-reinforced polymeric materials: A review. *Prog. Polym. Sci.* **35**, (2010) 1288-1310.
89. M. F. Ashby, Materials selection in mechanical design. *MRS Bull.* **30**, (2005) 995.
90. J. Schroers, W. L. Johnson, Ductile bulk metallic glass. *Phys. Rev. Lett.* **93**, (2004) 255506.
91. W. Clegg, K. Kendall, N. M. Alford, T. Button, J. Birchall, A simple way to make tough ceramics. *Nature* **347**, (1990) 455.
92. X. Zhang, A. Vyatskikh, H. Gao, J. R. Greer, X. Li, Lightweight, flaw-tolerant, and ultrastrong nanoarchitected carbon. *Proc. Natl. Acad. Sci. USA* **116**, (2019) 6665-6672.
93. X. Zhang, L. Zhong, A. Mateos, A. Kudo, A. Vyatskikh, H. Gao, J. R. Greer, X. Li, Theoretical strength and rubber-like behaviour in micro-sized pyrolytic carbon. *Nat. Nanotechnol.* **14**, (2019) 762-769.
94. C. Chen, Z. Wang, Z. Suo, Flaw sensitivity of highly stretchable materials. *Extreme Mech. Lett.* **10**, (2017) 50-57.
95. D. B. MARSHALL, M. V. SWAIN, Crack resistance curves in magnesia-partially-stabilized zirconia. *J. Am. Ceram. Soc.* **71**, (1988) 399-407.
96. Y. W. MAI, B. R. Lawn, Crack-interface grain bridging as a fracture resistance mechanism in ceramics: II, Theoretical fracture mechanics model. *J. Am. Ceram. Soc.* **70**, (1987) 289-294.
97. D. C. Hofmann, J.-Y. Suh, A. Wiest, M.-L. Lind, M. D. Demetriou, W. L. Johnson, Development of tough, low-density titanium-based bulk metallic glass matrix composites with tensile ductility. *Proc. Natl. Acad. Sci. USA* **105**, (2008) 20136-20140.
98. W. Curtin, The "tough" to brittle transition in brittle matrix composites. *J. Mech. Phys. Solids* **41**, (1993) 217-245.
99. S. Lin, C. Cao, Q. Wang, M. Gonzalez, J. E. Dolbow, X. Zhao, Design of stiff, tough and stretchy hydrogel composites via nanoscale hybrid crosslinking and macroscale fiber reinforcement. *Soft Matter* **10**, (2014) 7519-7527.
100. C.-N. Wu, Q. Yang, M. Takeuchi, T. Saito, A. Isogai, Highly tough and transparent layered composites of nanocellulose and synthetic silicate. *Nanoscale* **6**, (2014) 392-399.
101. F. Gao, N. Zhang, X. Fang, M. Ma, Bioinspired design of strong, tough, and highly conductive polyol-polypyrrole composites for flexible electronics. *ACS Appl. Mater. Interfaces* **9**, (2017) 5692-5698.

102. S. Kawabata, M. Matsuda, K. Tei, H. Kawai, Experimental survey of the strain energy density function of isoprene rubber vulcanizate. *Macromolecules* **14**, (1981) 154-162.
103. D. Haines, W. Wilson, Strain-energy density function for rubberlike materials. *J. Mech. Phys. Solids* **27**, (1979) 345-360.
104. T. Kawamura, K. Urayama, S. Kohjiya, Multiaxial deformations of end-linked poly (dimethylsiloxane) networks. 1. Phenomenological approach to strain energy density function. *Macromolecules* **34**, (2001) 8252-8260.
105. S. Torquato, M. Rintoul, Effect of the interface on the properties of composite media. *Phys. Rev. Lett.* **75**, (1995) 4067.
106. L. A. Estroff, A. D. Hamilton, At the interface of organic and inorganic chemistry: Bioinspired synthesis of composite materials. *Chem. Mater.* **13**, (2001) 3227-3235.
107. F. Aymerich, F. Dore, P. Priolo, Prediction of impact-induced delamination in cross-ply composite laminates using cohesive interface elements. *Compos. Sci. Technol.* **68**, (2008) 2383-2390.
108. L. Greve, A. Pickett, Delamination testing and modelling for composite crash simulation. *Compos. Sci. Technol.* **66**, (2006) 816-826.
109. V. Gupta, J. Yuan, D. Martinez, Calculation, measurement, and control of interface strength in composites. *J. Am. Ceram. Soc.* **76**, (1993) 305-315.
110. Z. Zou, S. Reid, S. Li, A continuum damage model for delaminations in laminated composites. *J. Mech. Phys. Solids* **51**, (2003) 333-356.
111. C. Yang, T. Yin, Z. Suo, Polyacrylamide hydrogels. I. Network imperfection. *J. Mech. Phys. Solids*, (2019).
112. J. Liu, C. Yang, T. Yin, Z. Wang, S. Qu, Z. Suo, Polyacrylamide hydrogels. II. elastic dissipater. *J. Mech. Phys. Solids* **133**, (2019) 103737.
113. M. Guo, L. M. Pitet, H. M. Wyss, M. Vos, P. Y. Dankers, E. Meijer, Tough stimuli-responsive supramolecular hydrogels with hydrogen-bonding network junctions. *J. Am. Chem. Soc.* **136**, (2014) 6969-6977.
114. T. Tanaka, E. Sato, Y. Hirokawa, S. Hirotsu, J. Peetermans, Critical kinetics of volume phase transition of gels. *Phys. Rev. Lett.* **55**, (1985) 2455.
115. J. P. Gong, N. Hirota, A. Kakugo, T. Narita, Y. Osada, Effect of aspect ratio on protein diffusion in hydrogels. *J. Phys. Chem. B* **104**, (2000) 9904-9908.
116. T. R. Hoare, D. S. Kohane, Hydrogels in drug delivery: Progress and challenges. *Polymer* **49**, (2008) 1993-2007.
117. K. R. Kamath, K. Park, Biodegradable hydrogels in drug delivery. *Adv. Drug Delivery Rev.* **11**, (1993) 59-84.
118. K. Y. Lee, D. J. Mooney, Hydrogels for tissue engineering. *Chem. Rev.* **101**, (2001) 1869-1880.
119. M. Shibayama, Spatial inhomogeneity and dynamic fluctuations of polymer gels. *Macromol. Chem. Phys.* **199**, (1998) 1-30.
120. J. Zarzycki, Critical stress intensity factors of wet gels. *J. Non-Cryst. Solids* **100**, (1988) 359-363.
121. Y. Tanaka, K. Fukao, Y. Miyamoto, Fracture energy of gels. *Eur. Phys. J. E* **3**, (2000) 395-401.
122. D. Bonn, H. Kellay, M. Prochnow, K. Ben-Djemiaa, J. Meunier, Delayed fracture of an inhomogeneous soft solid. *Science* **280**, (1998) 265-267.
123. C.-C. Lin, A. T. Metters, Hydrogels in controlled release formulations: network design and

mathematical modeling. *Adv. Drug Delivery Rev.* **58**, (2006) 1379-1408.

124. M. J. Zohuriaan-Mehr, K. Kabiri, Superabsorbent polymer materials: a review. *Iran. Polym. J.* **17**, (2008) 451.

125. G. Lake, A. Thomas, The strength of highly elastic materials. *Proc. R. Soc. London A* **300**, (1967) 108-119.

126. P. J. Flory, *Principles of polymer chemistry*. (Cornell University Press, 1953).

127. A. Ghatak, K. Vorvolakos, H. She, D. L. Malotky, M. K. Chaudhury. (ACS Publications, 2000).

128. A. M. Saitta, M. L. Klein, Polyethylene under tensil load: Strain energy storage and breaking of linear and knotted alkanes probed by first-principles molecular dynamics calculations. *J. Chem. Phys.* **111**, (1999) 9434-9440.

129. H. R. Brown, A model of the fracture of double network gels. *Macromolecules* **40**, (2007) 3815-3818.

130. M. T. I. Mredha, Y. Z. Guo, T. Nonoyama, T. Nakajima, T. Kurokawa, J. P. Gong, A facile method to fabricate anisotropic hydrogels with perfectly aligned hierarchical fibrous structures. *Adv. Mater.* **30**, (2018) 1704937.

Accomplishments

Original paper

1. Wei Cui, Daniel R. King, Yiwan Huang, Liang Chen, Tao Lin Sun, Yunzhou Guo, Yoshiyuki Saruwatari, Chung-Yuen Hui, Takayuki Kurokawa, and Jian Ping Gong, Fiber-reinforced Viscoelastomers Show Extraordinary Crack Resistance that Exceeds Metals, *Adv. Mater.*, 2020, Accepted.

Others

1. Amber M Hubbard, Wei Cui, Yiwan Huang, Riku Takahashi, Michael D Dickey, Jan Genzer, Daniel R King, Jian Ping Gong, Hydrogel/Elastomer Laminates Bonded via Fabric Interphases for Stimuli-Responsive Actuators, *Matter*, 1 (2019) 674-689.
2. Yiwan Huang, Daniel R King, Wei Cui, Tao Lin Sun, Honglei Guo, Takayuki Kurokawa, Hugh R Brown, Chung-Yuen Hui, Jian Ping Gong, Superior fracture resistance of fiber reinforced polyampholyte hydrogels achieved by extraordinarily large energy-dissipative process zones, *J. Mater. Chem. A*, 7 (2019) 13431-13440.
3. Chung-Yuen Hui, Zezhou Liu, Stuart Leigh Phoenix, Daniel R King, Wei Cui, Yiwan Huang, Jian Ping Gong, Mechanical behavior of unidirectional fiber reinforced soft composites, *Extreme Mech. Lett.*, 35 (2020), 100642.

Conference presentations

1. Wei Cui, Daniel R. King, Tao Lin Sun, Liang Chen, Yiwan Huang, Takayuki Nonoyama, Takayuki Kurokawa, Jian Ping Gong, Tough soft composites from elastomers and fabrics, *The 4th International Life-Science Symposium* at Hokkaido University, Sapporo, Japan, November, 2016. Poster presentation.
2. Wei Cui, Daniel R. King, Taolin Sun, Liang Chen, Yiwan Huang, Takayuki Nonoyama, Takayuki Kurokawa, Yoshiyuki Saruwatari and Jian Ping Gong, Tough soft composites from elastomers and fabrics, *Japan-Korea Joint Symposium on Polymer Science* at Hokkaido University, Sapporo, Japan, July, 2018. Poster presentation.
3. Wei Cui, Daniel R. King, Tao Lin Sun, Liang Chen, Yiwan Huang, Takayuki Nonoyama, Takayuki Kurokawa, Yoshiyuki Saruwatari, Jian Ping Gong, Extremely tough and strong soft composites from elastomers and fabrics, *67th Symposium on Macromolecules* at Hokkaido University, Sapporo, Japan, September, 2018. Oral presentation.
4. Wei Cui, Daniel R. King, Tao Lin Sun, Liang Chen, Yiwan Huang, Takayuki Nonoyama, Takayuki Kurokawa, Yoshiyuki Saruwatari, Jian Ping Gong, Extremely tough soft composites from elastomers and fabrics, *The 12th SPSJ International Polymer Conference* in Hiroshima, Japan, December, 2018. Oral presentation.
5. Wei Cui, Liang Chen, Yiwan Huang, Tao Lin Sun, Yoshiyuki Saruwatari,

Takayuki Nonoyama, Takayuki Kurokawa, Daniel R. King, Jian Ping Gong, Extremely tough and strong soft composites from viscoelastomers and fabrics, *68th SPSJ Annual Meeting* at Osaka International Convention Center, Osaka, Japan, May, 2019. Oral presentation.

6. Wei Cui, Yiwan Huang, Liang Chen, Tao Lin Sun, Yunzhou Guo, Yoshiyuki Saruwatari, Takayuki Nonoyama, Takayuki Kurokawa, Daniel R. King, and Jian Ping Gong, Tough soft composites from viscoelastomers and fabrics, *Gordon Research Conference* at Mount Holyoke College, Massachusetts, USA, July, 2019. Poster presentation.

Acknowledgements

First, I would like to express my sincere gratitude to my supervisor, **Professor Jian Ping Gong**, for giving me the opportunity to become a member of LSW. I really enjoy my stay here and appreciate her guide and patience on my research and care on my life. In fact, we encountered a lot of problems during exploring the material system at first. In my second year of PhD study, we employed quite a few theories and models to figure out the intrinsic energy dissipation mechanism of our materials, but they all did not fit very well with our data. It was always a dilemma for us to explain why our materials show such good toughness. At the worst time, I almost wanted to give up and was rather unmotivated about the research. However, Professor Gong nerve gives up, neither on me nor on my research. She was confident that we could find out the truth and encouraged me to carry on my research. When we were discussing together, she always kept smiling and was really patience. I was not so good at mathematics, so she sometimes even used real objects to explain equations, which helped me a lot understand difficult theories. To deeply understand the system, she also built cooperation with professors who are experts in mechanics. Finally, we were able to explain our system based on theories. By investigating the materials with Professor Gong, I have not only learnt how to do research, but also benefited from her advices about how to write a research paper.

Her respectable scientific attitude will benefit me in my whole life.

Meanwhile, I would like to express my deep thanks to **Dr. Daniel R. King**, who is an assistant professor in our lab and my sub-supervisor. Dr. Dan is from United States, so firstly I really appreciate that he always comes to talk with me, which improves my speaking a lot. He is a thoughtful person, during discussion he could always come up with some solutions for problems and fantastic ideas. It is a great enjoyment to discuss with him. On the other hand, since his age is very close to students, we behave also like friends besides teacher and student. To refresh our brain and help us relax from the stressful research life, he held many parties at izakaya or his apartment. He is so kind that I never see him get mad at anybody. When I was unmotivated at my research, he never pushed me, instead, he talked to me and encouraged me. He is fun and can always come up with jokes to make people happy, I am sure everybody in LSW likes him!

Also, I would like to express my thanks to **Dr. Tao Lin Sun**, who was a member in our laboratory, for his guide on my research; and to **Professor Takayuki Kurokawa**, for helping me a lot on experimental devices; and to **Dr. Tasuku Nakajima**, who is an associate professor in LSW, for plenty of help on my study; and to **Dr. Takayuki Nonoyama**, who is an associate professor in LSW, for helping me a lot on my study.

Besides, I also thank **Dr. Yoshinori Katsuyam**a and **Mrs. Yukiko**

Hane for their help with experiments and devices. I also really appreciate helps on my paper works from secretaries in LSW, **Mrs. Eiko Hasegawa**, **Mrs. Yuki Ookubo**, and **Mrs. Iseya Saeko**.

And I appreciate all other **LSW members**, no matter Japanese, or international students, for helping and caring me in my daily life, which makes me feel at home.

I also would like to express my special thanks to **Professor Chung-Yuen Hui**, from Cornell University, for fruitful discussions. He is an expert in mechanics. With his help, we were able to figure out the energy dissipation mechanism of our materials. I also thank **Dr. Yoshiyuki Saruwatari**, from Osaka Organic Chemical Industry Ltd, for providing us monomers to fabricate samples.

I sincerely thank the IGP (International Graduate Program) and MEXT scholarship for financial support during my PhD study.

Finally, I would like to express my deep thanks to my family, who always stand behind me and encourage me patiently.

Cui, Wei

Laboratory of Soft & Wet Matter

Graduate School of Life Science

Hokkaido University

Sapporo, Japan

September 2020